Earth-Science Reviews 151 (2015) 132–175

Contents lists available at ScienceDirect

Earth-Science Reviews

journal homepage: www.elsevier.com/locate/earscirev

Invited review

Steep Rock Lake: Sedimentology and geochemistry of an Archean carbonate platform

Philip Fralick [a], Robert Riding [b]

[a] Department of Geology, Lakehead University, Thunder Bay, ON, P7B 5E1, Canada
[b] Department of Earth and Planetary Sciences, University of Tennessee, Knoxville, TN 37996, USA

ARTICLE INFO

Article history:
Received 22 January 2015
Received in revised form 22 September 2015
Accepted 13 October 2015
Available online 17 October 2015

Keywords:
Carbonate platform
Archean sedimentology
Stromatolites
Archean hydrosphere
Precambrian atmospheric evolution

ABSTRACT

The ~2800 Ma Mosher Carbonate Formation at Steep Rock Lake in south central Canada is one of Earth's oldest limestone deposits. It is both thick (up to 500 m) and relatively well-preserved, and was one of the first Precambrian successions to be noted for evidence of early life. It continues to provide information on the antiquity of such processes as photosynthesis. The carbonate contains a variety of fabrics and facies, from apparently fine-grained, bedded limestones with domal and columnar stromatolites, atikokania radial fans, and sheet-cracks, to closely packed metric-scale hybrid domes of originally aragonite seafloor crust interlayered with fenestral fabric. Here we review previous work, provide new observations concerning these sediments and their geochemistry, and discuss the inception, overall development and ultimate demise of the Steep Rock platform. We divide the Mosher Carbonate into the lower Hogarth Member and upper Elbow Point Member. These units constitute a shallow-water carbonate platform succession. The Hogarth Member overlies eroded ~3000 Ma tonalite and is at least 120 m thick. Thin horizons of domal, pseudocolumnar, columnar and fenestral stratiform stromatolites, and occasional layers of 'atikokania' radial crystal fans, occur within relatively fine-grained, thin-bedded limestone with iron-carbonate horizons. In the upper part, meter-scale domes occur locally, with sheet cracks and stromatactis. The irregular laminae that build the small domal and columnar stromatolites are interpreted to be lithified mats and biofilms, presumably cyanobacteria-dominated. Fine-grained, well-bedded facies of the lower Hogarth Member and its varied association of small stromatolites is interpreted to have accumulated in a relatively protected inner platform environment. Numerous very thin horizons of iron-carbonate in the lower and upper parts of the Hogarth Member suggest temporally limited influence of iron-rich offshore waters. Vertical trends in Fe, Mn, Ba, Sr, Ce and $\delta^{13}C$ probably reflect progressive restriction of circulation with at least one abrupt, but short lived, change back to more open seawater conditions. The upper Hogarth Member with large banded domes and fenestral crusts and stromatolites is interpreted as back margin facies. The overlying Elbow Point Member is at least 70 m thick and appears to be entirely composed of innumerable juxtaposed, elongate, smooth and thickly layered domes lacking intervening sediment. Each dome is typically several meters across and composed of centimetric alternations of cuspate fenestral fabric, possibly microbial, and crystal fan fabric that is probably abiotic seafloor aragonite precipitate. Adjacent cuspate fenestral and crystal fan fabric show significant differences in concentration of $\delta^{13}C$, Sr, Ba, Fe and Mn. This 'Giant Dome' facies is interpreted as a platform margin deposit in which alternating calcite–aragonite mineralogies within each dome reflect a laterally fluctuating offshore redox boundary. Negative Ce anomalies, positive Gd anomalies and reduced positive Eu anomalies, relative to laterally correlative deep-water iron formation, occur in the majority of crystal fan samples and in some cuspate fenestral fabric samples. Ca-carbonate precipitation at the margin of an anoxic iron-rich sea would have been promoted by oxygenic removal of iron from seawater; otherwise Fe-carbonate would have been favored over Ca-carbonate precipitation. The Mosher Carbonate Formation is interpreted as an early marine oxygen oasis: a shallow-platform that favored cyanobacterial productivity, was sufficiently isolated from open marine circulation for the seawater to become relatively oxygenated, and where carbonate sediment aggradation was a positive feedback that sustained these shallow-water conditions. Limestone accumulation terminated as transgressive suboxic and anoxic seawater deposited first manganese oxide-rich and then manganese oxide-poor iron formation sediments.

Contents

http://dx.doi.org/10.1016/j.earscirev.2015.10.006
0012-8252/

1. Introduction

Carbonate platforms are large tabular bodies of shallow-marine limestone ($CaCO_3$) and dolostone ($CaMg(CO_3)_2$) that can survive in the geological record for billions of years. Together with deep-water limestone–dolostone deposits they constitute a crustal reservoir of inorganic carbon far exceeding the total organic carbon that occurs in biomass and fossil fuels (Holland, 1978; Stumm and Morgan, 1996). The long-term sequestration of CO_2 in these carbonate sediments (Holland, 1978) has played a key role in maintaining Earth's equable climate (Walker et al., 1981). The earliest known well-preserved carbonate sediments are ~3.4–3.5 Ga old deposits in Western Australia (Allwood et al., 2006; van Kranendonk, 2006) and South Africa (Lowe and Byerly, 2007). They are relatively thin, and no individual unit thicker than 60 m is known prior to 3.0 Ga (Riding et al., 2014). In contrast, Proterozoic and Phanerozoic carbonate platforms are typically 100s of meters thick and many kilometers in extent. The oldest limestone–dolostone sequences with these dimensions are ~2.78–2.94 Ga in age. One of the thickest and best-preserved of these is the ~2.8 Ga old limestone at Steep Rock Lake in Northwestern Ontario.

In an influential overview, Grotzinger (1989) argued that Precambrian platforms share essential features with their Phanerozoic counterparts: broad flat-topped areas with extensive shallow-water interiors and narrow high-energy margins, elevated above adjacent basins (Wilson, 1975; Read, 1985). Such rimmed carbonate areas develop when shallow-water carbonate sediments accumulate at rates exceeding relative sea-level rise. As Grotzinger (1989) noted, carbonate platforms can develop irrespective of differences in precipitation processes, as shown by platforms produced in the Phanerozoic by skeletal carbonates and in the Precambrian by stromatolites and abiogenic seafloor carbonate crusts. Two well-documented Precambrian platforms on which these comparisons are based are Rocknest (1.9 Ga; Hoffman, 1980; Grotzinger, 1986) and Campbellrand–Malmani (2.6–2.5 Ga; Beukes, 1987). In both of these, lateral facies changes from shelf to basin can be traced with confidence. Older platforms that are more deformed, and often steeply dipping, are less well-studied. At Steep Rock, major questions remain concerning the nature of the limestone components that constitute the deposit and the facies they represent. It remains debatable, for example, whether the sequence shallows (Wilks, 1986) or deepens (Grotzinger, 1989). At the same time, the greater age of Steep Rock focuses attention on factors that could have led to the inception of thick Ca-carbonate platforms; prompting fundamental questions concerning Ca-carbonate precipitation from Archean seawater that is widely thought to have been essentially anoxic and rich in dissolved iron (Holland, 1973; Cloud, 1972; Canfield, 2005; Holland, 2006).

2. Oxygenation

A number of proxies indicate that oxygen first accumulated in significant quantities in the Earth's atmosphere during the Great Oxidation Event (GOE) at approximately 2.4 Ga (Farquhar et al., 2000; Farquhar and Wing, 2003; Bekker et al., 2004; Holland, 2006; Lyons and Gill, 2010). Prior to this the atmosphere is thought to have been relatively anoxic (Kopp et al., 2005), though there may have been "whiffs" of oxygen for 50 to 200 Ma before the GOE (Anbar et al., 2007, 2011; Planavsky et al., 2014). Key to understanding the transition to free oxygen in the atmosphere has been extensive sedimentological and geochemical studies conducted on the Campbellrand–Malmani carbonate platform in South Africa (Sumner, 1996; Wright and Altermann, 2000; Kamber and Webb, 2001; Sumner and Grotzinger, 1996, 2004; Rouxel et al., 2005; Schneiderhan et al., 2006; Scott et al., 2008; Knoll and Beukes, 2009; Ono et al., 2009; Waldbauer et al., 2009; Fischer et al., 2009; Heimann et al., 2010; Voegelin et al., 2010) and the Hamersley carbonate platform in Australia (Becker and Clayton, 1972; Kaufman et al., 1990; Veizer et al., 1990; Simonson et al., 1993; Eigenbrode and Freeman, 2006; Czaja et al., 2010). These areas actively accumulated chemical precipitates, possibly reflecting seawater composition, 200 to 100 My before the GOE (Kaufman et al., 1990; Beukes et al., 1990; Bau and Dulski, 1996; Kamber and Webb, 2001; Eigenbrode and Freeman, 2006; Anbar et al., 2007; Kaufman et al., 2007; Kendall et al., 2010, 2011; Scott et al., 2011). The large Campbellrand–Malmani and Hamersley platforms existed at a time when the first "whiff" of oxygen may have developed in areas of the Earth's atmosphere–hydrosphere system (Kaufman et al., 1990, 2007; Wright and Altermann, 2000; Schneiderhan et al., 2006; Eigenbrode and Freeman, 2006; Anbar et al., 2007, 2011; Waldbauer et al., 2009; Kendall et al., 2010, 2011; Voegelin et al., 2010; Scott et al., 2011).

The generation of free oxygen in the hydrosphere via oxygenic photosynthesis during the Archean has been suggested from carbon isotopes (Schidlowski, 1988; Hayes, 1994; Grassineau et al., 2002; Kakegawa and Haikawa, 2007; Nisbet et al., 2007; Grassineau et al., 2005, 2006, Grassineau and Nisbet, 2008), lacustrine stromatolites (Buick, 1992, 2007, 2008), uranium abundances (Rosing and Frei, 2004), the timespan necessary to fill oxygen sinks (Catling and Claire, 2005), delta-top iron formations (Fralick and Pufahl, 2006), biomarkers (Eigenbrode et al., 2008), chromium isotopes (Frei et al., 2009; Crowe et al., 2013), molybdenum isotopes (Voegelin et al., 2010; Czaja et al., 2012; Planavsky et al., 2014), molybdenum–rhenium abundances (Kendall et al., 2010), geochemistry of altered basalts (Kerrich and Said, 2011), microbial mat properties (Kazmierczak et al., 2009; Tice et al., 2011), and sulfur cycling (Farquhar et al., 2011; Stüeken et al., 2012). At the same time, it has been inferred that any oxygen build-up in the hydrosphere at this time is likely to have been short-lived and spatially

restricted, as locally favorable conditions changed (MacGregor, 1927; Cloud, 1968; Fischer, 1965; Hayes, 1983; Kasting, 1992). Prime places to look for such 'oxygen oases' (Fischer, 1965) are shallow water areas containing abundant stromatolites and other evidence of primary productivity, such as the Steep Rock carbonate platform. Oxygenation of Steep Rock seawater, revealed by rare earth element (REE) analyses, could have promoted limestone precipitation through the oxidative removal of dissolved ferrous iron species, Fe(II), to insoluble Fe(III) oxyhydroxide (Fralick and Riding, 2012). At least 10.25 μM oxygen concentration in seawater would have been required to accomplish this at Steep Rock (Riding et al., 2014).

3. Steep Rock Lake

Steep Rock Lake, 5 km north of Atikokan ('caribou bones' in Ojibwe) in Northwestern Ontario, is at the southern margin of the Wabigoon Sub-province of the southern Canadian Shield (Fig. 1A). Although their age was unclear, relatively well-preserved early Neoarchean (~2800 Ma) metasediments in the area had attracted interest by the late 1800s (Smyth, 1891). Sandstones and conglomerates that fill erosional hollows in ~3.0 Ga tonalite are overlain by several hundred meters of carbonate, mainly limestone, from which fossils were reported in 1912 (Lawson, 1912; Walcott, 1912). Both the unconformity and the fossiliferous limestones were included in a field-visit during the 12th International Geological Congress in 1913. These purely geological interests were subsequently overshadowed by the economic importance of the much altered iron-rich sediments (iron and manganese oxides) that overlie the limestone. This major ore deposit, largely located beneath Steep Rock Lake, was mined from 1944 to 1979. The extensive operation commenced with isolation and draining of large sections of the lake, and revealed considerably more of the limestone than had

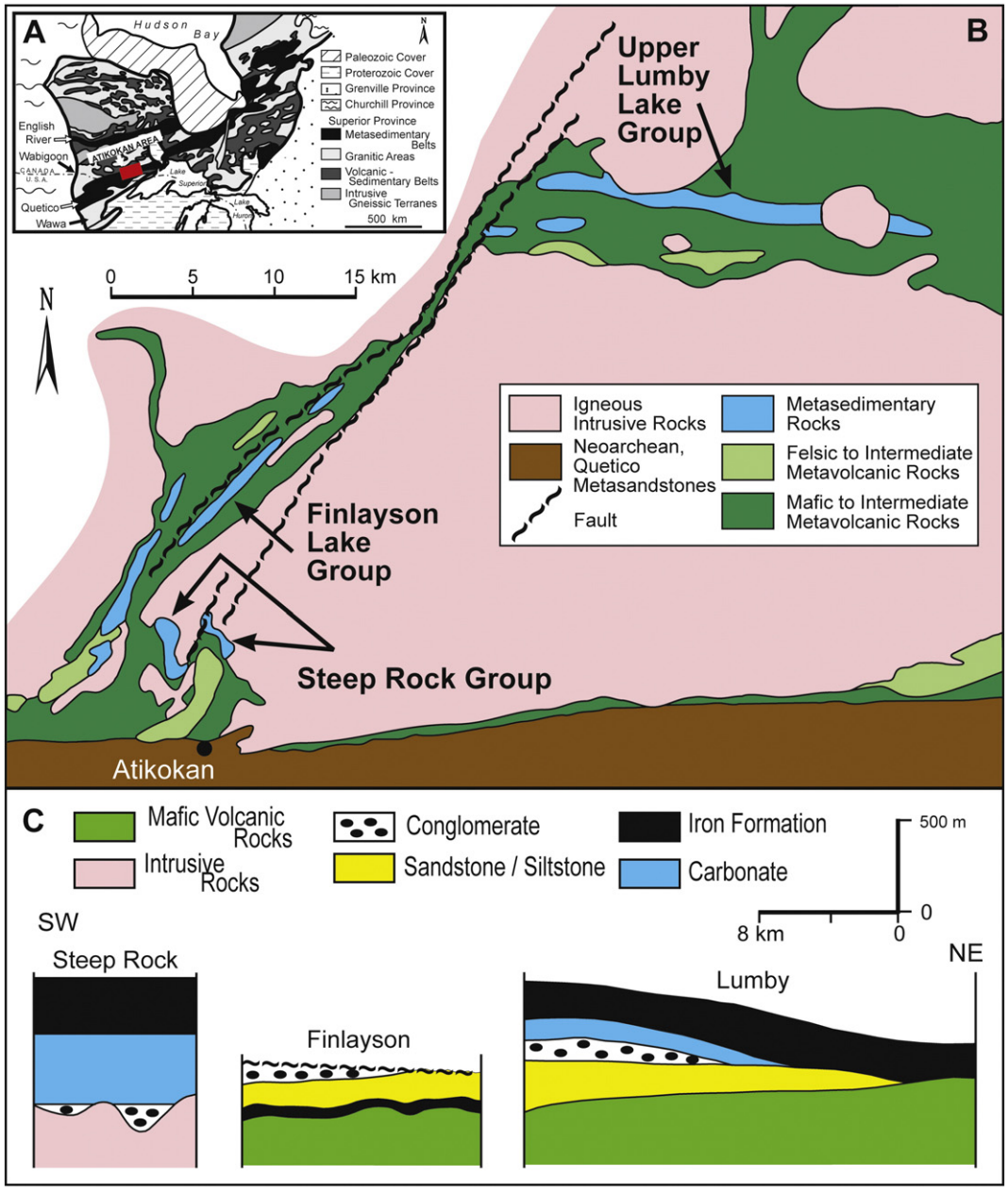

Fig. 1. A) Location of the Atikokan area in the Canadian Shield. B) Outcrop of the Steep Rock Group in relation to correlative sedimentary successions in the Finlayson Lake and Lumby Lake greenstone belts. Quetico metasediments to the south represent a sandstone dominated accretionary complex. Approximately 2692 Ma ago, this was thrust northward onto the 2750–2698 Ma Wabigoon Subprovince island arc succession by collision with the Wawa-Abitibi volcanic arc complex to the south (Barrett and Fralick, 1989; Williams, 1990; Fralick et al., 1992; Eriksson et al., 1994). C) Schematic cross-sections through the Steep Rock Group and laterally correlative Finlayson Lake and Lumby Lake groups (Fralick et al., 2008).

previously been visible (Supplemental Data: Steep Rock Iron Mines). Since mining ceased, the large and very deep excavations in the original lake floor have gradually been refilling with water, but have not yet re-submerged a number of important limestone outcrops.

The carbonate platform extends laterally for ~14 km in the Steep Rock area, and can be traced for at least 50 km in adjacent parts of the central Wabigoon sub-province. Greenschist facies metamorphism during the Archean affected much of the limestone microfabrics, and parts of the limestone also underwent ankerite replacement during Mesozoic karstification. Despite these effects, hundreds of meters of the carbonate succession remain moderately well-preserved limestone, with generally thin bands of siderite, ankerite and dolomite.

The nature of the first-reported Steep Rock fossils, sponge-like structures named *Atikokania* that initially were suggested to be 'the oldest forms of life yet discovered' (Lawson, 1912; Walcott, 1912), was soon questioned (Abbott, 1914) and *Atikokania* is now generally interpreted as abiotic crystal fans. Nonetheless, it was subsequently realized that the limestone also contains stromatolites that are unusually diverse for their age, and that some of these are major rock-builders at Steep Rock (Jolliffe, 1955; Hofmann, 1971; Walter, 1983). Numerous studies have made significant contributions to resolving the components and setting of the Steep Rock carbonate succession (e.g., Smyth, 1891; Lawson, 1912; Moore, 1938, 1939; Jolliffe, 1955; Shklanka, 1972; Hofmann, 1971; Walter, 1983; Wilks and Nisbet, 1985, 1988; Stone et al., 1992; Stone, 2008, 2010; Hayes, 1994; Beakhouse et al., 1996; Kusky and Hudleston, 1999; Sumner and Grotzinger, 2000; Grassineau and Nisbet, 2008; Grassineau et al., 2005, 2006). Nonetheless, despite being readily accessible and studied by geologists for many years, much remains to be discovered concerning this unusually old and relatively well-preserved limestone deposit.

4. Regional setting

The Steep Rock Group forms part of a laterally correlative series of rock units disrupted by a major shear zone (Fig. 1B) (Fenwick, 1976; Stone and Pufahl, 1995; Fralick and King, 1996; Wyman and Hollings, 1998; Tomlinson et al., 1999; Fralick et al., 2008). These units comprise the Finlayson Lake Greenstone Belt, Lumby Lake Greenstone Belt, and the Steep Rock Group. The sedimentary units that correlate with the Steep Rock Group form the upper portions of the Finlayson Lake and Lumby Lake Greenstone Belts, overlying thick successions of tholeiitic basalts and komatiites. The volcanic rocks span a time interval ranging from 3014 Ma (Tomlinson et al., 2003), near an intrusive contact at their base, to 2828 Ma (Tomlinson et al., 2003) in the upper portion of the Lumby Lake belt below the sedimentary rocks. The geochemistry of the volcanic rocks indicates that they were erupted in an oceanic plateau setting (Wyman and Hollings, 1998; Hollings and Wyman, 1999; Hollings et al., 1999). The Steep Rock Group sedimentary rocks and their correlative strata (Fig. 1C) were deposited on this >7 km thick oceanic platform after volcanism ceased (Fig. 2).

Correlative sedimentary rocks of the Finlayson Lake belt, lying to the north of the Steep Rock succession (Fig. 1B), consist of a coarsening upward siliciclastic marine to progradational strandline assemblage composed of tonalite and volcanic debris (Fralick et al., 2008). U–Pb age determinations on detrital zircons from the Finlayson and basal Steep Rock siliciclastics, combined with similar geochemistries, led to the conclusion that the fluvial systems which carved paleochannels in the tonalite underlying the Steep Rock Group delivered sediment to the strandline and flooded portion of the oceanic platform in the Finlayson area. As relative sea-level rose, slope reduction caused the channels to backfill, and continued marine flooding of the source area resulted in carbonate deposition (Fralick et al., 2008) (Fig. 1C). The units that overlay the siliciclastic succession in the Finlayson belt have been removed by faulting, but are preserved in the Lumby Lake Greenstone Belt, where the sedimentary succession varies from west to east. In the west, approximately 200 m of sandstone grades upwards to 50 m of conglomerate, overlain by 80 m of limestone (Fralick et al., 2008). Approximately 200 m of iron-rich lithofacies (iron formation), primarily composed of chert, magnetite, and carbonaceous, pyritiferous slate, with minor siderite layers, conformably overlies the limestone. To the east, over a distance of ~10 km, first the siliciclastics and next the limestone wedge out, leaving only iron formation directly overlying the basaltic basement. This has been interpreted as a deepening to the east. With isostatically induced flooding of the oceanic platform, a progressive facies shift towards the west culminated in further drowning of the platform at Steep Rock, which led to deposition of first manganese-rich then manganese-poor iron formation in that area (Fralick et al., 2008).

5. Steep Rock Group

Describing the sedimentary and associated volcanic rocks, Smyth (1891) listed a total of nine formations in the 'Steep Rock Series': (i) Conglomerate, (ii) Lower Limestone, (iii) Ferruginous Formation, (iv) Interbedded crystalline traps, (v) Upper calcareous green schist, (vi) Upper conglomerate, (vii) Greenstones and greenstone schists, (viii) Agglomerate, and (ix) Dark gray clay slate. He noted that the basal conglomerate and limestone rest unconformably on the underlying granitic rocks (Smyth, 1891), and that the Ferruginous Formation

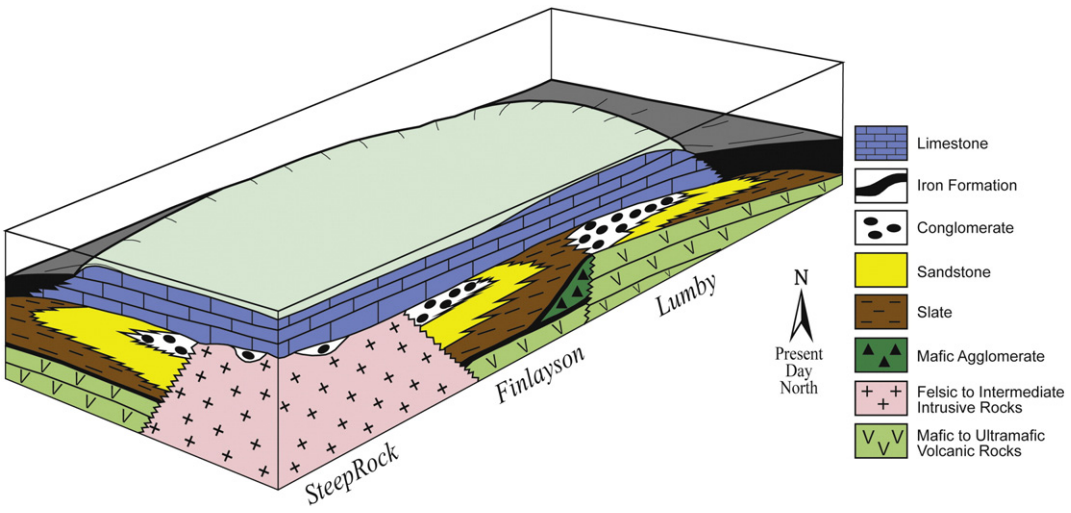

Fig. 2. Schematic interpretation of the igneous and sedimentary succession underlying the Steep Rock oceanic plateau. The Mosher Carbonate (marked as limestone) rests on siliciclastic sediments that record erosion of the igneous plateau. Transgressive drowning eliminated local siliciclastic supply and led to development of the carbonate platform (Fralick et al., 2008).

was mostly beneath Steep Rock Lake. Lawson (1912) recognized repetition in Smyth's (1891) units and reduced the Steep Rock succession to the first four formations. This approach was followed by Moore (1938). Jolliffe (1955) subdivided the volcanics above the iron formation into about 800 ft of 'ashrock' overlain by 1300 ft of 'sediments, flows, tuffs, and sills'. Subsequently, he defined the Steeprock Group and recognized it as comprising 'Conglomerate, Dolomite, Orezone, and Ashrock Formations' (Jolliffe, 1966) (Fig. 3).

Wilks and Nisbet (1988) renamed Jolliffe's (1966) Ashrock the 'Dismal Ashrock' and named the overlying volcanics and sediments the 'Witch Bay Formation'. At the same time, since they recognized the possibility of a structural break between the Dismal Ashrock and Witch Bay, they only provisionally included the Witch Bay in the Steep Rock Group (Wilks and Nisbet, 1988). They renamed Jolliffe's (1966) Dolomite Formation the Mosher Carbonate. Thus, Wilks and Nisbet (1988, Table 1) recognized the following units: (i) Wagita Formation (conglomerate, sandstone); (ii) Mosher Carbonate; (iii) Jolliffe Ore Zone; (iv) Dismal Ashrock, and (v) the Witch Bay Formation. Kusky and Hudleston (1999) suggested that both the Dismal Ashrock and the Witch Bay are allochthonous thrust units. If correct this would reduce the contiguous Steep Rock Group to just the first three units originally recognized by Smyth (1891): conglomeratic-sandstone, limestone, and iron formation. However, age determinations (Tomlinson et al., 2003; Denver Stone, personal communication) cast doubt on this conclusion. The age of the Steep Rock Group has long remained conjectural. As noted above, correlative sedimentary rocks in the Lumby Lake belt overlie a volcanic pile with a youngest age of 2828 ± 1 Ma (Tomlinson et al., 2003). This agrees with the youngest detrital zircon recovered from the Wagita Formation by Denver Stone (pers. comm.), which gave an age of 2779 ± 22 Ma; placing the basal unit in the Steep Rock Group as probably younger than 2801 Ma. Zircons from volcanic rocks in the overlying Dismal Ashrock gave an age of 2780 ± 1 Ma (Tomlinson et al., 2003), providing a youngest age for the Steep Rock Group. We infer that currently the best estimate for the age of the Steep Rock limestone is 2801–2780 Ma.

Here we use the formation names of Wilks and Nisbet (1988): Wagita Formation, Mosher Carbonate and Jolliffe Ore Zone. We subdivide the Mosher Carbonate into two members: Hogarth and Elbow Point. The Wagita and Mosher directly overlie 3003 ± 5 Ma (Davis and Jackson, 1988; also 3003 ± 3 Ma Tomlinson et al., 1999; and 3002 ± 2 Ma Tomlinson et al., 2003) tonalitic gneiss of the Marmion Complex that intrudes several greenstone belts in this area (Stone et al., 2002; Tomlinson et al., 2003; Percival et al., 2006). The relatively good preservation of the Wagita Formation and Mosher Carbonate at least partly reflects their deposition on the extensive rigid tonalitic basement. Regional metamorphic grade for these sediments in the Steep Rock area is lower greenschist facies (Wilks and Nisbet, 1985).

5.1. Wagita Formation

The contact separating the underlying Mesoarchean tonalite from the Steep Rock Group is a nonconformity (Smyth, 1891; Jolliffe, 1955; Wilks and Nisbet, 1985; Kusky and Hudleston, 1999). The Wagita Formation directly overlies this surface and consists mainly of lenticular beds of poorly-sorted sandstone and conglomerate (Smyth, 1891; Fralick et al., 2008) with angular to subrounded quartz and tonalite clasts up to 15 cm in size in a pelitic matrix (Wilks and Nisbet, 1988). Detrital zircons gave U–Pb ages of approximately 2999 Ma (Davis, 1993) and together with the preponderance of tonalite clasts indicate a very local source. The Wagita Formation is, in places, foliated and cleaved (Wilks and Nisbet, 1988; Kusky and Hudleston, 1999). In combination with local paleoweathering of the underlying tonalite (Schau and Henderson, 1983) this could account for the difficulty that Smyth (1891) noted in locating the lower contact in some places. The Wagita Formation forms the basal sediments of the Steep Rock Group. Although it is up to 150 m thick, it occupies depressions in the irregularly eroded tonalite and is locally absent (Jolliffe, 1955; Wilks and Nisbet, 1985); as a result, limestones can directly overlie the tonalite (Supplemental Fig. S3).

5.2. Mosher Carbonate

The Mosher Carbonate Formation (Wilks and Nisbet, 1988) was previously named the Dolomite Formation by Jolliffe (1966). Smyth (1891) described the limestone: 'The rock is very uniform in character wherever exposed. It is a dark to light bluish gray limestone not at all highly crystalline often banded with layers of lighter color along planes of original bedding. The light bands vary in width from a thin line up to 6 or 8 inches. Bedding planes are also often marked by thin cherty seams.' Coleman (1898, p. 225) noted that Steep Rock limestones 'have a very modern look, being scarcely at all crystalline in appearance', adding 'One almost expects to discover fossils in them'. Subsequent work (Lawson, 1912; Moore, 1938; Jolliffe, 1955, 1966; Shklanka, 1972; Wilks and Nisbet, 1985, 1988; Nisbet and Wilks, 1989; Kusky and Hudleston, 1999; Sumner and Grotzinger, 2000), together with mapping (Shklanka, 1972; Beakhouse et al., 1996), has built on these early observations. Hofmann (1971), Walter (1983) and Wilks and Nisbet (1985, 1988) recognized diverse stromatolite morphologies, with stratiform, pseudocolumnar and hemispherical stromatolites in the lower part of the limestone followed by branched and conical forms, and with large domal stromatolites dominating the upper part of the formation.

The topmost surface of the limestone is irregular. This has been attributed to regression and development of an unconformity (Wegenast, 1954; Jolliffe, 1955, 1966), with the overlying, up to 300 m thick, Manganiferous Paint Rock (see below) representing reworked weathered material. Jolliffe (1955) described the contact of the limestone with the ore zone as a sharply defined surface that broadly follows bedding in the limestone: 'in detail, it is most irregular and transgressive with local "relief" on the surface of the contact amounting to some tens of feet. Rounded protuberances of carbonate extend up into the orezone, and, conversely, salients of footwall 'paint' extend irregularly down into the carbonate' (Jolliffe, 1955, p. 383). He interpreted this as an ancient karst surface with pinnacles and sinkholes due to deep weathering. However, the Jolliffe Ore Zone is strongly altered and its irregular contact with

Smyth 1891	Jolliffe 1966	Wilks & Nisbet 1988	This study	
Crystalline Traps	Ashrock	Dismal Ashrock	Dismal Ashrock	
Ferruginous Formation	Orezone	Jolliffe Orezone	Jolliffe Orezone	
Lower Limestone	Dolomite	Mosher Carbonate	Mosher Carbonate	Elbow Point Member Hogarth Member
Conglomerate	Conglomerate	Wagita	Wagita	

Fig. 3. Steep Rock Group, summary development of stratigraphic names. If the Dismal Ashrock is contained in an allochthonous thrust unit, it may not be part of the Steep Rock Group (Kusky and Hudleston, 1999).

the limestone appears to be a much younger development (Kimberley and Sorbara, 1976). Several lines of reasoning suggest that this surface is not an Archean paleokarst. 1) The Manganiferous Paint Rock is consistently described as unconsolidated and earthy, whereas all other Superior Province rocks that experienced the 2.7 Ga Kenoran Orogeny are well lithified and metamorphosed. 2) The associated carbonate collapse breccia cements are neither deformed nor metamorphosed, although the surrounding rocks are. 3) There are vertical alteration zones in the carbonate that are not associated with the contact. 4) The alteration requires a highly oxidizing fluid, which is not a likely chemistry for Archean meteoric water. 5) Laterally correlative rocks show no evidence of Archean exposure. 6) The overlying iron formation is brecciated and altered, which is not consistent with sub-iron formation exposure. 7) The ore zone contains woody fragments (R. Bernatchez, in Wilks and Nisbet, 1988) and Machado (1987) believed that there is evidence of termite activity during formation of the ore. This suggests that the alteration affecting the ore and limestone is younger than Jurassic (Machado, 1987), consistent with the altered material being unmetamorphosed and in places unconsolidated. The alteration zones in the carbonate are quite discrete and easily recognized by the hematization. We conclude that the conformable contact between Mosher Carbonate and iron formation in the Lumby Lake belt was also originally present at Steep Rock, and was modified during the Phanerozoic. This concurs with Shklanka's (1972) opinion that there is 'no erosional disconformity' between Jolliffe's Dolomite and Orezone formations.

5.3. Jolliffe Ore Zone

The iron formation is extensively altered to relatively soft high grade goethite–hematite ore (Smith, 1942; Shklanka, 1972; Kimberley and Sorbara, 1976). It consists of a lower Manganiferous Paint Rock Member and an upper Goethite Member (Wilks and Nisbet, 1988). The Manganiferous Paint Rock Member is an unconsolidated, earthy deposit, 100–300 m thick, composed of clasts of goethite, hematite, chert and quartz in a matrix of these minerals plus kaolinite, illite, calcite, gibbsite and pyrolusite (Huston, 1956; Wilks and Nisbet, 1988). On average, it contains 3.8% manganese (Huston, 1956). The overlying Goethite Member is 50–100 m of goethite, with subsidiary hematite and minor kaolinite and quartz (Wilks and Nisbet, 1988). Some less altered fragments are similar to iron formation, whereas the highly altered ore that consists of hematitic pisolite resembles ferruginous bauxite (Wilks and Nisbet, 1988).

5.4. Structure

As a whole, these Steep Rock sediments dip steeply to the southwest and the sequence is disrupted by a series of NE–SW trending faults (Fig. 5A). Smyth (1891) realized that the iron ore, which is much softer than the limestone, mainly occurred beneath Steep Rock Lake, except on the 'south shore of the eastern arm', and that boulders of iron ore indicated its continuity 'at several widely distant points'. Smith (1893) was probably referring to this when he noted 'indications of extensive ore bodies' in the Steep Rock Series. Similarly, McInnes (1899) noted 'large angular blocks of a very good haematite' on the shore of Steep Rock Lake, adding that 'the beds from which the blocks of rich float were derived seem to be largely covered by the waters of the lake'. Because of its position, extraction of the iron ore required that much of Steep Rock Lake be drained. Work commenced in 1943 and the lake bed was extensively mined from 1944 to 1979.

6. Methodology

6.1. Samples

Samples were collected at all six localities examined (for locality details, see Localities in Supplemental Data). This provided coverage from the base to near the top of the Formation. Large solution pathways with hematitic and ankeritic alteration were avoided and only samples with well-preserved macrofabric were chosen. Forty-nine samples of carbonate were collected; most were slabbed and polished and fifteen, which showed good preservation of internal structure, were selected for geochemical analysis. Three of these were separated into crystal fan fabric, associated white void-filling cement, and immediately adjacent cuspate fenestral fabric (SR-16A crystal fans; SR-16B base of fans; SR-18A, 18E crystal fans, SR-18B cement, SR-18C, 18D area below fans; SR-22A crystal fans, SR-22b, 22C area above crystal fans). The white, void-filling cement was also separated from two domal stromatolite samples (8-24A flat-mat stromatolite, 8-24B cement; SR-5A small domal stromatolite, SR-5B cement). Two samples of digitate stromatolite were separated into column and inter-column areas (8-43A, 44A stromatolite, 8-43B, 44B inter-column debris). This resulted in 28 carbonate samples being analyzed by ICP-MS and AES. These samples, plus a sample of siderite from the iron formation, were also analyzed for oxygen and carbon isotopic ratios at the Facility for Isotope Research, Queen's University, Ontario, using a DELTA^{plus} XP Stable Isotope Ratio Mass Spectrometer.

The iron formation adjacent to the Mosher Carbonate was oxidized, probably during the Mesozoic (see Section 5.2), and so iron formation samples were collected from the laterally equivalent (Fralick et al., 2008) iron formation in the Lumby Lake greenstone belt northeast of Steep Rock Lake (Fig. 1B). Core samples of iron oxides, chert, pyrite, siderite and carbonaceous slate were collected from a hole drilled on the north-shore of Hematite Lake, 45 km NE of Steep Rock Lake. Eleven samples were analyzed by ICP-MS and AES.

Samples were analyzed for major and trace elements using ICP-AES (majors) and ICP-MS (traces) at the Geoscience Laboratories of the Ontario Ministry of Northern Development and Mines in Sudbury, Ontario. Sample dissolution was performed in a closed beaker using HF, HCl and $HClO_4$. Analyses were conducted on a Perkin-Elmer Elan 9000 ICP-MS following a variation on the protocol described by Burnham and Schweyer (2004). These samples were also analyzed for majors and selected traces using ICP-AES. Samples with large amounts of Ca and Fe were analyzed for these elements by ICP-AES at Lakehead University after the digest was diluted 2000 times. Detection limits for the trace elements determined by ICP-MS were set as 3 s of the procedural blanks. The Rare Earth Elements (REE) were analyzed at Lakehead University by ICP-MS. An open digestion using three treatments with nitric and hydrofluoric acids was employed. Accuracy and precision were evaluated by analyzing duplicate samples and standard reference materials embedded in the runs and were within acceptable limits. The REE data were standardized to post-Archean Australian Shale (PAAS) (Taylor and McLennan, 1985).

7. Lithofacies associations

Mosher Carbonate is dark and light blue-gray banded limestone (Smyth, 1891). Its lower part contains a variety of relatively small stromatolites and its upper part is dominated by meter-scale domes (Wilks and Nisbet, 1985, 1988). Here we formalize these two subdivisions of the Mosher Carbonate as the Hogarth Member (from Hogarth Pit, immediately west of Localities 1 and 2) and the Elbow Point Member (from Elbow Point north of Errington Pit where the Middle Arm and East Arm of Steep Rock Lake originally joined, Localities 5 and 6).

Sections of these members were measured at Localities 1, 2, 5 and 6 (Fig. 4A). Giant Dome Lithofacies occurs at a number of localities where domes form continuous horizons (Wilks and Nisbet, 1988). We only observed them in the upper part of the succession, and exposures up to ~70 m thick of the Elbow Point Member show that they entirely dominate this unit. This abundance contrasts with the relative scarcity of smaller domal and columnar stromatolites in the Hogarth Member that typically occur as thin horizons.

Approximately 150 m of the lower part of the Mosher Carbonate is exposed at Localities 1 and 2 (Supplemental Figs. S1A and S2) between

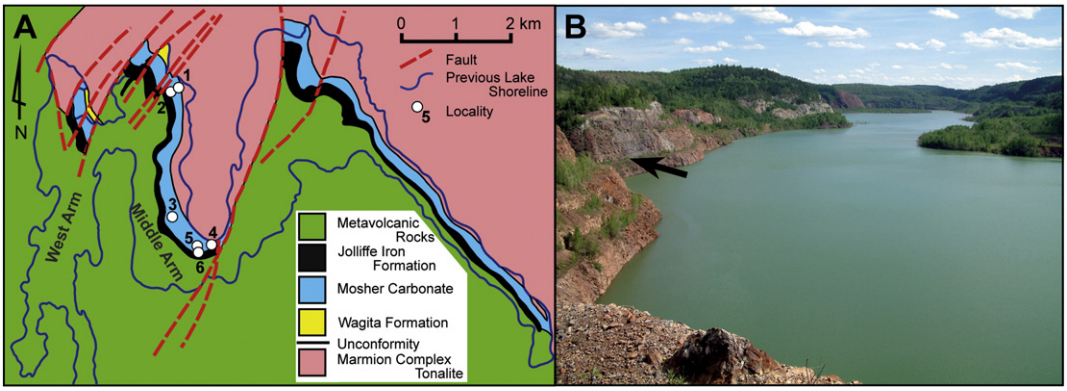

Fig. 4. A) Geology of the Steep Rock area. The M-shaped outline of Steep Rock Lake, which was mostly drained to permit mining of the iron ore, is shown by the thin blue line. The six localities examined and sampled are along the western side of the Mosher Peninsula facing the original Middle Arm of the lake. B) View south over reflooded Hogarth Pit and the former Middle Arm of Steep Rock Lake. Arrow indicates Locality 2.

the tonalite and the eastern edge of Steep Rock Lake. Locality 1 shows the lower 70 m of the Hogarth Member, overlain by approximately 65 m of altered ferruginous carbonate that is brecciated in places. This ~70 m of well-preserved Hogarth Member consists of 93% flat bedded limestone, 6% small stromatolites, and 1% atikokania (crystal fans). Locality 2 overlies the altered zone and consists of 14 m of what appears to be recrystallized packstone/grainstone, which we attribute to the Hogarth Member, overlain by 12 m of giant domes (basal Elbow Point Member) before the outcrop terminates at the lake (Fig. 4B). Further south, in the Elbow Point area (Supplemental Fig. S1B), the Hogarth Member is at least 120 m thick at Locality 5 and is overlain by at least 70 m of Elbow Point Member at Locality 6; a total of 190 m of Mosher Carbonate. Approximately 100 m of limestone is exposed at, and immediately north of, Locality 4. If this latter succession is contiguous with the succession at Localities 5 and 6 then there would be a total of 220 m of Hogarth Member plus 70 m of the Elbow Point Member in this area. However, it is possible that the succession at Locality 4, and to its north, is separated from Localities 5 and 6 by faulting, and also that it might represent altered rocks from the Hogarth-Elbow Point transition (see Section 10). Early estimates considered the Mosher as a whole to range from 'not less than 500 nor more than 700 ft' (i.e., 152–213 m) (Smyth, 1891), or up to approximately 1000 ft (i.e., 305 m) (Jolliffe, 1955). Wilks and Nisbet (1985) estimated the Mosher to be up to 500 m thick in the Steep Rock Lake area, and mapping (e.g., Beakhouse et al., 1996, fig. 24) shows the steeply dipping Mosher outcrop east of Elbow Point/Errington Pit to be approximately 400 m wide.

Despite being locally good, preservation of the limestone is very variable. In addition to the intense hematitic alteration that affects the Hogarth Member between Localities 1 and 2, there is locally strong folding and shearing (Kusky and Hudleston, 1999) and extensive recrystallization (Wilks and Nisbet, 1988), as at Locality 4. These effects hinder recognition and interpretation of primary textures, especially at the microscopic level.

8. Mosher Carbonate: Hogarth Member

8.1. Introduction

The Hogarth Member has a distinctive banded appearance. It is predominantly a thin-bedded (<20 cm) dark (black, gray) to pale (bluish, tan) limestone in which brown Fe-carbonate horizons and veins are locally common, especially in the lower and upper parts of the unit. Its succession can be followed from Localities 1 to 2, and at Locality 5. The succession at Locality 4 and its northern extension is uncertain (see Section 10). The lower part of the Member at Locality 1 contains decimetric beds of stratiform, pseudocolumnar, columnar and domal stromatolites, together with thin intraclastic breccia horizons and layers containing atikokania crystal fans. Better preserved thin (typically 2–10 cm) alternations of dark, mid- and pale-gray, commonly fenestral, limestone, apparently fine-grained, with well-defined and generally sharp layer contacts, are well exposed at Locality 5. The pale gray layers are locally penetrated by vertical synsedimentary cracks a few centimeters wide with irregular margins. This lithotype somewhat resembles ribbon rock, and includes large, commonly steep-sided, domes that differ from overlying giant domes of the Elbow Point Member in apparently being mainly composed of fine-grained banded limestone. The upper part (Unit 6) of the Hogarth Member at Locality 5 contains irregular and stromactoid fenestrae and laminoid sheet cracks, locally approaching zebra limestone. Domal stromatolites are also present, and these fenestral limestones probably include stratiform stromatolites. Thus, despite its relatively uniform overall bedded appearance, where it is well-preserved the Hogarth Member exhibits a wide variety of distinctive components, including atikokania (crystal fans), stromatolites, fenestrae, and a lithotype resembling ribbon rock; with domes locally occurring in both the fenestral limestones and the banded limestone that resembles ribbon rock.

8.2. Stratigraphic relationships — Hogarth Member section east of Hogarth Pit (Localities 1–2)

The lower part of the Member is well exposed at Locality 1 (the 'stromatolite pit' depression of Wilks and Nisbet, 1988), where it directly overlies tonalite (Supplemental Fig. S3). The member strikes N–S with dips between vertical and ~70° west, and is dominated by thinly and persistently layered pale to mid-gray limestone with occasional thin (mostly <0.5 m) horizons of small (decimetric) domical and columnar stromatolites and rare layers of radial crystal fans (atikokania). The limestone and stromatolites contain layers of, and are crossed by, numerous veins and patches, of brown Fe-carbonate. This 64 m section, well-exposed on a glacially smoothed surface, passes up into ~60–70 m of brown brecciated iron carbonate-replaced limestone at an abrupt irregular contact that cross-cuts Units 11 and 12. This brown altered rock (Unit 13) forms a hill, bounded by cliffs to the north and west, between Localities 1 and 2 (Supplemental Fig. S2) overlooking Hogarth Pit. Locality 2 is on the north-west side of the hill where there is a rapid transition back to the relatively unaltered sequence which recommences with 14 m of bedded limestone (Unit 14), which we regard as the uppermost part of the Hogarth Member. Unit 14 passes up into the Elbow Point Member at Locality 2. Thus, overall at Localities 1–2, the Hogarth Member is divisible into 14 units, of which one (Unit 13) is heavily altered (Fig. 5).

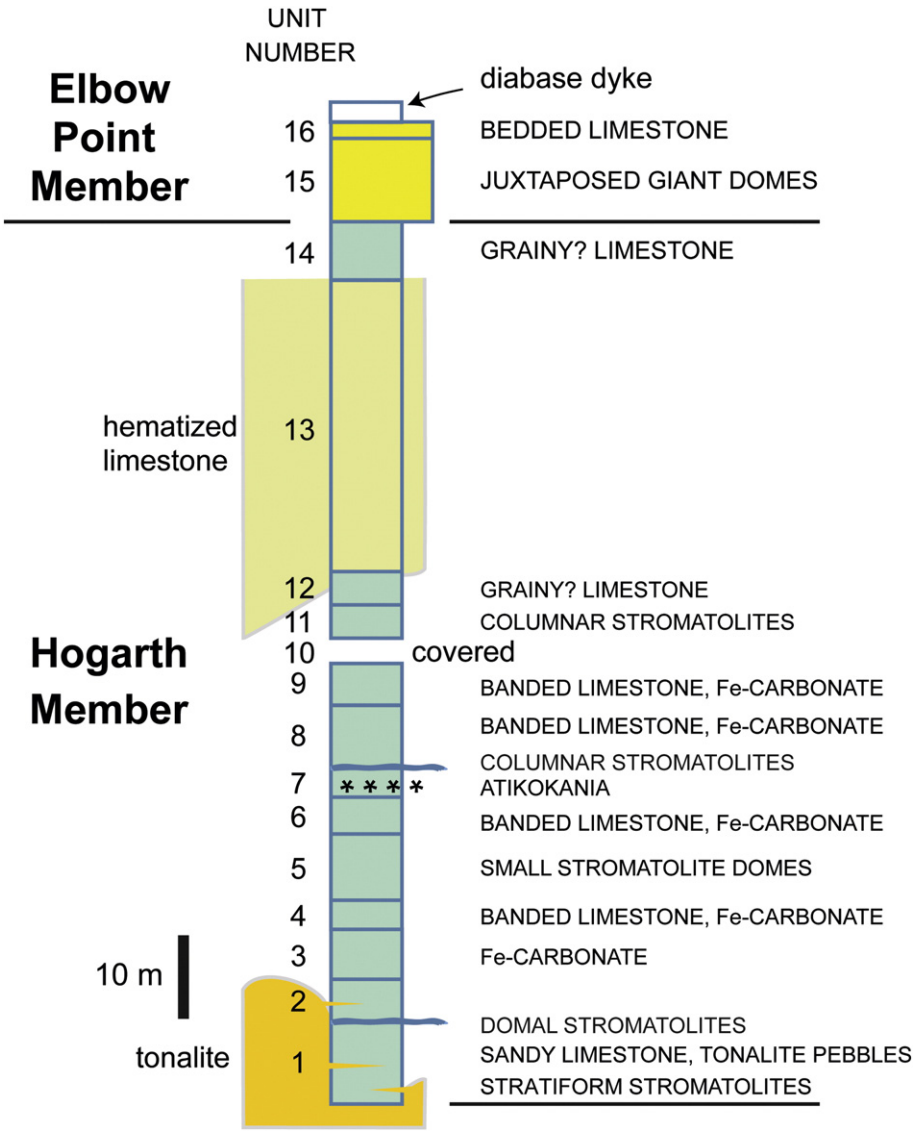

Fig. 5. Lithologic succession at Localities 1–2 through Hogarth Member (Units 1–14) to lowermost Elbow Point Member (Units 15–16). The Hogarth overlies irregularly eroded tonalite (see Supplemental Fig. 3), and the section is measured from the deepest depression in the tonalite at Locality 1. In this section the Hogarth (including the ~35 m thick hematized Unit 13) is ~106 m thick. The lowermost Elbow Point Member is ~12 m thick. The top of the section is truncated (to the west, at Locality 2) at Steep Rock Lake (Fig. 4B).

8.2.1. Units 1–13

8.2.1.1. Basal contact. The contact of the Hogarth Member with the underlying tonalite is well-exposed at the eastern end of Locality 1 (Supplemental Fig. S3). The siliciclastic Wagita Member which overlies the tonalite can be up to 150 m thick (Wilks and Nisbet, 1988), but here it is virtually absent and only represented by 80 cm of coarse sandstone derived from the underlying tonalite. This is overlain by Hogarth limestone with thin sandy layers and small rounded tonalite pebbles. The irregularly eroded tonalite has at least 10 m of original relief. Units 1 and 2 (total 15 m) are lateral to the tonalite hill. In the descriptions below, thicknesses 'above the tonalite' refer to thickness above the lowest level of the Hogarth bedded limestone in the hollows of the eroded tonalite.

8.2.1.2. Unit 1. 10 m. Thin (3–4 cm) sandstone layers and small rounded tonalite pebbles are present within the basal limestone (Sample 8-20, limestone with siliciclastic debris). Thin (~15 cm) laterally impersistent crinkly stromatolitic horizons of low domes (*Stratifera*-like of Wilks and Nisbet, 1988) occur within the basal interval, ~1.5 m above the tonalite, in thinly (mm to a few cm) layered pale gray limestones. In the upper part of Unit 1, ~10 m above the lowest level of tonalite and level with the top of the buried tonalite hill, there is a well-preserved stromatolite biostrome up to 30 cm thick (Fig. 6). It is composed of low domes ~5 cm across with well-defined moderately irregular, often enveloping, layering mostly 1–5 mm thick, picked out by brown Fe-carbonate layers (*Cryptozoon walcotti* of Wilks and Nisbet, 1988). There is ~20 cm of original relief on the well-defined steep sided margins of these thin biostromes, adjacent to channel-like depressions, although some tectonic folding complicates their structure. Sample 8-21: 6.9 m above base of Unit 1, thin-bedded pale and gray limestone.

8.2.1.3. Unit 2. 5 m. Limestone that becomes sandy as it approaches the tonalite at the top of the buried hill.

8.2.1.4. Units 3–12. 49 m. The remainder of the unaltered succession is pale to mid-gray thinly bedded limestone with occasional thin (mostly <0.5 m) layers of small (decimetric) domical and columnar stromatolites and rare horizons of radial crystal fans, well-exposed on mostly glaciated surfaces. The limestone and stromatolites contain layers of brown Fe-carbonate, and are cross-cut by numerous veins and patches of

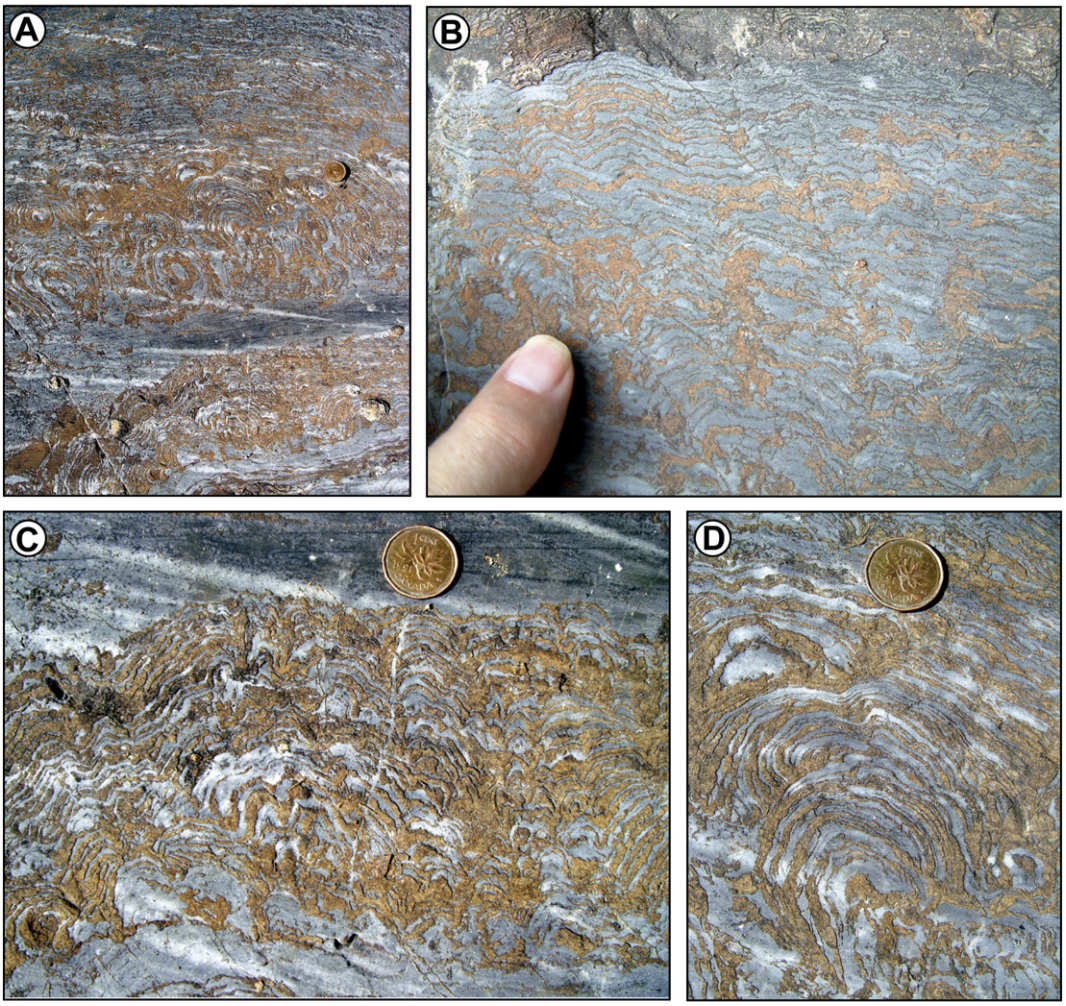

Fig. 6. Hogarth Member, Locality 1. Well-preserved stromatolites in the upper part of Unit 1, ~10 m above the lowest level of tonalite and level with the top of the buried tonalite hill (see Fig. 5). A) Domal-stratiform biostrome with laterally linked centimetric domes. B) Crinkly stratiform stromatolite associated with low domes. C) Layering accentuated by alternations of gray calcite and brown ferroan dolomite (ankerite). D) Enveloping laminae in successive domal forms. Coin diameter 19 mm.

similar material. Sample 8-24: from Unit 4, 23 m above base of section, laminated dark gray limestone (Sample 8-24A) with white calcite filled vugs (Sample 8-24B). In Unit 5, ~24.5–32.5 m above the tonalite, small stromatolite domes with millimetric layering mainly composed of dense mid-pale gray limestone, locally picked out by Fe-carbonate laminae, are common. Unit 6 contains laterally persistent centimetric beds of flat layered gray limestone showing bed disruption and intertonguing that may be synsedimentary. Unit 7 occurs 37–40.5 m above the tonalite. Small obliquely oriented, laterally linked stromatolite columns (2–3 cm wide, 10 cm high) that may reflect current influence

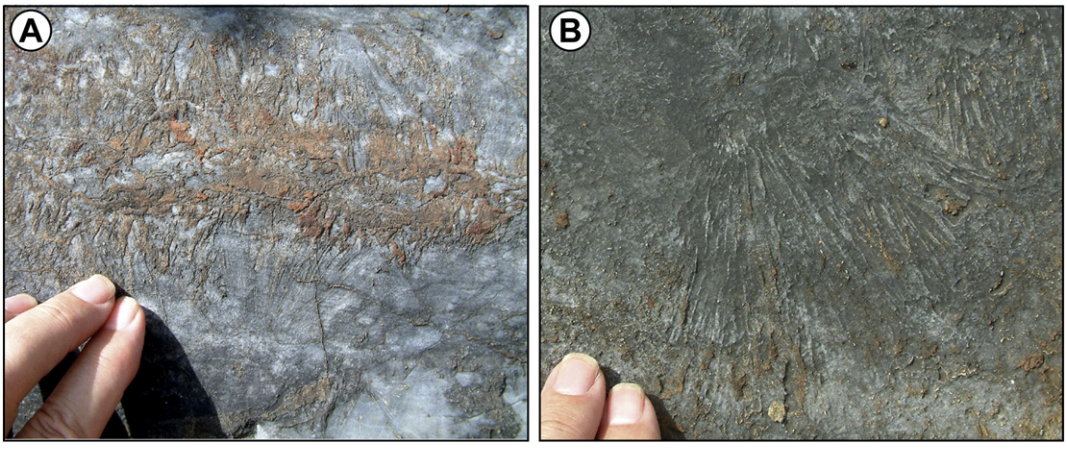

Fig. 7. Atikokania, Hogarth Member, Locality 1. A) Partly hematized decimetric horizon of mostly upward oriented radial clusters of narrow crystals, 2 m above base Unit 7. B) Similar radial crystals, mostly downward oriented, near base of Unit 7.

occur at the base of Unit 7. Masses (~5–15 cm across) and decimetric layers of radiating crystals (atikokania, Fig. 7) occur in the mid-part of Unit 7. Locally they face downwards (as noted by Wilks and Nisbet, 1988, p. 378) (Fig. 7B). Units 8–12 (40.5–64 m above the tonalite) are variably exposed and consist of parallel layered Fe-carbonate-rich limestones, some of which may be grainy, that locally show lunate structures somewhat resembling cuspate fenestrae. At the base of Unit 8 (40.5 m above the tonalite) an ~25 cm bed of narrow (3 cm) stromatolite columns is largely composed of Fe-rich dolomite and passes upwards into laterally linked wavy Fe-rich dolomite layers. The remainder of Unit 8 is composed of horizontally laminated limestone. Sample 8-28 from Unit 9 at 50 m above the tonalite, appears to be grainstone. A thin (20 cm) band of columnar and pseudocolumnar stromatolites (Fig. 8) is exposed some tens of meters to the north of the main glaciated outcrop. The columns, closely juxtaposed and locally laterally linked, are ~4 cm wide and up to 10 cm long, with crinkly laminae picked out by Fe-carbonate. This horizon is probably laterally equivalent to part of Unit 11. The stromatolites generally resemble those at the base of Unit 8, and also the well-preserved loose samples collected nearby: Sample 8-43, columnar stromatolite, loose at foot of slope; Sample 8-44, loose, 0.5 km to the north (Fig. 9). Units 11–12 (56–64 m above the tonalite) pass laterally into a zone of sharply bounded, cross-cutting altered limestone (Unit 13).

8.2.1.5. Unit 13. ~60–70 m of brown altered (presumably upper Hogarth Member), iron-replaced limestone; variably layered, massive, cavernous and brecciated and penetrated by doleritic dykes. Its abrupt irregular contacts cross-cut Units 11 and 12 below and Unit 14 above. This thick altered zone intervenes between the well-preserved limestones of Units 1–12 (Locality 1) and Unit 14 (Supplemental Fig. 2), which is at the base of the section at Locality 2; it could include faults that alter the apparent thickness of the succession.

8.2.2. Locality 2

On the north-west side of the hill, there is rapid transition from the altered zone (Unit 13) to Unit 14 (Fig. 10).

8.2.2.1. Unit 14. 14 m of mainly dark gray bedded limestone, locally possibly grainy and cross-bedded (Fig. 11), passing up into the lower part (Unit 15) of the Elbow Point Member. Sample 8-31, 2 m below top of Unit 14, appears to be grainstone. Sample 8-33 is from the giant domes of Unit 15.

8.3. Stratigraphic relationships — Hogarth Member section at Elbow Point (Locality 5)

The well-exposed cliff section at Locality 5 is at the top of the north face overlooking Errington Pit (Supplemental Fig. 1B). It exposes ~121 m of mid-to-upper Hogarth Member that passes up (westward) into Elbow Point Member (Fig. 12). The Hogarth is divisible into 7 units (plus two diabase dykes), consisting mainly of well-layered, dark–light banded, commonly fenestral limestones. Laminoid fenestrae that include sheet cracks are locally abundant in Units 1–2 and 5–7. Unit 3 contains smooth steep-sided domes with radial fan fabric, and Unit 4 is 10 m of weathered limestone associated with a dyke and fault whose displacement is uncertain. The section commences at the eastern end immediately above a pale green-gray diabase dyke, continues west beyond the level bench onto a scree slope above the lake, and ends to the west in a steep cliffed slope formed by the Elbow Point Member. An accessible section of the Elbow Point continues lower down the slope towards the lake, at Locality 6. The rocks strike NW–SE and generally dip at a high angle (~80°) to the south-west.

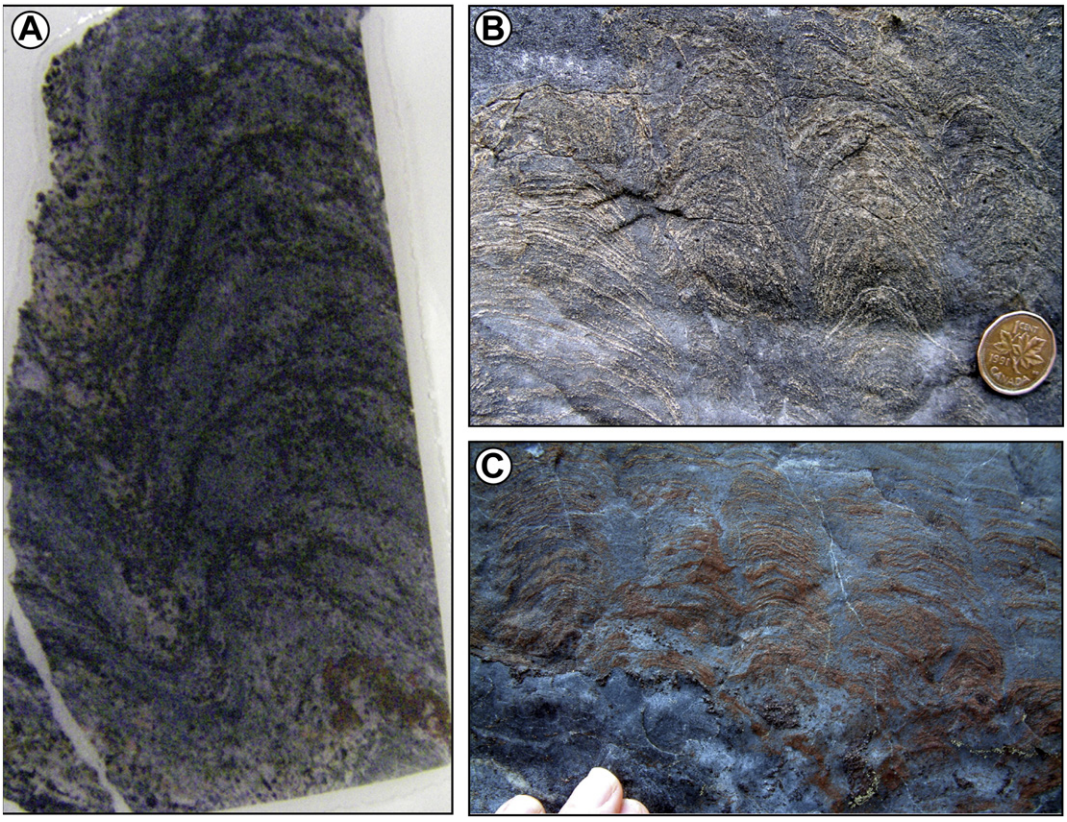

Fig. 8. Pseudocolumnar stromatolites, Hogarth Member, Unit 11, Locality 1. A) Thin section showing laminae highlighted by patchy organic carbon. Width of thin section 25 mm. B and C) Outcrop views of well-defined laterally linked columns with crinkly laminae picked out by Fe-carbonate. Locality 1, Unit 11. Coin diameter 19 mm.

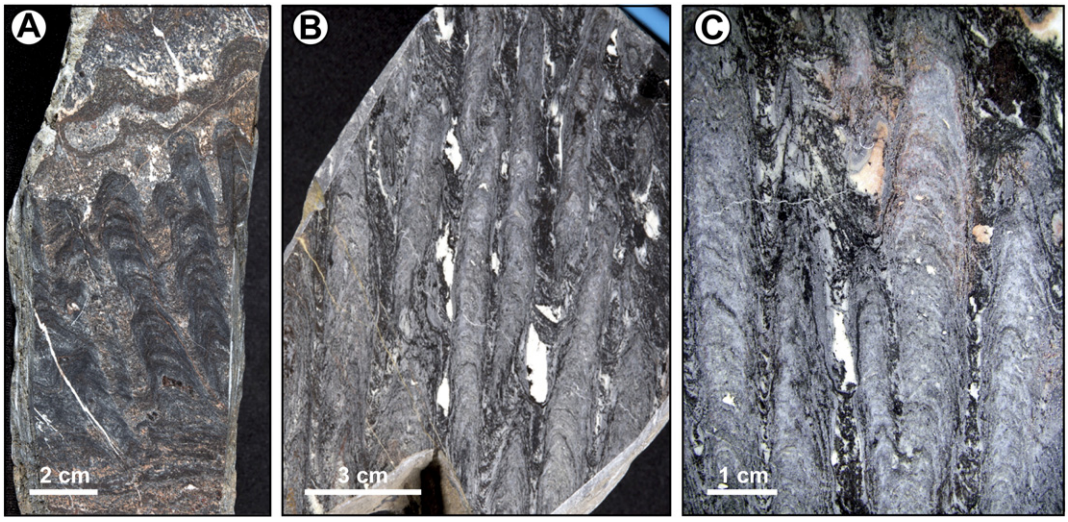

Fig. 9. Narrow columnar stromatolites, Hogarth Member, Unit 11, Locality 1. Vertical sections of columns showing bridging laminae. Most of the apparent coarse grains could be products of recrystallization. A) Shows local sub-parallel branching (loose Sample 8-43, from foot of slope). B, C) Elongate finger-like columns showing walls and sub-parallel branching (loose Sample 8.44, 0.5 km to north).

8.3.1. Unit 1

40 m, base not seen, section commences at a pale green-gray diabase dyke, dark–light cm–dm bedded limestone with locally abundant laminoid fenestrae, beds show good lateral continuity.

~6 m pale gray-green diabase dyke

8.3.2. Unit 2

9 m, as Unit 1.

8.3.3. Unit 3

15 m well layered light–dark limestone with large (0.75 m high, 1.5–2 m wide) smooth steep-sided (Ribbon Rock) domes (Fig. 13A) 2 m above base; composed of dark–light layers (Fig. 13E, F), some delicately laminated (Fig. 13C), overprinted by traces of radial fabric. 10 m above base, centimetric light layers (sheet crack fenestrae) are abundant (Fig. 14C) in complex stromatolitic macrofabrics with radial fan fabric (Fig. 14G). In the top 2 m of Unit 3, stromatolitic fabrics are well-developed, with laterally linked large and small domes with abundant fenestrae (Fig. 15A, B). Light–dark thrombolite-like mottled fabric, possibly disrupted/altered, also occurs (Fig. 16). Samples: SR-2, 2 m above base, SR-2A parallel laminated layers of dark gray possible granules and fine-grained sand, SR-2B parallel laminated possible very fine to fine-grained sand; SR-5, 10 m above base, SR-5A very dark parallel laminated limestone with small stromatolitic domes, SR-5B white blocky cement filling fenestrae.

8.3.4. Unit 4

10 m limestone with weathered surfaces associated with dyke and fault; fault displacement uncertain.

8.3.5. Unit 5

27 m well layered, thinly (cm/dm) banded, dark-gray and black limestone with abundant white spar filled fenestrae (Fig. 14). In the lower part of the unit (e.g., 4.5 to 7 m above the base) generally laminoid fenestrae make up ~30% of rock. Some are 1 cm thick sheet cracks but most are very irregular, almost hieroglyphic in shape, from 2 to 3 mm to 0.5 × 3 cm in size, with generally flatter bases than tops. They are separated by fenestra-poor bands of darker limestone, and locally are associated with Fe-carbonate layers (Fig. 14D, E). Similar fabrics are also seen in large fallen blocks at this location. The top 2 m of Unit 5 consists of 2–10 cm bands of (i) mottled fenestral fabric, (ii) pale wavy layered crusts, (iii) dark limestone with sheet cracks and/or large anastomosing fenestrae, and (iv) dark gray 'granular' limestone

Fig. 10. Upper Hogarth Member, Locality 2. Transition (marked by hat) from hematized zone (Unit 13) on left, to Unit 14 (center and right). Unit 14 consists mainly of bedded dark gray limestone, locally possibly grainy and cross-bedded (see Fig. 11), separated by darker apparently finer grained limestone. Hat 33 cm wide.

Fig. 11. Upper Hogarth Member, Locality 2, Unit 14. Limestone with lamination (black arrow) truncated by overlying lamination (red arrow), suggesting cross-stratification, possibly in grainstones. Coin diameter 19 mm.

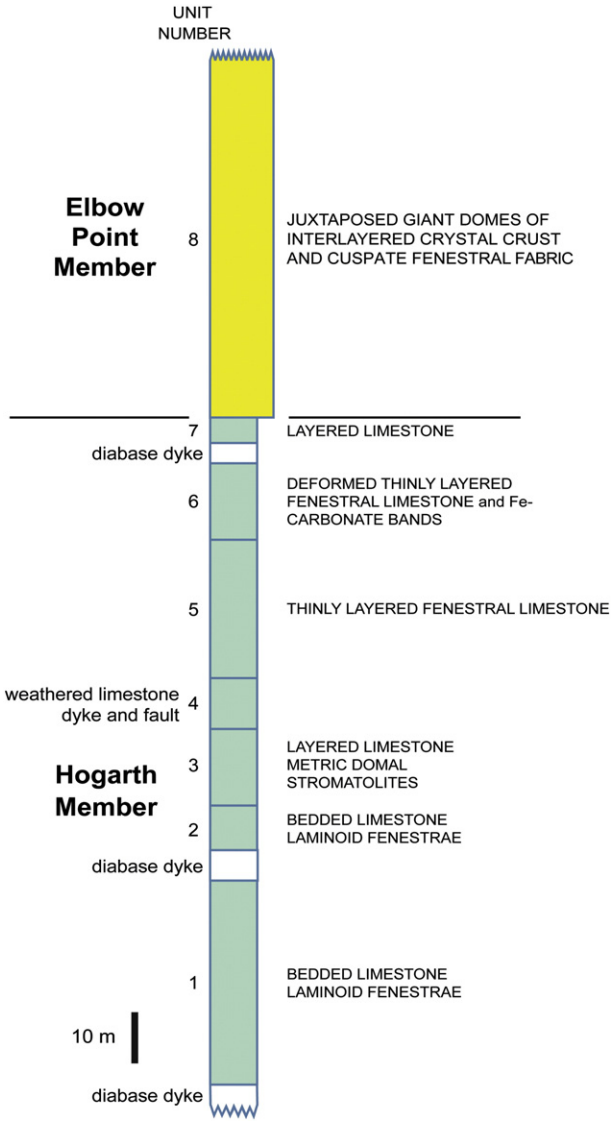

Fig. 12. Composite lithologic succession at Locality 5 (upper Hogarth Member, Units 1–7) and Locality 6 (Elbow Point Member, Unit 8). At Locality 5 the Hogarth (excluding dykes) is ~120 m thick; base not seen. At Locality 6 the Elbow Point Member is ~70 m thick; top not seen.

with dendritic crustose tops, together with numerous irregular and domical stromatolite-like laminae (Fig. 15C). Sheet cracks are common and traceable for 50 cm or more; small very irregular anastomosing fenestrae create intricate mottling (Fig. 14A). Both cracks and fenestrae can contain two cement generations. Loose samples at this locality show zebra limestone fabric. Samples: SR-7 one cm wide, sharp sided and parallel laminated dark and light layers, SR-9 50% ~3 mm thick broken and shuffled gray chips with 50% white cement.

8.3.6. Unit 6

15 m, deformed limestones similar to Unit 5, but with more Fe-carbonate bands.

Dyke, ~4 m thick.

8.3.7. Unit 7

~5 well layered dark–light limestone similar to that in the lower part of Unit 3.

The Elbow Point Member immediately overlies this, on a cliff outcrop with a steep descent to the lake. An accessible section continues below this, at Locality 6.

8.3.8. Transitional contact

Giant domes interbedded with bedded limestone at Localities 2 and 3 indicate that the contact between the Hogarth and Elbow Point members is gradational, at least locally.

8.4. Lithofacies in the Hogarth Member — Atikokania crystal fans

8.4.1. Description

Atikokania (after Atikokan town) is the name given by Walcott (1912) to Steep Rock deposits that A.C. Lawson thought might be fossils, but which are now generally regarded as synsedimentary crystalline precipitates (Fig. 7). Lawson (1912) described them as rounded or elliptical structures, 1–15 in in size, composed of rays 'that appear to radiate in all directions from a centre', 'so crowded together that they abut one against another', and locally so abundant that 'the rock is, in part, almost an aggregate of fossils'. He supposed that they might be 'the oldest forms of life as yet discovered'. He gave specimens to C.D. Walcott, who described them as cylindrical or semi-globose, with inner and outer walls united by small radial tubes and having a central cavity, and suggested they might be archaeocyaths or sponges (Walcott, 1912). Abbott (1914) compared *Atikokania* with coral-like Permian concretions in north-east England, and commented 'it seems very doubtful to me that these bodies have any organic origin'. Walcott (1914) immediately responded: 'with present information I should *not* be inclined to refer the latter [*Atikokania*] to the sponges or to the Archaeocyathinae'. Most subsequent researchers have regarded *Atikokania* as inorganic (e.g., Raymond, 1935; Glaessner, 1962; Hofmann, 1971; Swain, 2002).

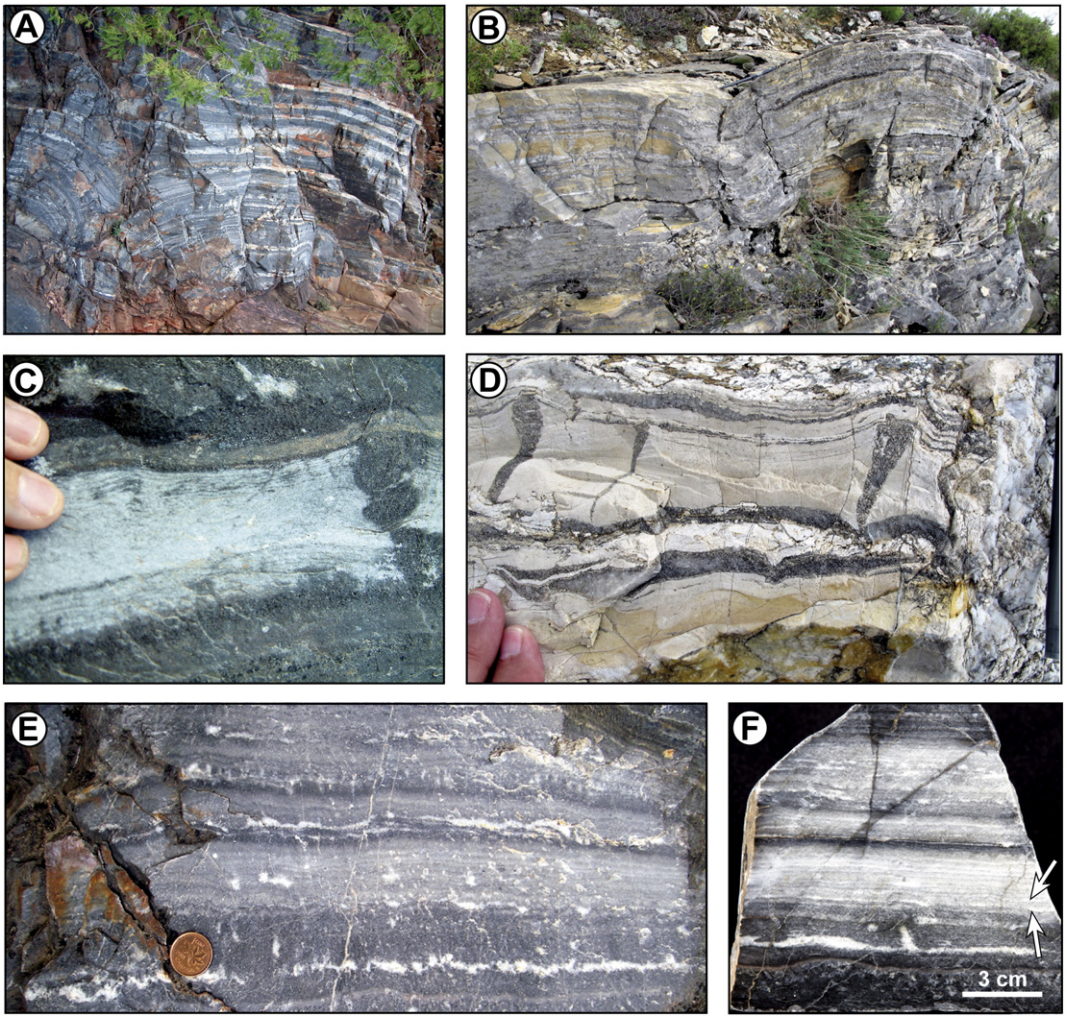

Fig. 13. A) Metric domes in banded limestone. Note large steep ended dome lower center right. Width of view 2 m (Locality 5, Hogarth Member, Unit 3). B) Similar Early Cretaceous barrel-shaped domes, Cameros Basin, 1 km west of Aguilar del Río Alhama, La Rioja, Spain; width of view 1.5 m. C) Parallel laminated limestone, with possible wave ripple lamination at its top, cut on the right by irregular crack filled with dark limestone (Locality 5, Hogarth Member, Unit 3). D) Comparable layer in the Early Cretaceous Cameros Basin, Spain. E) Banded limestone showing dark (possibly coarser) and light (possibly finer) laminated layers, both with sheet cracks and layers of fenestrae (Locality 5, Hogarth Member, Unit 3). F) Polished slab similar to E, showing laminated light and dark layers, both with sheet cracks and fenestrae (arrows indicate indistinct fenestrae).

8.4.2. Interpretation

Recognition of atikokania was probably the first discovery of the macroscopic crystal fan fabrics that can be conspicuous in Archean carbonates, and which have often been interpreted as originally gypsum or aragonite (Bertrand-Sarfati, 1976; Martin et al., 1980; Walter, 1983; Hofmann et al., 1985; Buick and Dunlop, 1990; Grotzinger and Kasting, 1993; Sumner and Grotzinger, 1996; Hofmann et al., 1999; Sumner and Grotzinger, 2000; Hardie, 2003; Shen and Buick, 2004). Downward directed structures somewhat similar to those that occur in Unit 7 at Locality 1 (Fig. 13B) were described by Grotzinger and Read (1983, fig. 1a) as cavity fills beneath peritidal tepee structures in the ~1.9 Ga Rocknest Formation. All these deposits have variously been termed seafloor cements, botryoidal fans, crystal pseudomorphs, and sparry seafloor crusts (Riding, 2008). Their interpretation is complicated because the crystals are now generally calcite, silica, or barite. Our samples of atikokania crystals from Locality 1 have high Sr and Ba values similar to those of crystal fan fabric that forms bands within giant domes in the Elbow Point Member, whereas their sulfur values are similar to those of other Steep Rock carbonate samples. These levels are consistent with a primary aragonite composition for atikokania.

Although atikokania falls within the broad category of Precambrian seafloor crystal fan fabric that ranges from millimetric veneers to thick beds of hemispherical botryoids (Grotzinger and Read, 1983; Sumner and Grotzinger, 2000; Riding, 2008), it should not be regarded as representative of all of these. Lawson (1912) described it as radial structures 1–15 in (2.5 to 38 cm) across. Since then both larger masses and also thin beds have been compared with atikokania. For example, Walcott (1914) appears to have accepted comparison of atikokania with concretions that Abbott (1914) termed 'coralloids' which have a distinctive tubiform structure. Swain (2002) figured a specimen from Rainy Lake, Minnesota, that is 40 cm across, and specimens attributed to atikokania at Red Lake, Ontario, are approximately 50 cm thick (Hofmann et al., 1985). In addition, structures (and layers) within Steep Rock giant domes (Walter, 1983), as well as single crystals within fenestral cuspate fabric (Walter, 1983, photo 8.11a) have been compared with atikokania.

We recommend restricting the name atikokania to specimens similar to those described by Lawson (1912) and Walcott (1912), i.e., globose radiating masses, some of which point down as well as up (Wilks and Nisbet, 1988, fig. 6b) (Fig. 7B). We recommend spelling atikokania uncapitalized and non-italicized, in common with general usage for sedimentary structures/deposits originally named as fossils, e.g., stromatactis. Atikokania-like crystals are not restricted to the Archean, and there are sporadic reports of similar younger examples, e.g., ~1.0–0.5 Ga (James et al., 2001, fig. 11b; Pruss et al., 2008, fig. 2d), and 250 Ma (Baud et al., 2007, fig. 4e; Kershaw et al., 2011).

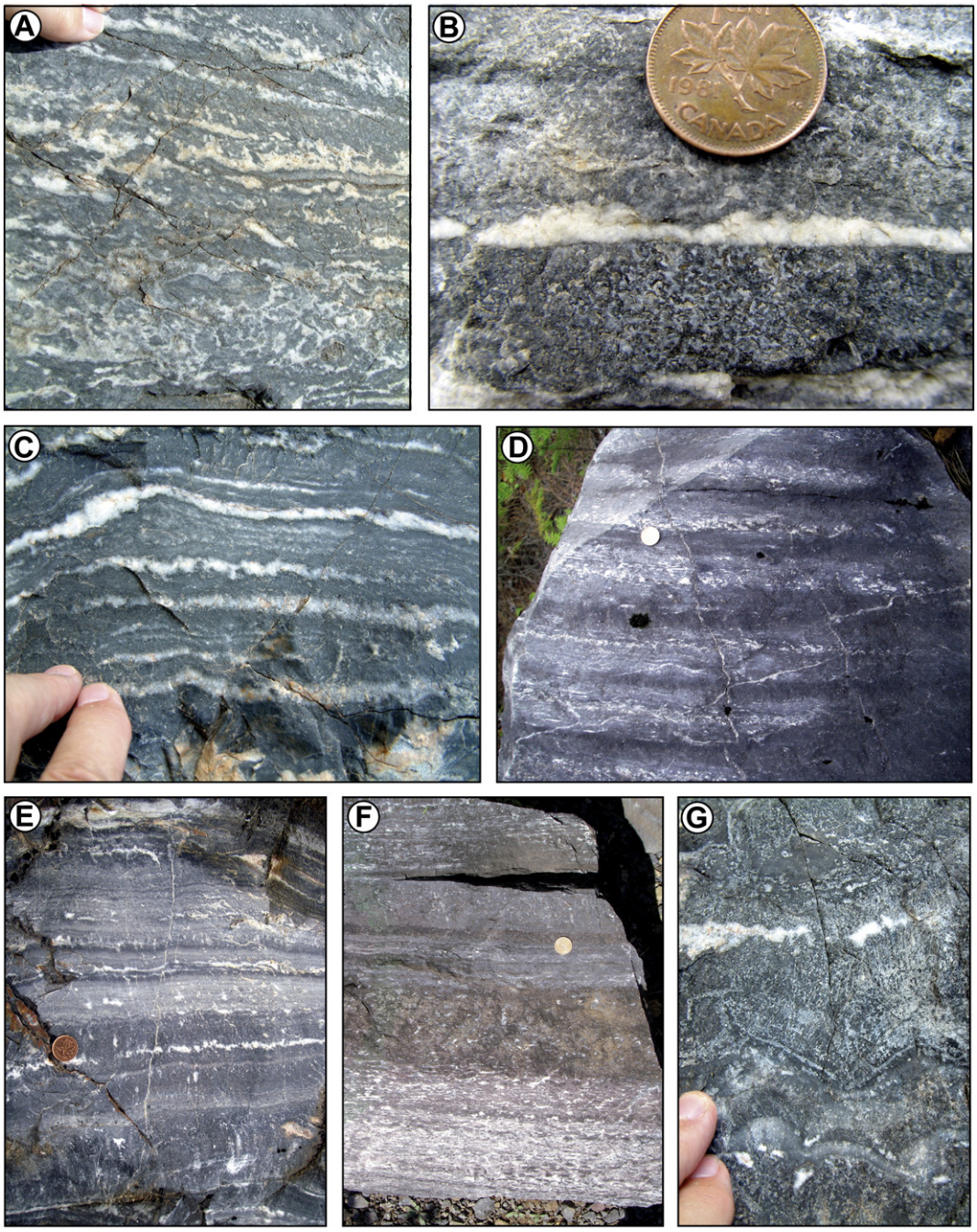

Fig. 14. Hogarth Member, All Locality 5, except D, which is from the northern extension of Locality 4. A) Extensive development of stromatactis (Unit 5). B) Close-up showing smooth base and irregular top. C) Bedding plane-parallel sheet cracks approaching zebra limestone fabric (Unit 3). D) Laterally linked irregular vugs. E) Thin, irregular stromactoid fenestrae. F) - Section showing vertical variability in amount of stromatactis. G) Radial fan fabric and laterally linked irregular vugs (Unit 3).

8.5. Lithofacies in the Hogarth Member — stromatolites

Stromatolites are commonly described according to morphotype: e.g., stratiform, pseudocolumnar, domal, conical, columnar, and branched. These terms are self-explanatory, except for pseudocolumnar (also known as columnar-lamellar), which denotes that the columns are laterally linked, whereas in columnar forms the columns are mutually isolated and in some cases have greater primary relief (Walter, 1972; Hofmann, 1973). In contrast to the giant domes of the Elbow Point Member (Section 9.1), a variety of relatively small (mostly decametric) stromatolites, including pseudocolumnar, columnar, domal and bulbous forms, occur in the Hogarth Member. These form thin (<0.5 m) horizons in the lower part (Units 1–12) of the Member at Locality 1 and in the upper part of the Member (Unit 3) at Locality 5. Stratiform stromatolites also occur near the base of the Member at Locality 1, and are probably present in thickly-developed fenestral limestones near the top of the Member (Units 5, 6) at Locality 5. Large domes of banded limestone also occur in Unit 3 at Locality 5, but their origins are uncertain. All these deposits have been somewhat affected by alteration and deformation.

8.5.1. Pseudocolumns

Juxtaposed, obliquely sloping, pseudocolumnar stromatolites form a bed ~20 cm thick at the base of Unit 7, 37 m above the tonalite, at Locality 1. These are similar to the linked domes of Wilks and Nisbet (1985, fig. 6), and to examples in the 2600 Ma Huntsman Limestone (Schopf

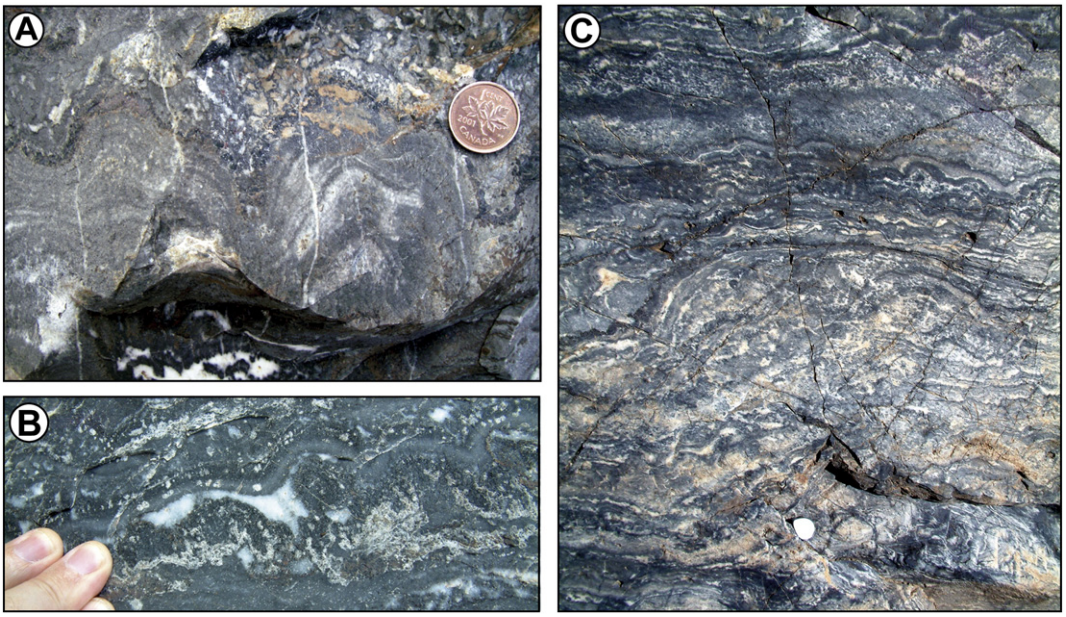

Fig. 15. Stromatolite macrofabrics, Hogarth Member, Locality 5. A) Low laterally linked domes (top of Unit 3). Coin diameter 19 mm. B) Dome-like structures with well-defined layers in fenestral limestone (Unit 3) associated with layers of radial crust (see also Fig. 14G). C) Large and small domes with abundant fenestrae (Unit 5). Hand lens 3.5 cm long.

et al., 1971). Similar pseudocolumnar–columnar stromatolites (Fig. 8) occur in a 20 cm bed within Unit 11, 56–61 m above the tonalite at Locality 1. They closely resemble an example described by Walter (1983, photo 8-12A; 1994) as a pseudocolumnar to columnar-layered stromatolite with columns up to 3 cm wide. Our columnar–pseudocolumnar sample also, although less closely, resembles that attributed to *C. walcotti* by Hofmann (1971), which shows well-laminated narrow (~5 cm) juxtaposed columns that are structurally deformed and which he described as wall-less, passively branched columns of fine-grained carbonate and silica surrounded by coarse sand. These seem less similar to the cigar-shaped stromatolites described but not figured by Wilks and Nisbet (1988) consisting of 'branching furcate columns with ragged margins. The branching is γ style (Walter, 1972). The height of these columns can reach up to 20 cm but is commonly around 10 cm.' Our specimens have laminae that are less smooth and possess lateral links across intercolumn spaces. They are broadly similar to those in the 2.7 Ga Manjeri Formation (Bickle et al., 1975, fig. 5; Martin et al., 1980, fig. 4), to pseudocolumnar 2725 Ma forms in Québec (Hofmann and Masson, 1994, fig. 4), and to small ~2.7 Ga laterally linked domes of the Ventersdorp Supergroup interpreted as lacustrine (see Altermann and Lenhardt, 2012, fig. 10b, c).

8.5.2. Bridged columns and pseudocolumns

These occur at the base of Unit 8 (Locality 1, 40.5 m above the tonalite) in an ~25 cm thick bed of columnar stromatolites passing up into laterally linked pseudocolumns, plus stratiform deposits that could also be stromatolitic. The finger-like columnar stromatolites are 1–3 cm wide and up to ~10 cm high, and have ovoid cross-sections (possibly structurally deformed) that show iron-rich dolomite cores.

Better preserved columns in a loose sample, probably derived from Unit 11 at Locality 1, have highly convex laminae turn down to vertically envelope ('wall') the column sides and then cross ('bridge') the narrow

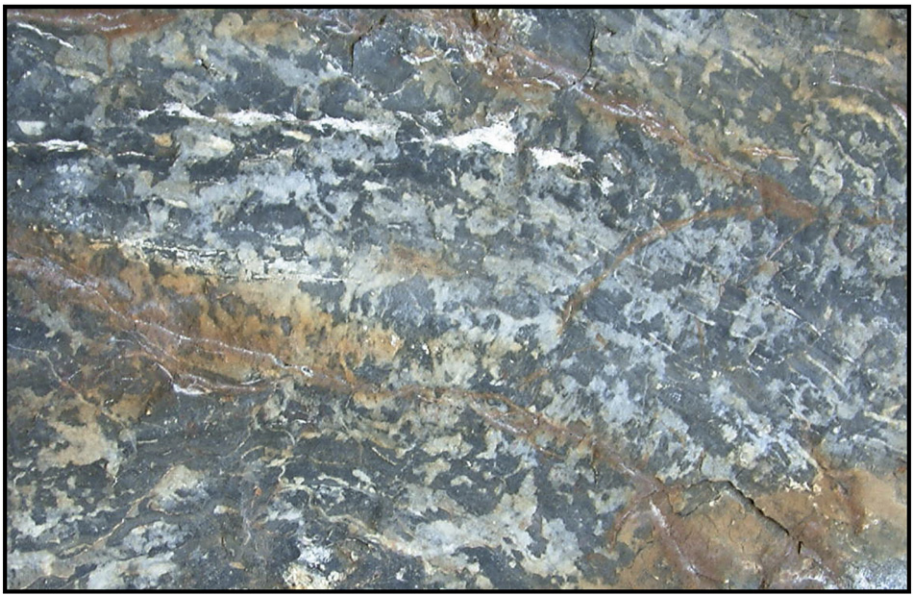

Fig. 16. Hogarth Member, Locality 5, Unit 3. Mottled thrombolite-like light–dark fabric. Stratigraphic top is up. Width of view 55 cm.

interspaces that appear to be otherwise filled by grainy material (Sample 8-43, Fig. 9A). Short passively branched (non-divergent) columns pass up into pseudocolumns. Dark gray/black moderately well-defined irregular laminae approximately 1–3 mm thick alternate with less well-defined dark gray to pink spotted layers about 1–5 mm thick. Connecting laminae (bridges) are thin and smoothly concave and, together with the steep-sided laminae that partly envelop the columns, indicate synoptic relief of at least 1–2 cm. These are the branching columnar stromatolites of Wilks and Nisbet (1985, fig. 7). They closely resemble an example from Kogelbeen, South Africa, figured by Beukes (1987, fig. 5a). Steep Rock columnar stromatolites are broadly similar to those in the 2650 Ma Cheshire Formation (Martin et al., 1980, Figs. 21, 23).

8.5.3. Walled columns

Another well preserved loose sample collected ~0.5 km north of Locality 1, has elongate narrow walled fingerlike columns, at least 15 cm long and <2 cm wide, with poorly developed alpha parallel branching (i.e., in which the width of the initial column remains unchanged), and occasional laminae crossing the narrow interspaces (Sample 8-44, Fig. 9B, C). It closely resembles the columnar walled stromatolite of Wilks and Nisbet (1985, fig. 8) that has similar geopetal cavities.

8.5.4. Domal-stratiform biostrome

A well-preserved stromatolite biostrome up to 30 cm thick occurs at the top of Unit 1 at Locality 1, near the base of the Hogarth Member and lateral to an elevation in the irregularly eroded tonalite. It consists of laterally linked centimetric to rarely decametric domes (Fig. 6A) together with ones that approach being stratiform (Fig. 6B), both of which show irregular crinkly-wavy layering picked out by brown ankerite (iron-rich dolomite) and light to dark gray calcite layers 1–5 mm thick (Fig. 6C, D). The domes are the *C. walcotti* described by Rothpletz (1916); Hofmann (1971), and Wilks and Nisbet (1985, figs. 4, 5). The well-defined steep sided margins of the biostromes have approximately 20 cm of original relief relative to adjacent channel-like depressions. Wilks and Nisbet (1985, fig. 3, 1988, fig. 7) noted that *Stratifera* with flat to undulose laminae can be traced up into *Irregularia*-like (Korolyuk, 1960) laterally linked pseudocolumns up to 2 cm high, and then into the cumulate, hemispherical, laterally linked (*Cryptozoon*) stromatolites that are 2–10 cm high and 5–15 cm in basal diameter with wavy laminae 0.5–3.5 cm thick (Wilks and Nisbet, 1988).

8.5.5. Domes

In addition to large domes of banded limestone (Section 8.5) whose origins are uncertain, stromatolitic domes occur in Unit 3 of the Hogarth Member at Locality 5 (Fig. 15). These include low laterally linked domes (Fig. 15A), and well-rounded steep sided domes. Some of these resemble domes found in the Cheshire Formation (Martin et al., 1980, fig. 19).

8.5.6. Small low coniform domes

At Locality 1, Unit 5 contains an approximately 50 cm thick horizon with decametric, laterally linked domes (about 5–10 cm wide) and stratiform stromatolites. They have 2–10 mm thick layers with moderate inheritance and a light gray marble-like appearance. Some of the laterally linked domes appear to have low, slightly coniform laminae. Wilks and Nisbet (1985, 1988) recognized 'simple, small conical' stromatolites 2–10 cm across and up to 5 cm high.

8.5.7. Stratiform stromatolites

In addition to the laterally impersistent *Stratifera*-like crinkly layers up to approximately 15 cm thick in the basal Hogarth Member at Locality 1 (Wilks and Nisbet, 1988) (top of Fig. 12B; cf. Martin et al., 1980, fig. 12), thick stratiform fenestral layers associated with domes in Unit 5 at Locality 5 also appear stromatolitic (Fig. 15C).

8.5.8. Stromatolite names and morphotypes

Linnean-type names that have been applied widely to Proterozoic stromatolites have also been used at Steep Rock. These include *Irregularia*, *Stratifera*, and variants of *Cryptozoon* (e.g., *Cryptozoan*) (Hofmann, 1971; Wilks and Nisbet, 1985, 1988). *Cryptozoön* (Hall, 1883) was originally applied to inflated Late Cambrian domes ~50 cm across in New York State. *Stratifera* was first described by Korolyuk (1959) from the Early Cambrian of Siberia, and describes essentially planar-laminated stratiform stromatolites whose laminae can be topographically complex in detail. Forms (morphospecies) of *Stratifera* may have restricted stratigraphic distribution (e.g., Semikhatov and Raaben, 2000) but as a whole the group probably has the widest spatial and temporal distribution of all stromatolites and has been equated with Aitken's (1967) term cryptalgalaminite (Walter, 1972). *Irregularia*, described by Korolyuk (1960), is also stratiform. It is distinguished by having laterally linked pseudocolumns (but also see Krylov, 1976).

Stromatolite morphology has long been thought to reflect both biotic and environmental factors (Fenton and Fenton, 1933; Rezak, 1957; Logan et al., 1964; Hoffman, 1967; Serebryakov, 1976), and the effects of both can be emphasized in very shallow-water environments where physical and chemical gradients are steep (Hoffman, 1976a). In Proterozoic platform interiors, low relief columns and sheets of microstromatolites can occur in very shallow environments, commonly in cyclic arrangements of small laterally linked domes and pseudocolumns, together with stratiform stromatolites; in slightly deeper water they are replaced at the platform margin by bioherms of columnar to domal forms that can be very large (Hoffman, 1976b; Grotzinger, 1989, Fig. 16a). Similar patterns are seen in late Archean platforms (Beukes, 1987). However, confident interpretation of individual morphotypes within this spectrum often remains difficult with regard to factors such as depth, water movement and sedimentation, and also biotic controls (e.g., Beukes and Lowe, 1989; Grotzinger and Knoll, 1999; Murphy and Sumner, 2008; Planavsky and Grey, 2008). The succession of stratiform to domal stromatolites noted by Wilks and Nisbet (1985) near the base of the Hogarth Member, especially apparent at Locality 1, could reflect a deepening trend in the initial stage of flooding of the platform. The walled columnar stromatolites slightly higher in the sequence (Wilks and Nisbet, 1985, Fig. 8) (Fig. 9B, C) commonly show synoptic relief of at least 5 cm. Their narrow columns and ability to outpace ambient sediment accumulation indicate relatively rapid accretion and suggest pervasive early lithification.

8.6. Lithofacies in the Hogarth Member — fenestrae

In addition to cuspate fenestral fabric, sheet cracks and closely-spaced vugs aligned parallel to bedding are present in the Hogarth Member (Figs. 13, 14). These fenestrae are conspicuous in the better preserved upper part of the sequence at Locality 5, but fenestrae may also be present in the lower part of the Hogarth Member at Locality 1 (Wilks and Nisbet, 1988, fig. 7). Laminoid fenestrae are common in Unit 3 and Unit 5 at Locality 5. They are thin (mm to a few cm) vugs or sheets of sparry calcite up to >50 cm long, apparently in fine-grained matrix. They range from thin but extensive stromatactis with relatively smooth bases and very irregular festooned tops (Fig. 14A, B), to bedding-plane parallel sheet cracks, locally sufficiently closely spaced to produce zebra limestone ('limestone banded by parallel sheet cracks', Fischer, 1964) (Fig. 14C) and laterally linked irregular vugs (Fig. 14D–G). So far as we are aware, these are the oldest examples of sheet cracks and stromatactis so far reported.

8.6.1. Interpretation

Bedding-parallel arrangement and local development of complex irregular upper surfaces (stromatactis), suggest that these laminoid sheet-like fenestrae are essentially synsedimentary. A wide variety of synsedimentary origins has been suggested for these types of fenestrae, including settling from suspension and mud slurries (Schofield and

Keen, 1929; Hladil, 2005); desiccation and early lithification, e.g., in microbial mats (Ham, 1952; Fischer, 1964) and tidal flats (Shinn, 1968; Grover and Read, 1978); gas escape (including methane from gas hydrates, Peckmann et al., 2002) and/or dewatering and sediment collapse (Schäfer, 1954; Cloud, 1960; Fischer, 1964; Furniss et al., 1998); organic decay (Lees, 1964; Cloud et al., 1974); sediment slumping (Bourque and Boulvain, 1993); seismic shocks (Pratt, 1995); and fluid overpressure (Corkeron, 2007; Hoffman and Macdonald, 2010). Despite the large age-difference, some Steep Rock fenestrae closely resemble Devonian examples of stromatactis (e.g., Hladil, 2005). Examples in Unit 5 at Locality 5, near the top of the Hogarth Member (e.g., Fig. 14A), closely resemble the 'stratified stromatolite with laminoid fenestrae' that cap 2–6 m cycles in Campbellrand Kogelbeen lagoon sediments (Beukes, 1987, figs. 4c, 5c) (see also Bishop and Sumner, 2006, fig. 4e), and can reasonably be similarly interpreted.

8.7. Lithofacies in the Hogarth Member — banded limestone

This distinctive lithotype typically consists of well-defined alternations of darker and light gray limestone layers approximately 2–10 cm thick, some of which can be traced laterally for tens of meters. The macrofabric appears fine-grained but this cannot be confirmed due to microfabric recrystallization. We have not indubitably observed either coarse-grains or cross-bedding in these rocks. The darker layers may originally have been coarser than the light ones (see interpretation, below). In Unit 3 at Locality 5 this lithology forms broad, smooth, locally steep-sided domes, up to 0.75 m high and 1.5–2 m wide, here termed banded limestone domes (Fig. 13A). These contain sheet-like fenestrae (Fig. 14C). The pale layers are locally broken by narrow sub-vertical cracks filled by darker limestone, a few centimeters wide, that penetrate part or all of the bed and in which the light layer often has irregular margins (Fig. 13C).

8.7.1. Interpretation

The banded limestone somewhat resembles ribbon limestone (Taylor and Cook, 1976), ribbon carbonate (Pfeil and Read, 1980) and ribbon rock (Demicco, 1983), in the Late Cambrian of Laurentia, which consists of centimetric alternations of carbonate sand-silt ripples, draped by selectively dolomitized carbonate mud. Ribbon rock commonly exhibits scour and fill structures, cracks and soft-sediment deformation, and is interpreted as a low to moderate current energy deposit in shallow subtidal to intertidal environments. The cracks could be dewatering structures, although Cowan and James (1993) termed similar, although often narrower, disruption structures in Cambrian carbonate mudstone 'diastasis' cracks, attributing them to differential compaction that produced cracks in layers of stiff mud (dolomitic mudstone) interbedded with sand (peloid grainstone). Sumner (2002) interpreted ribbon rock with diastasis features in Neoarchean Campbellrand carbonates as 'fine-grained (silt-sized?)' sediment. Bishop and Sumner (2006) describe thinly (mm/cm) bedded ribbon rock composed of alternations of carbonate-quartz silts with shales in the Neoarchean Monteville Formation at the base of the Campbellrand Platform. At Steep Rock, locally disrupted light carbonate layers superficially closely resemble present-day siliciclastic examples illustrated by Demicco (1983, fig. 7b), and also contain sheet cracks. This could indicate that light layers in the banded limestone at Steep Rock are finer than the dark ones. If some of the Hogarth Member lithotypes are as fine-grained as they appear, then they could represent water-column precipitated carbonate mud. So far as we are aware, banded limestone domes have not been described before. These Steep Rock examples closely resemble the lithotype that forms barrel-shaped domes (Fig. 13B, D) in Early Cretaceous lacustrine limestones of the Cameros Basin, Spain. Their origin is also uncertain. Some Hogarth Member lithotypes have mat-like parallel lamination (Fig. 13C). Banded limestone domes remain enigmatic. Lehrmann et al. (2001) report Early Triassic ribbon rock; noting that it had otherwise disappeared from carbonates since the Early Paleozoic, they regarded it as an 'Anachronistic Facies'.

8.8. Lithofacies in the Hogarth Member — carbonate sands

The upper (non-hematized) part of the Hogarth Member at Localities 1–2 (Units 11–12 and 14, Fig. 5) is composed of mostly 5 to 40 cm thick laterally continuous strata interlayered with intervals of thinly, mm to 1 cm scale, laminated darker carbonate (Fig. 10). Recrystallization has destroyed the original grain-size and sedimentary structures in these beds, but one 40 cm thick, trough cross-stratified bed erosively cuts into the underlying parallel laminated carbonate (Fig. 11).

8.8.1. Interpretation

These strata bear a resemblance to tempestites in the Paleoproterozic Gunflint Formation (Fralick, 1989). However, the lack of primary internal structure and texture, except for one bed, makes this conclusion speculative. All that can be stated is that these units could be carbonate sands separated by what originally were finer grained units possibly deposited from suspension.

9. Mosher Carbonate: Elbow Point Member

9.1. Introduction

Giant domes that dominate the Elbow Point Member provide one of the best known images of the Steep Rock limestone (Fig. 18A). The giant domes are elongate and meter-scale, with regular convex upper surfaces and always appear closely juxtaposed. The base of the Member (with domes intercalated with bedded limestone) is well seen at Localities 2 and 3 which both show relatively limited but impressive three-dimensional exposures of the domes. The thickest section of the Elbow Point Member that we encountered is at Locality 6.

Most giant domes are in the range 2–3.5 m wide and 2–6 m long, with primary relief of 0.5–1 m (Fig. 18A). They have a regularly geometric appearance with smooth steep sided outlines, dimple-patterned upper surfaces, elongate orientation, and neat angular marginal contacts. A remarkable feature is their lateral and vertical juxtaposition, apparently to the exclusion of other sediment. Closely packed domes form a continuous succession at least 70 m thick in the Elbow Point Member at Locality 6. Each giant dome is well-layered and appears to be entirely composed of regular alternations of bands of dark radial crystal fan fabric (Figs. 17C–E, 19A, B) and paler gray cuspate fenestral fabric (Fig. 19C–F), each typically 5–20 cm thick, with intervening thin brown coatings rich in Fe-carbonate (Fig. 17B). Layers of crystal fan and cuspate fenestral fabric can locally be traced unbroken from dome to dome. In other cases, in adjacent domes the angle of the layers increases until they are almost parallel, forming a sharp 'v'.

Steep Rock giant domes seem to have been first noticed when mining operations exposed large bedding plane surfaces in the upper Mosher. Jolliffe (1955) showed 'gentle domes' up to 50 ft (15 m) across at Errington Pit. Such large examples seem exceptional. Giant domes have subsequently been referred to as 'linked nodular' (Walter, 1983, photo 8-10), 'giant columnar', 'giant domal' (Wilks and Nisbet, 1985, figs. 2, 10) and 'large-scale' (Wilks and Nisbet, 1988) stromatolites, and as 'giant mound structures' (Kusky and Hudleston, 1999, fig. 6). Sumner and Grotzinger (2000) described crystal fan fabric interbedded with fenestral microbialite fabric in 'columnar stromatolites' at Steep Rock; these appear to be from within the giant domes. Giant domes are not typical stromatolites; they consist mainly of contrasting centimetric layers of cuspate fenestral fabric and crystal fan fabric. Assuming that the cuspate fenestral fabric is microbial in origin, then giant domes could be classed as hybrid stromatolites in which a microbial component alternates with essentially inorganic crystal fan fabric, although such alternations in Hybrid Crust (see Riding, 2008) are typically millimetric.

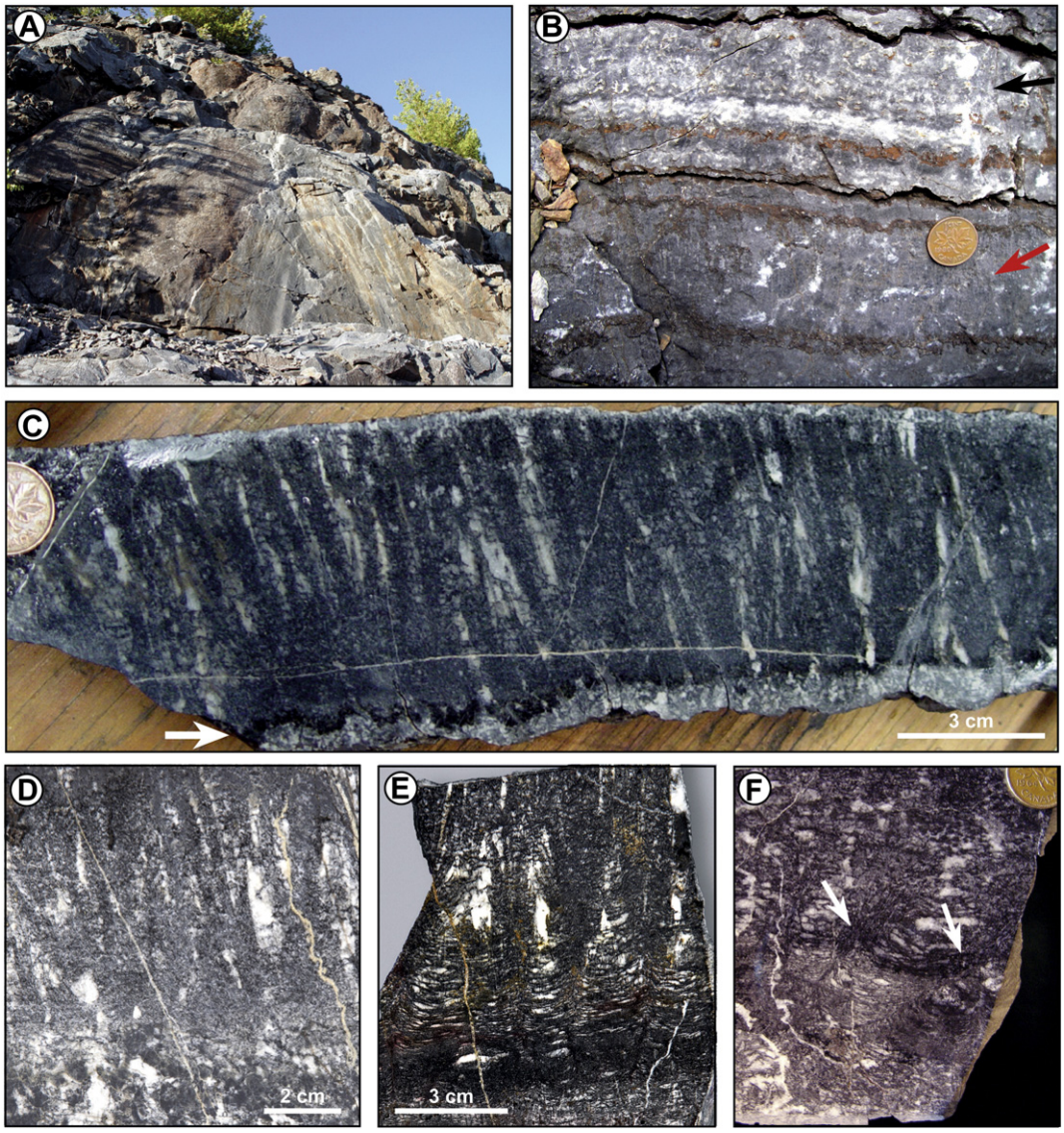

Fig. 17. Giant domes, Elbow Point Member, Locality 6. A) General view of giant dome outcrop. B) Giant domes are composed of cuspate fenestral fabric (black arrow) and crystal fan fabric (red arrow). Conspicuous iron-rich zones separate some layers. Coin diameter 19 mm. C) Slab of layer of crystal fan fabric growing from what appears to be an irregular dissolution surface with iron- and carbon-rich residue (white arrow). D) Crystal fans growing from the underlying sediment. E and F) Crystal fans nucleated on the upturned edges of the underlying cuspate fenestral fabric (white arrows on F) and also appearing to overprint the cuspate fabric. Coin diameter 19 mm.

9.2. Elbow Point Member section at Locality 2 (Hogarth Pit)

Overlooking the Middle Arm of Steep Rock Lake at Hogarth Pit, the top of the Hogarth Member is exposed immediately above the hematized unit (Unit 13) and forms Unit 14, which passes conformably up into 12 m of Elbow Point Member (Units 15–16) before the section ends at a dolerite dyke. The uppermost part of Unit 15 at Locality 2 is the much photographed surface showing the tops of several giant domes (Fig. 18A).

9.2.1. Unit 15

~10 m of meter-scale giant domes that increase in size and height through the unit. They first appear as very low arcuate beds resembling gentle folds but linked by angular depressions, by 3 m above the base of the unit the domes are ~1-3 m across, ~0.2–0.4 m high, and consist of thinly (~5–20 cm) bedded light/dark limestone with abundant laminoid to lunate rather poorly organized fenestrae ~5 mm across. At 5 m above the base of the unit the domes are ~4 m across and 1 m high. In the top 2 m of Unit 15, domes are generally 2–3 m wide, 2–6 m long, and with 1 m of original relief. The much photographed horizon in the top 2 m of the unit shows the upper surfaces of about 10 inflated steep-sided domes with well-defined parallel, somewhat en echelon orientation (Fig. 18A). The more elongate ones are depressed in the center and slightly sinuous in plan. The contacts of adjacent domes show smooth abrupt changes in angle of 100–140°. Dome surfaces have an overall smooth and very even appearance but in detail are regular patterned by small 1–1.5 cm shallow dimples. Domes are entirely constructed by well-defined beds, often 2–20 cm thick, of dark and pale gray limestone that maintain their thickness into adjoining domes. The principal lithotypes are cuspate fenestral fabric (generally mid-light gray) and sparry crust (generally dark gray to black) that commonly appears to partially overprint cuspate fenestral fabric or is intermingled with it.

9.2.2. Unit 16

2 m of bedded limestone. The sequence is cut by a dolerite dike, and then altered.

Fig. 18. A) Steeply dipping well-preserved giant domes in plan view in the lower Elbow Point Member at Locality 2. B) Cross-section through broad, low-relief domes at Locality 4. Red arrow indicates a layer of silicified crystals. Black arrow indicates one of the many prominent stylolites in this succession. These domical structures at Locality 4 could represent deformed and altered domes of either the Elbow Point Member or upper Hogarth Member. C) Smoothly layered dome at Locality 4. D) Detail of laminated fabrics that occur in the domes figured in B and C. Hand lens case is 4.5 cm long at Locality 4.

9.3. Elbow Point Member section at Locality 3

This 5 m high cliff section above a bench by the lake shows large domes exposed for 20–25 m along strike overlooking the southern end of the Middle Arm of Steep Rock Lake, near the current lake level. This outcrop includes large low domes 2–3.5 m wide and at least 4.5 m long, with 0.5 m relief. Their smooth dimpled surfaces meet at regular intersections with wide angles. The domes consist of beds 10–20 cm thick with a vertical fabric, which may be crystal fan but is much less well-preserved than at Locality 2, and has a friable granular texture. The dimples are ~1 cm in size. These large domes appear to represent part of the Elbow Point Member but, as at Locality 2, intercalated bedded limestone suggests they are in a transition zone between the Hogarth Member and the Elbow Point Member.

9.4. Elbow Point Member section at Locality 6

The lower ~70 m of the Elbow Point Member is well-exposed, often in three-dimensions, on the irregular floor of the bench and in the cliff immediately above, that overlooks Errington Pit and is located immediately below Locality 5 (Supplemental Fig. S1B). The iron ore whose extraction created Errington Pit is a massive mottled, vuggy orange-brown-gray rock with occasional hematite botryoids that borders the limestone on the south and east.

9.4.1. Unit 8

~70 m of closely juxtaposed elongate giant domes ~5 m long, 2 m wide and 1.4 m thick with their long axes oriented vertical up the cliff face. The domes lack conspicuous intervening sediment and formed against and upon one another. The well-developed banding continues from dome to dome. Their Fe-carbonate coated upper surfaces are patterned by 1–2 cm linear ridges and grooves with an elongate dimpled pattern that parallels the dome's long axis (Fig. 20A, B). Internally the domes consist of ~1–12 cm alternations of dark gray radial crystal crust and paler gray cuspate fenestrae (Figs. 17, 19). The radial fans appear to be arranged in mm/cm tufts and crusts within the bands, although these seem to be traversed by crystal needles. The radial crust has a serrate upper surface and commonly overprints the fenestral fabric, locally producing narrow vertical v-shaped clefts up to 4 mm wide and 5 cm long. Cuspate fenestrae (Figs. 17E, 19C–F) can contain short ladder-like fenestrae, 1–3 mm wide and 1–2 mm high (Fig. 17E).

Fenestral fabric locally develops a laminar appearance (Figs. 17E, 19D) and the radial fabric can develop a granular appearance.

9.4.2. Samples

SR-16A crystal fans 8 cm high; SR-16B base where 16A fans grow together; SR-18A crystal fans; SR-18B white cement from between 18A fans; SR-18C cuspate fenestral fabric underlying SR-18A fans; SR-18D dark, 2 mm thick, probably iron-rich corroded layer immediately under fans of 18A; SR-18E both crystal fans and cement; SR-22A 5 cm long crystal fans; SR-22B dark gray limestone, probably cuspate fenestral fabric above 22A; SR-22C very dark gray zone below 22A, probably fenestral cuspate fabric.

9.5. Layering

Each giant dome consists of relatively thin, even, and laterally continuous alternating layers (Fig. 18A) of crystal fan and cuspate fenestral fabric (Figs. 17, 19). Additional, presumably secondary, development of radial crystals may in places partially overprint cuspate fenestral fabric. The upper surface of the cuspate fenestral fabric is regularly patterned by small dimples that appear to occupy hollows between adjacent cusps of the cuspate fenestral fabric (Fig. 20A, B) and commonly veneered by brown stained Fe-carbonate (Fig. 20D). Crystal fan and cuspate fenestral fabric may not be entirely restricted to the Elbow Point Member. We observed thin crystal fan layers associated with stromatolites in Unit 3 at Locality 6. The ~100 m thick section at and north of Locality 4, also contains alternating layers of cuspate fenestral fabric and black crystal fan fabric; however, this sequence could be the downfaulted and somewhat altered transition from the Hogarth to Elbow Point members (see Section 10). The sections below describe crystal fan and cuspate fenestral fabric as they occur in well preserved giant domes at Localities 2 and 6.

9.6. Lithofacies in the Elbow Point Member — crystal fan fabric

This forms approximately 5–20 cm thick, dark gray to black, laterally persistent layers with variably distinct radial millimetric to centimetric tufts and crusts. Well-preserved crystal fabric can show numerous small dark sub-botryoidal radial clusters with serrated upper surfaces (Fig. 17C), locally producing narrow vertical v-shaped clefts up to 4 mm wide and 5 cm long (Fig. 17C–E) as well as larger thin penetrative crystals that partially overprint overlying cuspate fenestral layers with radial acicular fibrous fabric (Walter, 1983, photo 8-11), suggesting prolonged replacive crystal extension.

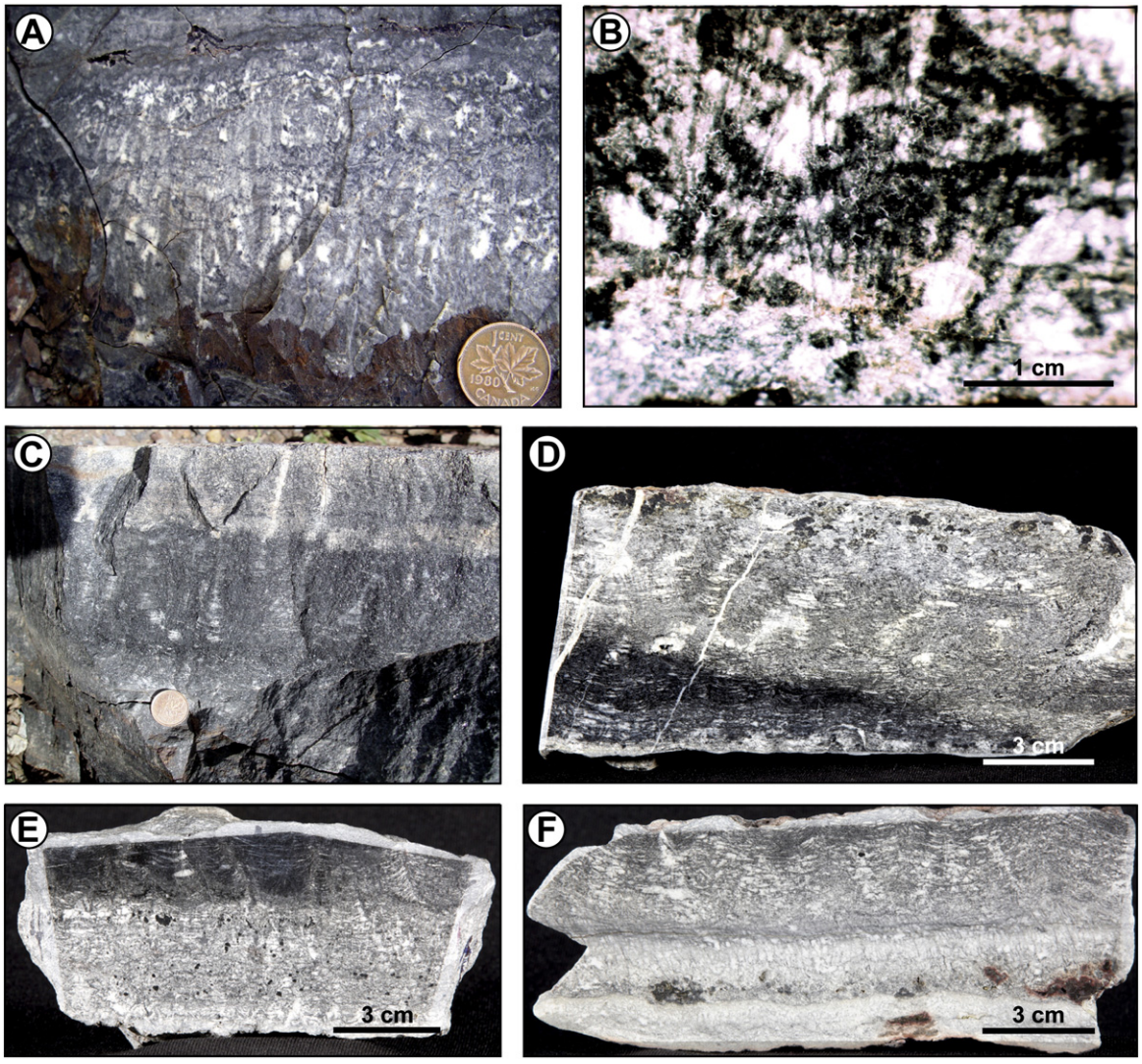

Fig. 19. Fabrics within giant dome layers, Elbow Point Member, Locality 6. A) Crystal fans growing through what appears to be laminated sediment. Coin diameter 19 mm. B) Small crystal fans with internal chevron-style arrangement. C) Dark layer of cuspate fenestral fabric shows laminated appearance that might be created by flattening of the cuspate layers. Coin diameter 19 mm. D) Polished slab of cuspate fenestral fabric. E) The lower, lighter layer has an open cuspate fenestral fabric whereas the overlying dark layer has a more compact, possibly collapsed, laminar structure. F) Polished slab showing vertical structure in the lower lighter layer, and more typical cuspate fenestral fabric in the overlying slightly darker layer.

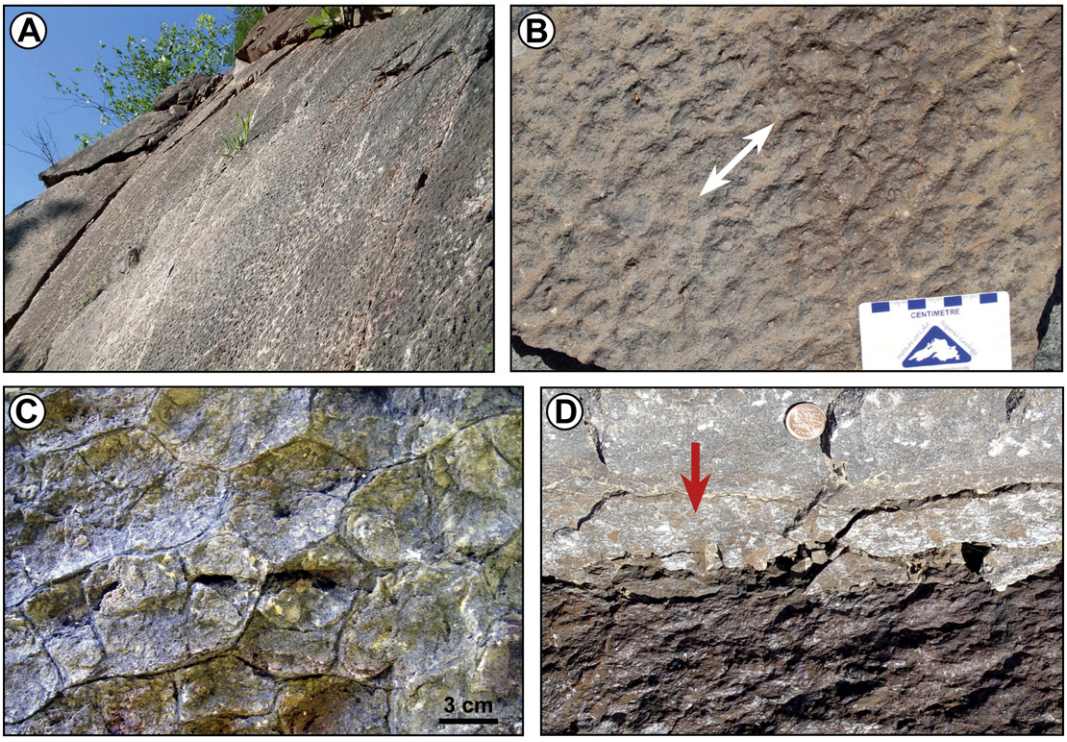

Fig. 20. A) Dimpling on the otherwise even surface of a giant dome (Elbow Point Member, Locality 3). B) Close-up of dimpled surface showing orientation of small ridges (Elbow Point Member, Locality 3). C) Desiccation-like cracks separating areas with up-turned edges on the surface of a giant dome (Elbow Point Member, Locality 2). D) Upper part: vertical section through a giant dome layer containing possible rip-up clasts of iron-rich sediment (arrow). Lower part shows the iron-rich bedding plane underlying the upper layer (Elbow Point Member, Locality 6). Coin diameter 19 mm.

Walter (1983) recognized atikokania-like structures within giant domes; he thought they could be either aragonite or gypsum and were most likely gypsum due to their size. He noted that lamination is discontinuous and only locally and crudely developed, and marked by 'wispy layers of kerogen and by closely spaced lenses of sparry calcite' which he interpreted as possibly originally gypsum. He noted 'abundant patches of sparry carbonate locally produce a "chicken-wire" texture suggestive of the disruptive growth of a sulfate mineral, although the smaller patches also resemble fenestrae' (Walter, 1983), although the example he cites is from a columnar stromatolite (Walter, 1983, photo 8-12). Kusky and Hudleston (1999) noted that giant domes 'show internal traces of recrystallized aragonite fans, suggesting that these large mounds are largely chemical precipitates'. Sumner and Grotzinger (2000) described crystal fan fabric associated with fenestral microbialite at Steep Rock, but they do not appear to have linked this association with the Giant Dome Lithofacies.

9.6.1. Interpretation

Crystal fan layers in the giant domes appear to be a type of synsedimentary seafloor carbonate precipitate, of which various kinds, differing in thickness, extent, size, crystal size, density and original mineralogy, have been described from the Archean and Paleoproterozoic. Examples include those present in the ~3.45 Ga Pilbara (Hofmann et al., 1999; Shen and Buick, 2004, Fig. 9g), 2.6 Ga Carawine and 2.9 Ga Uchi (Sumner and Grotzinger, 2000), and ~1.64 Ga McArthur Group (Winefield, 2000). These diverse seafloor crusts have variously been regarded as originally barite, gypsum or aragonite (Bertrand-Sarfati, 1976; Hardie, 2003; Sumner and Grotzinger, 1996, 2000). Crystal fan fabric in the giant domes at Steep Rock is unusual in forming relatively thin, dense and even layers (Fig. 17C). In this respect it differs from, for example, thick botryoidal domes such as those at Campbellrand (e.g., Sumner and Grotzinger, 2000) and also from less dense and more obviously crystalline masses, such as atikokania, although protruding sparry crystals can locally be seen (Fig. 19A), especially where emphasized by overlying Fe-carbonate. These, together with some delicate crystal fans in the upper part of the Hogarth Member in Unit 3 at Locality 5 (Fig. 14G), resemble radiating crystals interbedded with stromatolites in the ~2.65 Ga Cheshire Formation, that Martin et al. (1980, fig. 19) interpreted as aragonite pseudomorphs.

9.7. Lithofacies in the Elbow Point Member — cuspate fenestral fabric

9.7.1. Description

This equally prominent component of the giant domes consists of nested, flattened, lensoid, concave-up fenestrae, a few millimeters to 2 cm wide and up to 2 mm in height, delineated by thin fine-grained draping laminae, sometimes between well-defined vertical supports, arranged in wavy layers. They generate a ladder-like internal appearance and terminate upward in concave-up hollows separated by upward-pointing cusps, creating a dimpled upper surface. In well-preserved examples, crystal fans can be seen nucleated on the upturned areas of the cuspate fenestral fabric (Fig. 17E, F). Locally, what appears to be extreme flattening of the cuspate layers creates a more laminated fabric (Fig. 19C). In places, fabric resembling miniature chicken wire structure (Fig. 19F) grades into the cuspate fabric. As a result of these effects, and crystal overprinting (see above), crystal fan fabric and cuspate fenestral fabric layers can vertically blend into one-another (cf., Walter, 1983, photo 8-9b, c). The cuspate layers commonly become Fe-rich at their upper dimpled surfaces (Fig. 20D).

9.7.2. Interpretation

Fabrics similar to cuspate fenestral fabric are well-developed in 2.6–2.52 Ga Campbellrand-Malmani platform carbonates (Beukes, 1987; Sumner, 1997a; Altermann and Siegfried, 1997). These and similar Archean fabrics have been termed 'disrupted algal mat' (Malmani Dolomite, Button, 1973, 1976, fig. 3), contorted cryptalgalaminae in thin bedded carbonates associated with *Conophyton* stromatolites in carbonate slope and deep shelf deposits (Beukes, 1987, figs. 2, 10), tufted

fenestral fabric (Beukes, 1987, Fig. 10), 'net-like fenestrate' fabric in subtidal platform lagoon facies (Beukes, 1987, fig. 6), *Thesaurus* (Hofmann and Masson, 1994), thesauroid mat (Altermann and Siegfried, 1997; Wright and Altermann, 2000, fig. 3), tented/cuspate/irregular columnar microbialite and plumose structure (Sumner, 1997a), fenestrate microbialite (Sumner, 2000), and nodular fenestrate fabric (Gandin and Wright, 2007). 'Roll-up' structures, interpreted as microbial mats, occur in the ~2600 Ma Wittenoom and Carawine formations (Simonson et al., 1993, fig. 24), and at Campbellrand–Malmani (Wright and Altermann, 2000, fig. 4).

Beukes (1987) noted that 'net-like fenestrate' fabric at Campbellrand was of uncertain origin, and outlined three possibilities: gas bubbles, chicken-wire evaporite, and wispy tufted microbial mats. 1) *Bubbles*: Schopf et al. (1971, pl. 56) suggested that cuspate fenestral fabric is infilled gas bubbles. Both Walter (1983) and Sumner (1997a) considered this unlikely. Calcified bubbles in travertine range widely from spherical and elongate ('foam-rock') (Chafetz and Folk, 1984, figs. 30, 31) to irregular (Pentecost, 2005). Although some resemble the dish-shaped fenestrae in Steep Rock cuspate fenestral fabric, they are generally surrounded by much thicker layers (e.g., Chafetz and Guidry, 2003, figs. 4g, h). 2) *Evaporites*: Walter (1983) and Beukes (1987) noted similarities between cuspate fenestral fabric and evaporite fabrics, and this interpretation has been advocated by Gandin et al. (2005) and Gandin and Wright (2007) who suggested that cuspate and plumose fabrics originated by growth of nodular and enterolithic calcium sulfate. 3) *Mat/film*: Button's (1973, 1976) proposal that cuspate fenestral fabric represents calcified wispy tufted microbial mats/films was supported by Beukes (1987) using comparisons with Yellowstone cyanobacterial mats (Walter et al., 1976). As Beukes (1987) noticed, there are close similarities in size and shape between present-day Yellowstone silicified tufted cyanobacterial cones (e.g., Walter et al., 1976, fig. 19) and details of Campbellrand carbonate tufted fenestral fabric (Beukes, 1987, fig. 10b). It is possible that the 1–2 cm wide lensoid fenestrae in Beukes (1987, fig. 10a) could reflect accretion of cones with ridges and spines such as those shown in Walter et al. (1976, figs. 12–14). This approach was followed by Hofmann and Masson (1994) (see Thesaurus section) and Altermann and Siegfried (1997), and further developed in detail by Sumner (1997a, 2000). It has been linked to gliding motility and phototactis in cyanobacteria (Walter et al., 1976) although this remains to be clarified (Shepard and Sumner, 2010; Tamulonis and Kaandorp, 2014). In a very detailed study, Sumner (1997a) interpreted thin filmy laminae in the Gamohaan and Frisco formations as remnants of microbial mats and termed these diverse fabrics, composed of laminae, supports and sparry cement-filled spaces, 'fenestrate microbialite' (Sumner, 2000). Organic films could account for the strong but flexible laminae, and Sumner (1997a) suggested that they defined the fenestrae by being suspended in water between supports that could also be organic films, so that the fenestrae need not be produced by gas bubbles. Sumner (1997a) suggested mats in Antarctic lakes (see also Rivera and Sumner, 2014), Yellowstone hot springs and Laguna Mormona as possible partial present-day analogs. Bartley et al. (2014) attributed cuspate microbialites in the ~1.3 Ga Sulky Formation of northern Canada to upwardly motile filamentous bacteria that could be either cyanobacteria or sulfide-metabolizing bacteria.

9.7.3. Thesaurus

Fabrics similar to Steep Rock cuspate fenestral fabric were described by Hofmann and Masson (1994) in ~2728 Ma limestone blocks at Abitibi, Québec, as *Thesaurus*, a stromatolite originally described from the Mesoproterozoic (Vlasov, 1977), although they noted that *Thesaurus* is generally much larger. *Thesaurus* is normally grouped with the Thyssagetaceae (Vlasov, 1977), a family of *Conophyton*-like stromatolite in which the cones are laterally linked by abundant laminae that cross the intercolumnar spaces (Hofmann et al., 1991). Thyssagetacean-like stromatolites have been described over a wide time-range from the Archean (Grey, 1981; Hofmann et al., 1991; Allwood et al., 2007), mid-early Proterozoic (Vlasov, 1977; Misra and Kumar, 2005), and latest Mesoproterozoic (~1035–1005 Ma, Petrov and Semikhatov, 2001). However, it appears that few if any of these examples are constructed by the small cuspate fenestrae characteristic of cuspate fenestral fabric. For example, both *Thyssagetes* from the 2729 Ma Wawa siderite (Hofmann et al., 1991) and the cuspate swales compared with *Thesaurus* in 3430 Ma Pilbara deposits (Allwood et al., 2007) appear quite distinct from cuspate fenestral fabric.

9.7.4. Orientation

Whereas columnar stromatolites are convex-up, cuspate fenestral fabric fenestrae and laminae are usually concave-up, producing a distinctive wavy cuspate appearance (Figs. 17E, 19D–F). This can mislead hand-specimen orientation. Sumner (1997a) pointed out that specimens of Zimbabwe cuspate fenestral fabric have been figured upside-down (e.g., Macgregor, 1941; Cloud and Semikhatov, 1969, pl. 1, fig. 1; Schopf et al., 1971, pl. 56; Walter, 1983, photo 8-9a), as if they were columnar, and this was also done for a Steep Rock sample by Walter (1983, photo 8-11).

9.7.5. Comparisons

Steep Rock cuspate fenestral fabric differs from some examples of 'fenestrate' fabric, particularly those that are more coarsely fenestral, better preserved, and interbedded with laminated mat (e.g., Sumner, 2000, Figs. 2–5) rather than alternating with crystal fan layers. In well-preserved Campbellrand examples, Sumner (1997a, fig. 7) recognized several varieties of fabric: draped laminae ('tented'), nested fenestrae (cuspate) and those with more vertical supports (plumose). She inferred that the vertical supports and draped laminae probably indicated a low energy environment (Sumner, 1997b). These fenestrate fabrics generally have often been regarded as low energy/quiet water deposits (Hofmann and Masson, 1994; Murphy and Sumner, 2008). These structures have also been documented in the Campbellrand–Malmani platform, where microbialite textures and stratigraphic context also suggest a deep subtidal depositional environment with low sediment influx (Sumner, 1997b, 2000; Sumner and Grotzinger, 2004; Sumner and Beukes, 2006). In Steep Rock cuspate fenestral fabric vertical supports are often poorly defined, the fabric commonly contains numerous sub-millimetric fenestrae (Fig. 19C–F), and usually occurs in relatively thin beds interlayered with crystal fan fabric (Fig. 17B).

9.8. Giant Dome discussion

Steep Rock is unusual, not only in the diversity of its small stromatolites but also in its thick development of distinctive Giant Dome Lithofacies. Whereas Steep Rock's small stromatolites are diverse crinkly laminated domes and columns that can readily be interpreted as calcified mats, the giant domes consist of thick layers of apparently abiotic crystal fan fabric that alternate with the possible calcified microbial films of cuspate fenestral fabric. These putative abiogenic/biogenic accretions created an accumulation of up to 70 m of closely juxtaposed domes, individually up to 1 m thick, 3 m wide and 6 m long, without intervening sediment. Interpretation of cuspate fenestral fabric as calcified microbial filaments (Beukes, 1987; Hofmann and Masson, 1994; Sumner, 1997a) is the main reason for considering these large domes as stromatolites; they lack the thinner layering normally considered a diagnostic feature of stromatolites, and the crystal fan fabric appears abiotic. Giant domes therefore represent relatively unusual, thickly layered, hybrid structures.

Jolliffe (1955) compared Steep Rock stromatolites with Kona Dolomite (~2.3 Ga) examples that Twenhofel (1919) described at Marquette, Michigan. Metric domes are not uncommon in the Proterozoic; e.g., ~2.1 Ga, Nash Fork Formation (Blackwelder, 1926; Knight and Keefer, 1966; Bekker and Eriksson, 2003) and Whalen Group, Wyoming (Hofmann and Snyder, 1985; Bekker et al., 2003), ~1.9 Ga Rocknest

(Hoffman, 1973, 1980, 1989), ~1.8 Ga Mavor Formation, Tukarak Island (Ricketts and Donaldson, 1989), ~1.3 Ga Coppermine River (Donaldson, 1976), ~1.0–1.35 Ga Burovaya Formation (Petrov and Semikhatov, 2001). Large Archean domes are best known, and probably largest in the 2.5–2.6 Ga Campbellrand Group (Truswell and Eriksson, 1973; Beukes, 1987), but also occur in the 2.6 Ga Carawine Dolomite (Simonson et al., 1993) and in the ~2.6 Ga Huntsman Limestone (Sumner, 2000), as well as at Steep Rock. Crystal fan fabric and/or cuspate fenestral fabric occur in all these locations (Sumner and Grotzinger, 2000), but so far as we know they only occur as repetitive alternating layers in Steep Rock giant domes. At present it appears that interlayered cuspate fenestral fabric and thick crystal fan fabric is an essentially Neoarchean phenomenon, and that the Steep Rock Giant Dome Lithofacies is a unique example of their combined ability to create thick carbonate sequences.

9.8.1. Arrangement and orientation

Giant domes commence as low domes that enlarge and inflate upward; as in Units 14 and 15 at Locality 2 where they become up to 3 m wide and 6 m long, with 1 m of relief over a thickness of a few meters. Successive domes occupy space between lower domes. This creates a dome-dominated vertical and spatial juxtaposed en echelon arrangement that at Locality 6 generates a 70 m thick succession that appears to lack intervening sediment, either as beds or pockets, between adjacent domes. Wherever giant domes are exposed in plan-view (Localities 2, 3, 6) they show well-defined elongate orientation (Fig. 18A) that appears to be primary. Wilks and Nisbet (1988) observed that the domes are elongate perpendicular to the inferred shoreline of the Marmion Complex. We infer that the Elbow Point Member giant dome unit at Steep Rock probably represents a rimmed shelf: a shallow wave-swept platform margin where currents molded dome elongation, orientation and en echelon arrangement, possibly aligned the surface dimples (Fig. 20A, B) and removed any particulate sediment. This apparent sustained current influence created the regular juxtaposed dome-dominated sequence. Elongation normal to platform margins occurs in Paleoproterozoic stromatolites, e.g., 1.9 Ga Pethei Group (Hoffman, 1967, 1974, Fig. 8) and Mavor Formation (Ricketts, 1983, Fig. 15), and is also displayed in very large 2.52–2.59 Ga barrel-like Campbellrand domes (Knoll and Beukes, 2009, Fig. 9) that are patterned by millimetric crinkled stromatolitic bedding (Truswell and Eriksson, 1973, Figs. 3, 4).

9.8.2. Surface patterning

From a distance, giant dome surfaces appear evenly curved and smooth. In detail the upper surfaces of the cuspate fenestral fabric layers are commonly uniformly patterned by centimetric dimples, locally producing a regular lineation paralleling dome-orientation (e.g., at Localities 2, 3, 6, Fig. 20A, B). These are possibly the mammillose structures depicted by Wilks and Nisbet (1988, fig. 6a), although larger elongate stromatolites also occur rarely on the upper surfaces of domes. Patterned cusp-cone-concavity stromatolite-like structures are not uncommon in the Proterozoic (e.g., Vlasov, 1977; Misra and Kumar, 2005) and Archean (e.g., Allwood et al., 2007) but are generally relatively large (~0.2–2 m in width). The polygonal pattern on some giant dome surfaces has been compared with desiccation cracks (Walter, 1983), such as those on present-day emerged columnar stromatolites in Hamelin Pool, Shark Bay (see Playford and Cockbain, 1976, Fig. 5a) (Wilks and Nisbet, 1988). Probable, but very rare, desiccation cracked surfaces are present on the giant domes. These seem morphologically distinct from the common dimpled surfaces at Steep Rock (compare Fig. 20B, C), which is much more regular and appears to be directly related to the small dish-shaped surface depressions on the surfaces of layers of cuspate fenestral fabric. The surface dimples resemble generally better preserved dentate patterns attributed to 'tufted cryptalgal structures' (associated with the crinkled laminae described by Truswell and Eriksson, 1973, fig. 4) on the surfaces of giant Cambellrand domes (Beukes, 1987, fig. 3d, e; Altermann, 2008, Fig. 5 c-e), as well as the 'concavas' in ~2.7 Ga structures described as *Thesaurus* stromatolites at Abitibi by Hofmann and Masson (1994, fig. 3).

10. Mosher Carbonate at Locality 4 and its northern extension

Approximately 100 m of Mosher Carbonate is exposed at Locality 4 and its northern extension, south-east of Elbow Point. The stratigraphic position of this sequence is uncertain.

10.1. Locality 4

Locality 4 is a prominent steeply sloping glaciated surface (Fig. 18B) ~150 m north-east of Localities 5 and 6 (Supplemental Fig. S1B). It exposes ~20 m of thin (2–10 cm), regular layered and laterally persistent parallel banded carbonate consisting of alternations of black crystal fan and mid-gray fenestral fabric. Pale gray smoothly layered domes of cuspate fenestral stromatolites occur occasionally, together with stratiform stromatolite-like layers, with the appearance of broad low domes (Fig. 18B), that lack Fe-carbonate layers but resemble some domes in Unit 5 at Locality 1. These limestones have a strong pervasive penetrative lineation and somewhat powdery texture, developed in aggregates of quartz crystals that may represent replaced crystal crusts that were structurally rotated and aligned (Fig. 18D). Although the smoothly layered domes show relief up to 1 m (Fig. 18C) most of the original doming may have been flattened by strain (Fig. 18B).

10.2. Northern extension

A low cliff north of Locality 4, along the west side of the lower trail (Supplemental Fig. S1B), exposes ~80 m of near vertical, approx. E–W striking, limestone, consisting of thin (typically 2–3 cm) planar banded alternations of black radial fan fabric and mid-gray fenestral fabric (Fig. 21) with occasional pale gray domical to cuspate fenestral fabric. We have not recorded this section in any detail.

10.3. Position within the overall succession

The general location of the succession at Locality 4 and to its north suggests that it is mid-Mosher, and this is how it has been mapped (Shklanka, 1972; Beakhouse et al., 1996 Fig. 24). If this is correct and this succession is in-place, then it would stratigraphically underlie Localities 5 and 6. This would suggest a total of ~291 m of Mosher in the vicinity of Localities 4–6. However, Locality 4 is immediately west of a large NNE/SSW fault (Shklanka, 1972). This could account for the alteration and pervasive lineation seen at Locality 4. In addition, it is possible that the succession at Locality 4 and immediately north of it is displaced by currently unmapped faults that down-fault it from higher in the Mosher (cf. Shklanka, 1972). This is consistent with general similarities between domical lithologies at Locality 4 and those in the Elbow Point (Figs. 13A, 18A–C), and also with similarities between layered fenestral fabrics in its northern extension (Fig. 21) and in the upper Hogarth at Locality 5 (Fig. 14E). These comparisons therefore suggest that the succession at Locality 4 and its northern extension could represent altered rocks of the Hogarth-Elbow Point transition, similar to those which are much better preserved at Localities 5 and 6. If this is correct then the ~100 m thick sequence at Locality 4 and its northern extension is downfaulted (and displaced towards the north-east) from the succession at Localities 5–6.

11. Geochemical data

In a comprehensive study, Veizer et al. (1982) showed that of fifteen Archean carbonate successions they examined, Steep Rock exhibited the least post-depositional chemical alteration. Our results support this finding. On scatter-diagrams, isotopic ratios tend to plot according to lithofacies (Fig. 22). The columnar stromatolites in Fig. 22 are ferroan

Fig. 21. Detail of banded lithotype in Fig. 14D showing alternations (each typically 2–3 cm thick) of dense dark layers and of paler layers with white fenestrae resembling flattened cuspate fenestral fabric. Section north of Locality 4.

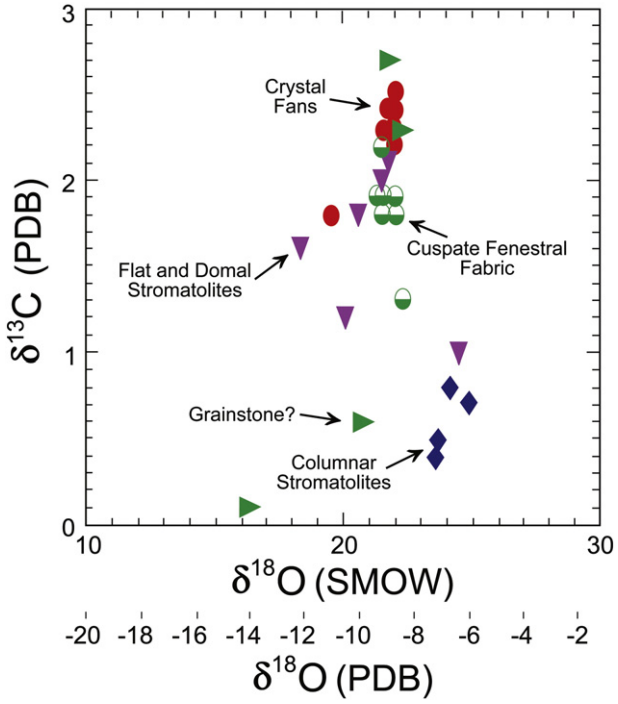

Fig. 22. Cross-plot of $\delta^{13}C$ and $\delta^{18}O$ for the 28 carbonate samples. The majority of the crystal fan samples are more enriched in heavy carbon than the layers of cuspate fenestral fabric immediately adjacent to them. One sample (8-28, grainstone?) has significantly lower $\delta^{13}C$ and $\delta^{18}O$ than the rest. It was collected near a hematite altered zone and is likely showing the effects of alteration. The siderite iron formation sample, not plotted here, has the values: $\delta^{13}C = -5.6‰$ (PDB) and $\delta^{18}O = 21.8‰$ (SMOW).

dolomite (ankerite), whereas the other lithologies, with the exception of two samples, are calcite. Dolomites formed by replacement of calcite in predominantly calcite units commonly have slightly elevated $\delta^{18}O$ and similar to slightly elevated $\delta^{13}C$ (Ray et al., 2003); a trend that is amplified during metamorphism (Sheppard and Schwarcz, 1970). The lower $\delta^{13}C$ exhibited by the Steep Rock iron-rich dolomites (ankerites) is the opposite of this trend and therefore probably original. Furthermore, the Steep Rock $\delta^{13}C$ and $\delta^{18}O$ values are similar to those from the Campbellrand (Fischer et al., 2009), Hamersley (Veizer et al., 1990), Cheshire (Abell et al., 1985a) and Mushandike (Abell et al., 1985b) platforms. Samples of different lithofacies, such as crystal fan fabric and cuspate fenestral fabric, collected 1 cm apart exhibit distinct isotopic differences (Fig. 22). Chemical alteration tends to homogenize carbonate composition via increased element mobility. Lithofacies control of isotopic composition at the centimeter scale suggests minimal post-lithification chemical alteration.

Alteration caused by highly oxidized fluids percolating downwards from the iron formation, commonly associated with brecciation, is present in the Steep Rock outcrop area. These locations are well defined due to iron enrichment producing gossan-like zones, and have relatively sharp contacts with the much more pristine surrounding carbonate. The carbonate, where samples were collected, is predominantly limestone with average atomic ratios of Ca = 48.1, Mg = 0.62, Fe = 0.31 and Mn = 0.51 (scanning electron microscope, energy dispersive spectrometer point analyses). Dolomite, with atomic ratios of Ca = 25.2, Mg = 18.8, Fe = 3.8 and Mn = 1.3, commonly composes less than four percent of the limestones. One layer, approximately two meters wide is primarily composed of dolostone, with atomic ratios of Ca = 26.5, Mg = 21.2, Fe = 1.14 and Mn = 0.81. Calcite present in this layer has atomic ratios of: Ca = 49.4, Mg = 0.26, Fe = below detection and Mn = 0.19. The low iron values are not compatible with alteration by the iron enriched fluids that formed the dissolution pathways. Also, the internal variance in these four data sets is low with the values not showing an increase in iron geographically towards major alteration pathways. This, combined with the reasons discussed in the preceding paragraph, the trace element geochemistry and Sr isotope studies of Veizer et al. (1982) and the pristine carbon isotopic signatures in both the inorganic and organic fractions reported by Nisbet et al. (2007); Kakegawa and Haikawa (2007) and Grassineau and Nisbet (2008), indicates that alteration is not significant in rock not intimately associated with the distinct alteration pathways. Difficulty in using geochemical results to investigate the chemical environment of deposition can also arise if siliciclastic material in the samples affects the measured concentrations of elements of interest in the chemical sediments. Scatterplots, pairing elements that are abundant in most siliciclastic sediment but not in chemical sediment, with elements of interest in the chemical sediment, show no correlation (Fig. 23). This indicates that the presence of very minor amounts of siliciclastic material has not significantly influenced the abundance of elements incorporated into the chemical sediments. An exception is the lowest sample of carbonate, collected from directly above the unconformity, which contained grains of tonalite-derived material.

Some elements, such as phosphorus, exhibit a broad correlation between their concentration and lithofacies. Most of the carbonate samples had concentrations of phosphate that were below detection (approximately 0.001%). The exceptions were six samples from the giant domes that had an average phosphate content of 0.003%. These very low values contrast with the iron formation (average of 0.138%), where even the chert samples had phosphate concentrations about five times more than the carbonate samples that had values above detection limits. This may reflect very efficient phosphate recycling in the carbonate precipitating environment, where most phosphate is lost from the biogenic sediment, but that trapped in crystal fan precipitates has a greater chance of not being recycled.

The controlling effect that lithofacies has on the distribution of certain elements is also apparent when the samples are plotted at their appropriate stratigraphic position (Fig. 24). At Locality 1, the graphs show increases in Sr, Ba, Y/Ho and $\delta^{13}C$ from the unconformable contact with the tonalite to the layers of atikokania (crystal fans) in Unit 7; matched by decreases in Fe, Mn and Mg. Columnar stromatolites near the base of Unit 8, which directly overlie the atikokania crystal fans, form a 1.5 m thick ferroan dolomite layer that is laterally traceable for at least 0.5 km. It represents a significant change in the composition of the

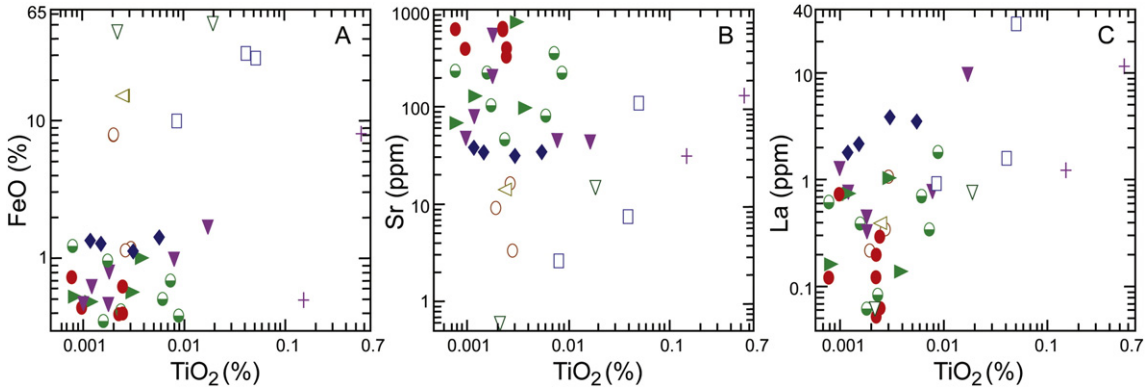

Fig. 23. Scatterplots of FeO, Sr and La concentrations against TiO_2. The TiO_2 is concentrated in the siliciclastic fraction. This is particularly evident for the two crosses, which represent carbonaceous slates interbedded with the iron formation. Correlation between FeO, Sr or La and TiO_2 would indicate that the concentration of the latter element is dependent on the siliciclastic content of the sediment and therefore will not provide information on water chemistry. However, correlation is not apparent. Note the very low abundance of TiO_2 in most samples. This reflects the isolation of the Steep Rock oceanic platform from siliciclastic sediment sources (Fralick et al., 2008). Legend for symbols is shown in Figs. 22 and 25.

Mosher Carbonate, with much lower Sr, Ba and $\delta^{13}C$, and higher Fe, Mn, Mg and Y/Ho. From this level at Locality 1 there is a gradual upward increase in Sr and Ba in what may be packstone/grainstone.

The giant domes that constitute the Elbow Point Member exhibit two trends. The crystal fan fabric layers in the domes show elevated Sr and Ba abundances and lowered Fe and Mn concentrations, whereas the cuspate fenestral fabric layers that alternate with the crystal fan fabric exhibit opposite trends with respect to these two groups of elements. This relationship can also be observed in scatter-plots and ratio-plots (Fig. 25). The partitioning of the samples into separate — albeit overlapping — areas based on their lithofacies is apparent. The samples of columnar stromatolites and iron formation show similar Ba/FeO and Sr/La ratios (Fig. 25B), although their $\delta^{13}C$ values (ankerite columnar stromatolites 0.6, siderite iron formation −5.6) are quite different. The groupings of samples belonging to discrete lithofacies progresses successively: from iron formation, to columnar stromatolites, to stratiform and domal stromatolites, to cuspate fenestral fabric and possible packstone/grainstone, and finally to crystal fan fabric, with overlap between the fields (Fig. 25B). This implies that these distinct lithofacies were deposited from water with differing chemistries.

Some aspects of the chemistry of the water from which the carbonate precipitated can be investigated by examining REE abundances, as their original pattern, reflecting the water from which they formed, is commonly retained in ancient limestones (Nothdurft et al., 2004; Kamber et al., 2004; Webb et al., 2009). Modern seawater, fresh surface water and ground water commonly exhibit a number of positive and negative anomalies (see Bolhar et al., 2004, for a brief discussion), which cause them to deviate from a flat pattern when normalized

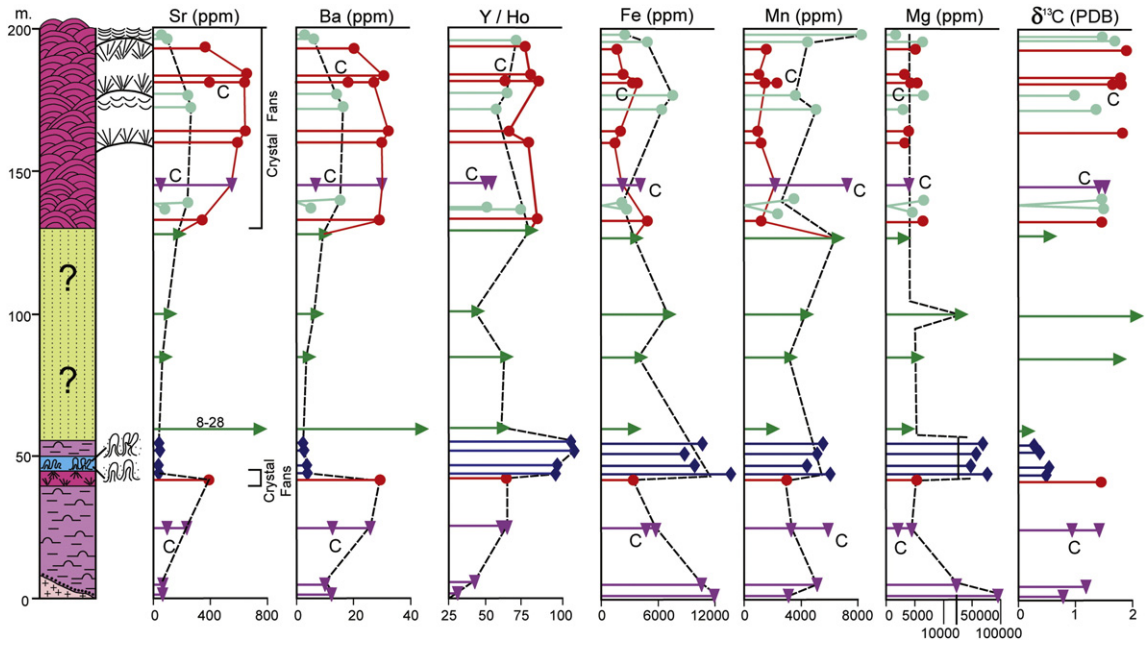

Fig. 24. Concentrations of Sr, Ba, Y/Ho, Fe, Mn, Mg and $\delta^{13}C$ through the Mosher Carbonate succession. Concentrations of Sr and Ba initially increase from the basal contact with the tonalite up to the layer of crystal fans (atikokania) in Unit 7, after which they show a marked decrease, and then a slight increase through what is probably grainstone. The upper part of the Mosher Carbonate, the giant dome-dominated Elbow Point Member (domical ornament), is similar to the lower crystal fans in having high concentrations of Sr and Ba, whereas the interlayered cuspate fenestral fabric has only moderate values for these elements. Even samples from cuspate fenestral–crystal fan pairs only 2 cm apart show this geochemical dichotomy. The Y/Ho ratio exhibits a similar pattern, except that the columnar stromatolites have high values that contrast with their low Sr and Ba values. Fe and Mn behave the opposite of Sr and Ba with low values in the crystal fans and raised concentrations in the lowermost limestone. The cuspate fenestral fabric has higher values than the interlayered crystal fans. Mg displays a similar pattern to Fe and Mn though without the dichotomy between the cuspate fenestral fabric and crystal fans. C on the diagrams represents white, blocky cement samples separated from the stromatolite and crystal fan samples. The blocky cements have lower amounts of Sr, Ba and Y/Ho ratios and higher amounts of Mn. Sample 8-28 again displays abnormal concentrations indicating alteration and is not included in the description of geochemical stratigraphic trends. Symbol legend is shown on Figs. 22 and 25.

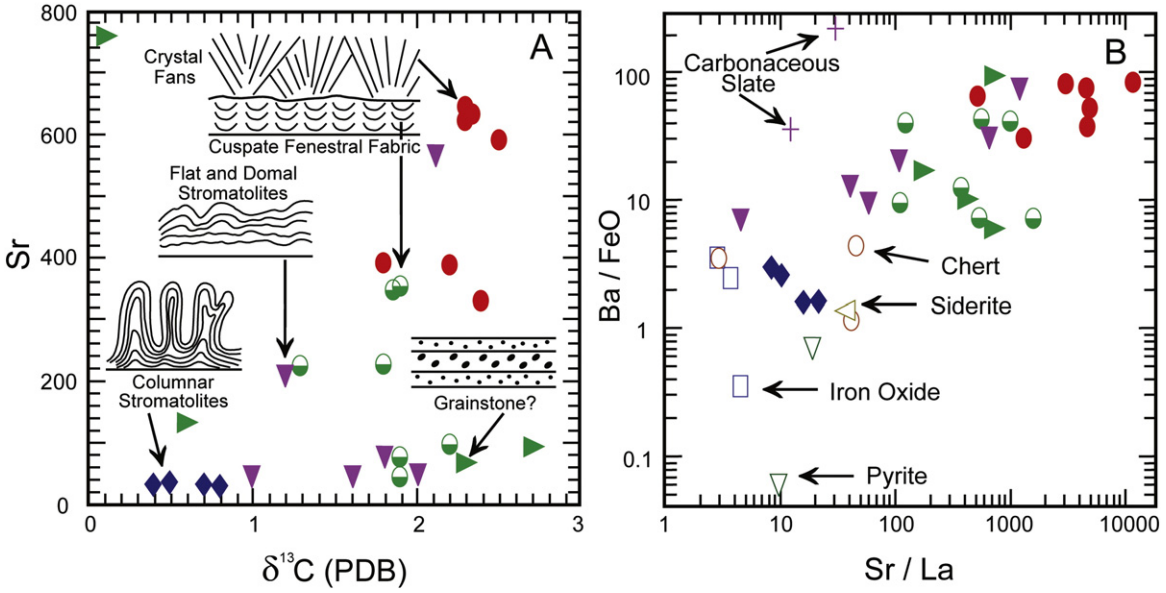

Fig. 25. Scatterplots of Sr against $\delta^{13}C$ (A) and Ba/FeO against Sr/La (B). On both diagrams the carbonate samples form arrays from the columnar stromatolites with low values to the crystal fan fabric with high values. The relationship between lithofacies and geochemistry of the samples is striking. Even though in some cases the samples of cuspate fenestral and crystal fan fabric are from layers only centimeters apart, they consistently show distinct compositions of these elements. Also of note are the columnar stromatolites plotting in the same area as the iron formation samples on B. In A, sample 8-28 (upper left corner) is outside the main sample trend, probably due to alteration of this sample.

against PAAS (Taylor and McLennan, 1985). These waters are commonly enriched in heavy REEs (Fig. 26A) (Elderfield et al., 1990), with the exception of some middle REE enrichment in low pH, fresh waters (Hannigan and Sholkovitz, 2001) that typically originate in saturated, organic-rich areas. They also commonly have negative Ce anomalies, a result of oxidation of Ce^{3+} to Ce^{4+} in the natural environment and removal of the less soluble Ce^{4+} from solution (Moffett, 1990; Sholkovitz and Schneider, 1991; DeCarlo et al., 1998). REE abundances in Archean chemical sediments, which can reflect seawater composition at that time (Barrett et al., 1988; Derry and Jacobsen, 1990; Murray et al., 1992; Alibert and McCulloch, 1993; Bau, 1993; Bau and Moller, 1993; Danielson et al., 1992; Bau and Dulski, 1996; Kamber and Webb, 2001; Kato and Nakamura, 2003; van Kranendonk et al., 2003; Bolhar et al., 2004; Klein, 2005; Planavsky et al., 2010; Bekker et al., 2010), also may have heavy REE enrichment, but commonly do not possess a negative Ce anomaly. They generally have a distinct, positive Eu anomaly, caused by extensive hydrothermal leaching of Eu from ocean crust rocks (Klinkhammer et al., 1983, 1994; Derry and Jacobsen, 1990; Danielson et al., 1992), and positive La and Gd anomalies (Kamber et al., 2004). The latter are probably the result of an empty 4f electron shell in the La atom and a half-filled 4f shell in Gd causing behavioral differences with the surrounding REEs (De Baar et al., 1985; Byrne and Kim, 1990; Kim et al., 1991; De Baar et al., 1991; Bolhar et al., 2004), though the effectiveness of this tetrad effect in creating anomalies has been disputed (McLennan, 1994).

REE spider diagrams for the iron formation samples (Fig. 27D–F) are all similar and comparable to both typical exhalative Archean iron carbonate (Fig. 27B) and modern deep-sea venting hydrothermal fluid (Fig. 27A). One chert sample has a subdued Eu anomaly and a positive Gd anomaly, but the general curve shape is similar to the other iron formation samples. The REE patterns for the carbonate samples are somewhat different than the iron formation. The former all have pronounced positive La and Gd anomalies. Most also exhibit a drop in value for the three heaviest REEs, Tm, Yb and Lu. Five of the crystal fan samples (Fig. 26B) and three of the cuspate fenestral fabric samples (Fig. 26C) also have pronounced negative Ce anomalies. Equations designed to measure the anomalies or slope when cross-plotted (Fig. 28) can provide information on REE data trends (see Bau and Dulski, 1996, for further discussion). The trends for the iron formation and carbonate samples form continuous arrays on three of the cross-plots: La* vs Ce* (Fig. 28A) (where La* = La anomaly); slope of the mid- too heavy portion of the REE patterns vs La* (Fig. 28B); and slope vrs Gd* (Fig. 28F), giving the impression that, in addition to being laterally transitional stratigraphically, they may also be transitional with respect to their REE signatures. The carbonate samples generally have higher slopes, more pronounced positive La, which may be combined with negative Ce, and lower Eu anomalies, but greater Gd anomalies.

12. Discussion

12.1. Geochemistry

Samples collected to study the geochemistry of Precambrian chemical sediments should be lithofacies specific, and their sequence stratigraphic context, depositional environment, and diagenetic/metamorphic modification understood as far as possible (Pufahl and Hiatt, 2012). This allows recognition of localized depositional trends, which commonly reflect lateral and vertical changes in water column chemistry (for examples, see Kamber and Webb, 2001; Schneiderhan et al., 2006; Allwood et al., 2010; Allwood et al., 2006; Planavsky et al., 2010; Poulton et al., 2010; Godfrey et al., 2013). The first three of these studies are particularly relevant as they apply to carbonate platform successions where both lateral and temporal changes in water chemistry are apparent from the lithofacies. Steep Rock lithofacies also exhibit striking changes in lithofacies and geochemistry both temporally, up-section (Fig. 24), and laterally from carbonate to iron formation (Figs. 25B, 28).

12.1.1. Iron formation

Lithologies in the iron formation commonly have sharp contacts and are centimeters to meters thick. Internal lamination is present in some layers, but is not always obvious. The interbedding of lithologies does not appear to follow a regular pattern. The succession was starved of siliciclastics, as indicated by the fine grain-size of the sediments, lack of obvious silt or sand, and the very high carbon content (up to 15 wt.%) of the slate layers that are present. Since it is unlikely that fine rainout of clay and dead organisms varied substantially through time, this was probably the background sediment, as in today's ocean.

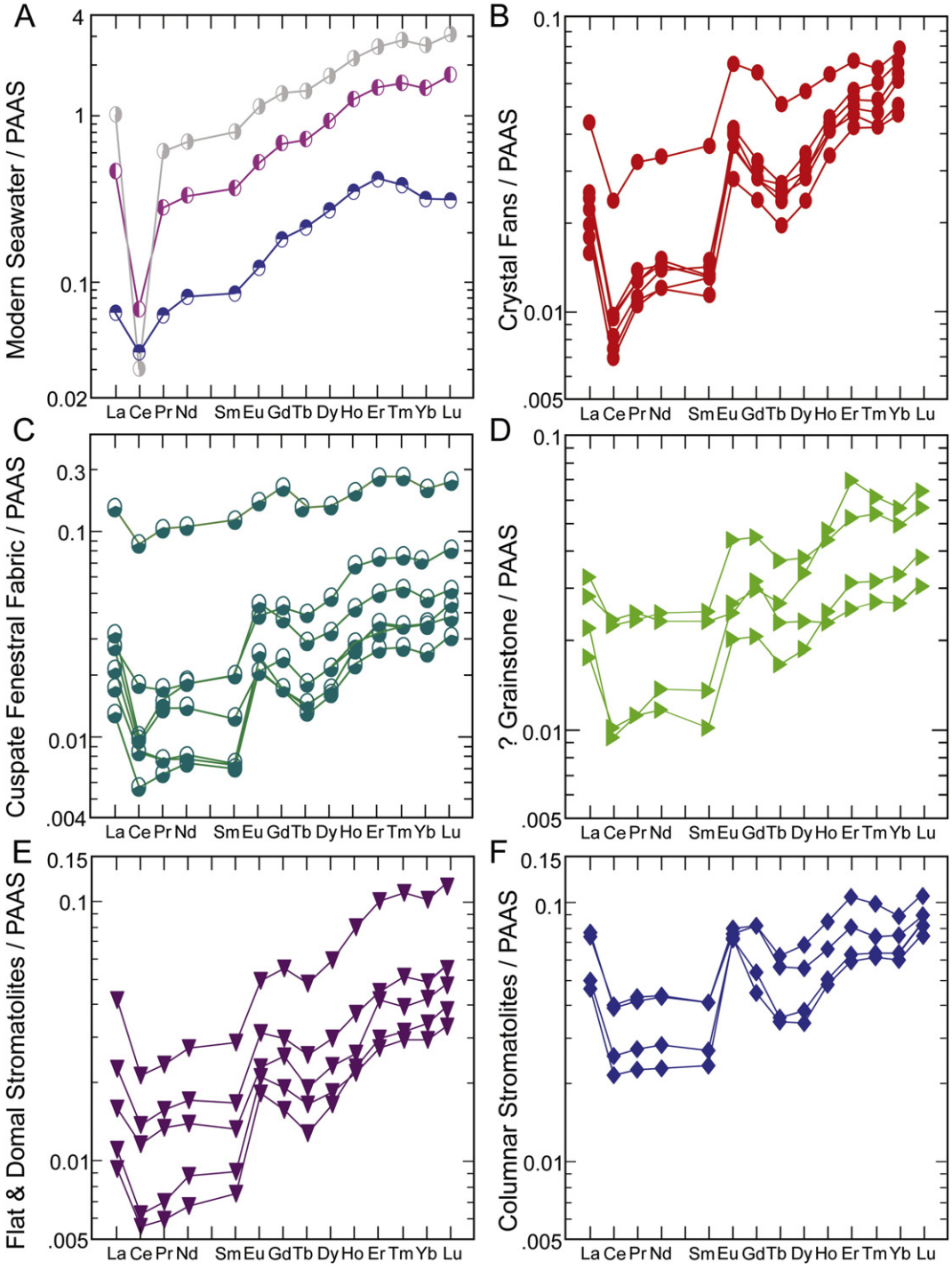

Fig. 26. Rare earth element patterns for the carbonate samples compared with modern open ocean water (A) (Zhang and Nozaki, 1996). Modern seawater patterns represent samples collected from the deep (uppermost pattern), mid-depth (middle pattern) and shallow (lowest pattern) waters of the western South Pacific (Zhang and Nozaki, 1996). Most crystal fans and some cuspate fenestral fabric have negative Ce anomalies similar to shallow seawater. The slope and most enriched HREE area in the Er region of most samples is also similar to modern shallow seawater. However, the large positive La, Eu and Gd anomalies in the carbonate samples are not representative of modern seawater. The significance of these anomalies is discussed in the text. Samples are normalized with Post Archean Australian Shale values of Taylor and McLennan (1985). The limited span of the vertical axis exaggerates deflections of the curve shape, highlighting pronounced positive Gd and Eu anomalies, distinct negative Ce anomalies, and elevated Er, and less commonly, Ho.

This highly reducing sediment, combined with the ferruginous water column and sulfur from degrading prokaryotic cells, would account for some of the pyrite present. Deposition of the chert and iron hydroxides must have fluctuated, periodically overwhelming the background clay and dead organisms. This requires changes in water column chemistry, which can only be facilitated in this system by water masses with different compositions moving into the deeper portions of the platform where chert and iron formation accumulated. This could have been accomplished by either deep oversaturated ocean water upwelling onto these portions of the platform, or oxygenated water from the shallow carbonate portion of the platform moving offshore.

The geochemistry of the magnetite, chert, pyrite and siderite in the iron formation is similar to that of other Archean iron formations (e.g., Mel'nik, 1982; Barrett et al., 1988; Danielson et al., 1992; Bau and Dulski, 1996) and consistent with formation in an anoxic environment (Pufahl and Hiatt, 2012, and references therein). The −5.6 $\delta^{13}C$

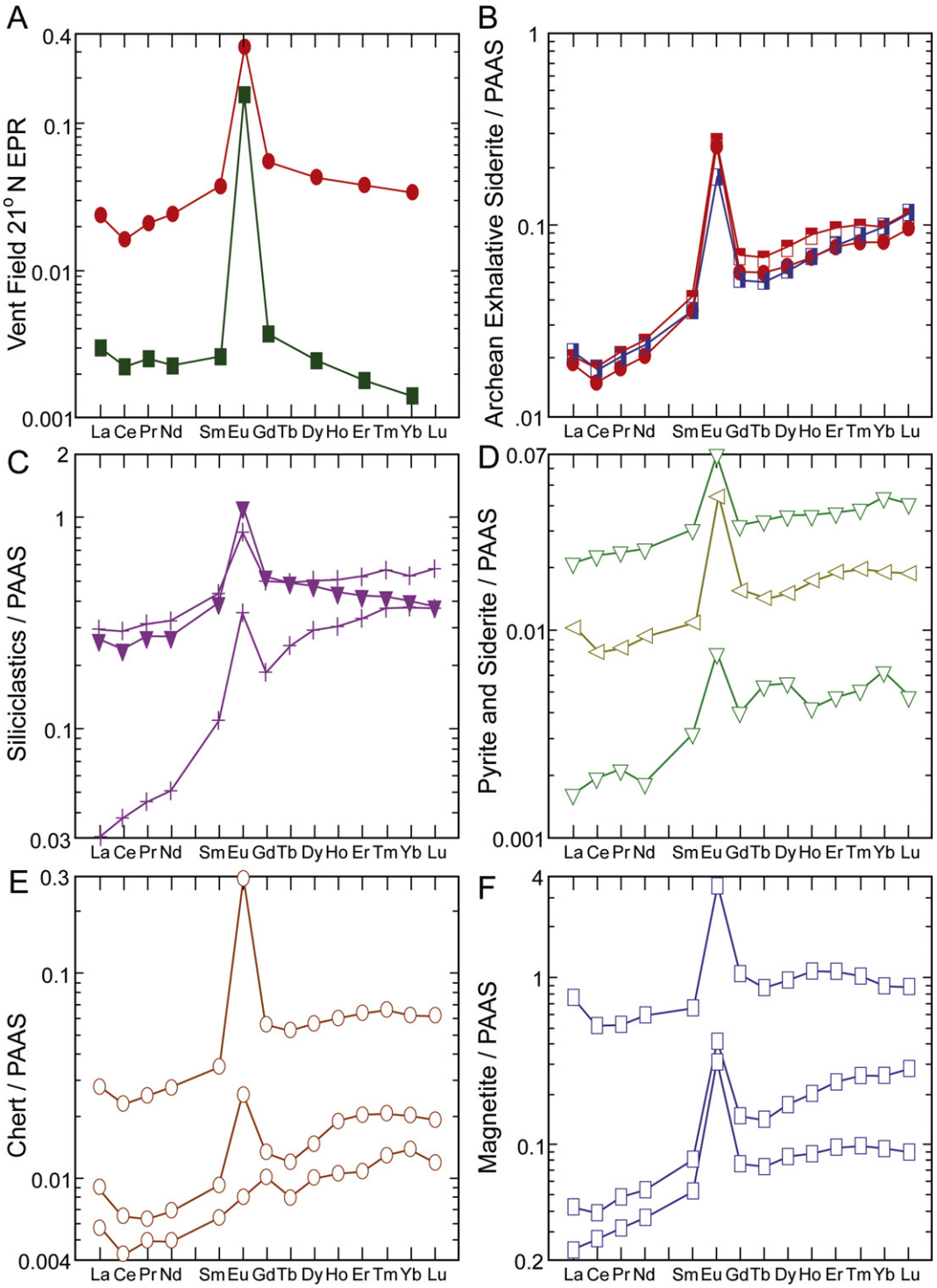

Fig. 27. Rare earth element patterns for samples associated with the iron formation, compared to modern deep seafloor vent fluids (A, lower pattern) and metalliferous sediment (A, upper pattern) (German et al., 1999), and Neoarchean interflow deep-sea siderite iron formation (B). The carbonate sample from immediately above the basal unconformity (C, triangles) is grouped with the iron formation associated carbonaceous slates (C, + symbols) as it has a large siliciclastic content. The lowermost siliciclastic sample (C) was very carbonaceous. The magnetite, siderite, pyrite and chert iron formation samples all, to varying degrees, resemble the Neoarchean deep-water hydrothermal deposits (B) and modern deep ocean hydrothermal deposits (A), except for the slope of the HREEs compared to A.

of the siderite iron formation is similar to the $\delta^{13}C$ of other iron formations associated with Archean carbonate platforms. Early work on the Brockman and Dales Gorge produced $\delta^{13}C$ of −9‰ to −11‰ (Becker and Clayton, 1972). Kaufman et al. (1990) obtained similar results, with averages at two areas of −7‰ and −10.5‰, which they attributed to deep Archean seawater with $\delta^{13}C$ of approximately −5‰, combined with further lowering of the isotopic ratio by reactions between organic carbon and iron hydroxide during diagenesis. Beukes et al. (1990), working on the Kuruman Iron Formation, reached a similar conclusion. Schneiderhan et al. (2006), investigating younger strata in the Transvaal Supergroup found that $\delta^{13}C$ increased from values as low as −18‰ in the iron formation to −1‰ in the overlying dolostone. Systematic

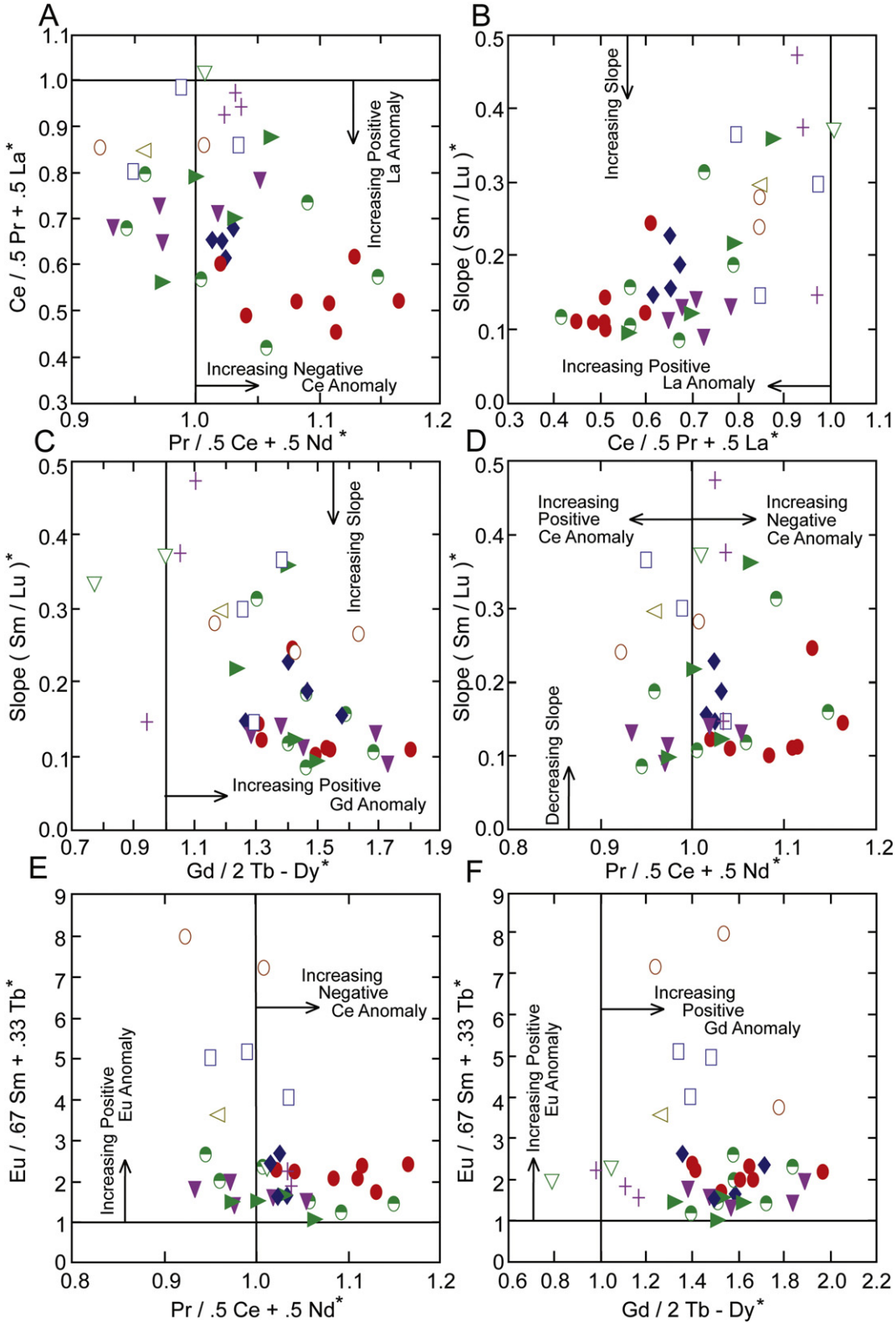

Fig. 28. Scatterplots of the various anomalies of the REE patterns. A) La anomaly (Y axis) versus Ce anomaly (X axis). See Bau and Dulski (1996) for formulae and explanation of rationale. Values above and below 0.05 of unity are taken as significant (Bekker et al., 2010). A general correlation exists between the increasing negative Ce anomaly and increasing positive La anomaly, though this may be caused by the formula for the La anomaly containing Ce. Five of the crystal fan samples and three cuspate fenestral fabric samples have significant negative Ce anomalies. B) A positive correlation exists between increasing slope of the middle and heavy portion of the REE patterns and increasing La anomaly. Siliciclastic and pyritic iron formation samples have low slopes and no La anomalies, whereas crystal fans have pronounced La anomalies and higher slopes. C) A positive correlation also exists between positive Gd anomalies and higher slopes, with the siliciclastics and pyritic samples having the lowest slopes and no positive Gd anomalies. D) Any correlation between slope and Ce anomaly is not well defined for most of the samples. E) Iron formation samples have considerably larger positive Eu anomalies than carbonate samples, but do not significantly vary in Ce anomalies from most of the carbonate samples; the exception being most of the samples of crystal fans and some of the cuspate fenestral fabric. F) Most of the iron formation samples have higher Eu anomalies and lower Gd anomalies than the average carbonate. The asterisk * in the formulae indicates that values are normalized by dividing by PAAS. A pyrite sample and chert sample were omitted from graphs of the Ce anomalies as slightly elevated Pr in these samples produced false negative Ce anomalies.

increase can also be seen in the data of Fischer et al. (2009, fig. 6), from the iron-rich area at the tops of cores into the dolostone, although they interpreted the low $\delta^{13}C$ values in the iron-rich areas as entirely the result of diagenetic reactions between iron hydroxides and organic carbon; a view supported by Heimann et al. (2010) for the Kuruman Iron Formation. It is therefore probable that the −5.6‰ value for the Steep Rock siderite layer reflects a deeper Archean seawater composition of approximately −5‰ (Kaufman et al., 1990), as the sample is from a siderite layer with sharp planar contacts and insignificant iron oxide or carbon content, making it unlikely to have been of diagenetic origin.

12.1.2. Ca-carbonate

Carbon isotopic values in the carbonate range from 0.1‰ to 2.7‰ $\delta^{13}C$. These values are slightly higher than those in Late Archean carbonate platforms at Campbellrand, Hamersley and in Zimbabwe, which commonly have averages close to zero (Becker and Clayton, 1972; Abell et al., 1985a, 1985b; Fischer et al., 2009). However, Veizer et al. (1990) reported $\delta^{13}C$ values of 0.9 to 2.1 for samples from the Pongola Supergroup. It is notable that the Steep Rock carbon isotopic values are correlated with lithology for the columnar stromatolites, flat and domal stromatolites plus cuspate fenestral fabric, and crystal fan fabric (Fig. 22). The cuspate fenestral fabric and crystal fan fabric samples were obtained from paired layers of these lithofacies that are within 2–5 cm of each other in giant domes, yet the values are, for the most part, consistently different. This supports the pristine nature of the samples (e.g., cf. Allwood et al., 2010), as diagenetic alteration would be expected to homogenize the values. The $\delta^{13}C$ values also correlate somewhat with Sr (Fig. 25A) and Ba concentrations, indicating that the isotopic variation reflects only one aspect of changes in the chemistry of the fluids from which the carbonates precipitated. Sr, Ba and $\delta^{13}C$ vary inversely with Fe and Mn concentrations (Fig. 25B). All of these values vary systematically with stratigraphy (Fig. 24). Fe and Mn decrease and Sr and Ba increase, from the basal contact to the atikokania layer. Change in lithofacies to columnar stromatolites in the next layer corresponds with a precipitous decrease in Sr and Ba and a large increase in Fe and Mn. The change in water chemistry needed to accomplish this may have been increased restriction in circulation in the inner part of the shelf as the carbonate platform developed. Gradual rise in the $\delta^{13}C$ ratio from the base of sequence to the atikokania horizon in Unit 7 at Locality 1 may also reflect evaporation that promoted heavier isotopic values as restriction increased. Restricted connectivity to the world ocean would allow evaporative loss of CO_2 over extended residence times to raise the isotopic ratio (Stiller et al., 1985; Schidlowski et al., 1985; Casanova and Marcell, 1993; Valero-Garcés et al., 1999). Lazar and Erez (1990) have a contradictory view, though their model also shows enrichment in heavy carbon of up to 3.5‰ $\delta^{13}C$ (PDB) at salinities of up to twice the modern ocean. In addition, removal of organic carbon from recycling into the water in a restricted setting will raise $\delta^{13}C$ in the water mass (Craig, 1954; Schidlowski, 1988). It is also possible that, with restricted circulation, precipitation of calcium lowered Ca^{2+} concentration in the water column, resulting in progressively higher Mg^{2+}/Ca^{2+} and Fe^{2+}/Ca^{2+} ratios causing precipitation of aragonite to supersede that of calcite, and then ankerite developed as the stable phase. With removal of Ca, the Sr/Ca and Ba/Ca ratios in the calcite would also increase up-section until aragonite atikokania precipitation allowed a large increase in Sr and Ba, which substitute for Ca in the crystal lattice. Possibly, increased connectivity with the open sea occurred at the level of the columnar stromatolites, triggering a fall in $\delta^{13}C$, change in lithofacies, and precipitation of ankerite, or another iron-rich precursor, as the carbonate phase. High Fe and Mn values, lowered Sr and Ba content, and a 2.5‰ fall in $\delta^{13}C$ over <1 m stratigraphically, together with an abrupt change from atikokania precipitation to columnar stromatolite development, all agree with increased interchange with offshore seawater at this level. However, the high Y/Ho ratios in the columnar stromatolites are difficult to explain by increased connectivity with the open sea.

Geochemical trends related to lithofacies, and thus related to depositional environment, have also been noted in other Archean carbonate platforms. Kamber and Webb (2001) found that REE patterns in Campbellrand carbonate sediments correlate with water depth. The Eu and La anomalies decrease with decreasing water depth (from deeper offshore, to shallow offshore, to lagoonal), as does the total REE abundance (from 2×10^{-2} to 1×10^{-3} for PAAS-normalized average curve position). They interpreted this to indicate less mixing of the water masses, from offshore to inner parts of the platform (Kamber and Webb, 2001). The Steep Rock REE PAAS-normalized average curve position is similar for the samples above the basal sample (which is siliciclastic contaminated) at Locality 1 to the sample from the atikokania crystal fan horizon. However, in the columnar stromatolites (which are 1 m higher in the succession than the crystal fans) the concentration of REEs is approximately twice as high as the lower samples. The Y/Ho ratio increases from 29 for the stratigraphically lowest sample, which contains abundant siliciclastic material producing this ratio, to 42 for the relatively pure carbonate sample slightly higher in the succession, and then to 63 for the atikokania horizon (Fig. 24). This is compatible with increasingly restricted conditions in the first 40 m of the Hogarth Member, followed by increased connectivity with offshore waters at the change from atikokania to columnar stromatolites. This is also consistent with the Campbellrand findings of Kamber and Webb (2001). A strong correlation between REE geochemistry and sedimentary facies has also been detected in the ~3.45 Ga Strelley Pool Formation of the Pilbara Craton, where REE patterns indicate that chemical sediment deposition in an environment dominated by hydrothermal fluids was succeeded by stromatolite development in open seawater (Allwood et al., 2010). A previous study of carbon isotopes in the Steep Rock Group also found lithofacies control of geochemistry and concluded that aerobic microbial activity occurred during formation of the stromatolites, whereas the carbonaceous shales, which accumulated in deeper water with the iron formation, were dominated by methanotrophs (Kakegawa and Haikawa, 2007). Carbon isotopic studies carried out by Nisbet et al. (2007) also concluded that the shallow water carbonates at Steep Rock accumulated under oxic conditions.

Lateral redox gradient migration would have had consequences for iron formation deposition on the deeper portions of the platform. Initial flooding, followed by progressive restriction of circulation on the carbonate platform, could have led to the formation of two chemically distinct water masses: seawater typical of the time-period offshore, and higher salinity, locally oxygenated seawater over shallower parts of the platform. We infer that minor perturbations in this overall pattern are highlighted by thin, stratiform Fe-carbonate layers replacing and sporadically interbedded with the limestone (Fig. 29). These represent periods of offshore water mixing and movement into the carbonate area. During these episodes, the rate of iron hydroxide precipitation would be reduced in the offshore areas previously accumulating iron formation, allowing organic-rich mud or chert to dominate. This situation recurred on a larger scale during the increased mixing marked by deposition of the columnar stromatolites. In this view, changes in water chemistry reflected in sediment composition on the carbonate platform should correspond with coeval changes in the offshore iron formation area.

The negative Ce anomaly in some carbonate samples (Figs. 26B, C, 28A, D, E) indicates that the water from which these chemical sediments precipitated encountered oxygen and that cerium oxide was preferentially removed from solution (Riding et al., 2014). These negative Ce values are markedly different than values from other Archean carbonate platforms, although data from Campbellrand carbonate have the beginnings of the same trend (Fig. 30). These negative anomalies should be matched by positive anomalies in the iron oxides and possibly in some of the carbonates. This is the case with some of the samples (Fig. 28A, D, E), although the negative anomalies are, on average, more pronounced than the few, more subtle, positive ones. This could either reflect a larger initial volume of iron hydroxide than carbonate precipitate with positive Ce anomalies, or that the limited iron

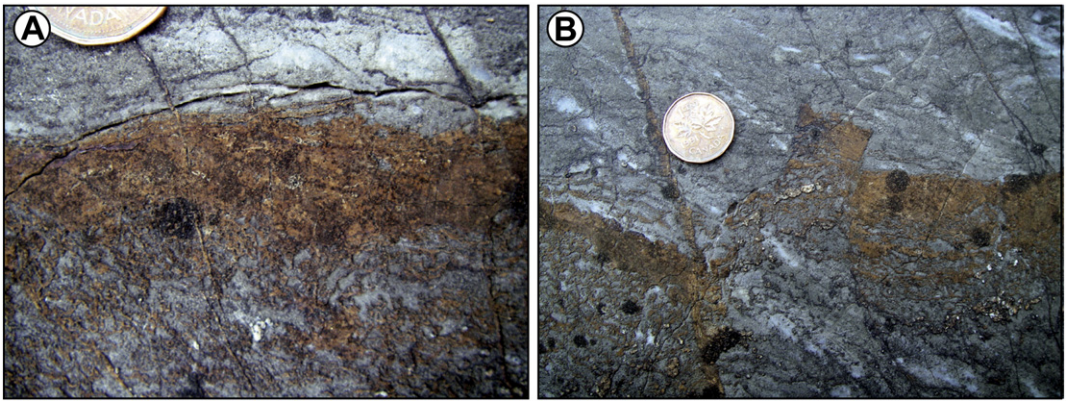

Fig. 29. Hogarth Member, Unit 5, Locality 1. It is not uncommon for tops of limestone beds to be replaced by ferroan dolomite (ankerite). A) Replacement decreases in intensity downward from the sharp contact with the overlying limestone bed. This indicates replacement through reaction with the overlying seawater. B) A plug was ejected from the top of a layer during dewatering of the sediment. This confirms that the replacement occurred prior to dewatering and complete lithification, further suggesting that replacement was the result of interaction with the overlying seawater. Late stage, ankerite veins are also seen in the joint system cutting both the limestone and the ankerite replaced areas. Coin diameter is 19 mm.

formation outcrop hinders sampling of areas with larger positive Ce anomalies.

Samples from thick limestone layers above the columnar stromatolites, with the exception of 8–28, which has signs of alteration (Figs. 22, 25A), show up-section increases in Sr and Ba and decreases in Fe (Fig. 24). These trends continue into the Elbow Point Member, especially in the crystal fan fabric layers. At first sight, they appear to represent another interval of restricted circulation, culminating in development of the Giant Dome Lithofacies. However, the increase in Sr and Ba and decrease in Fe and Mn in the crystal fan fabrics may reflect

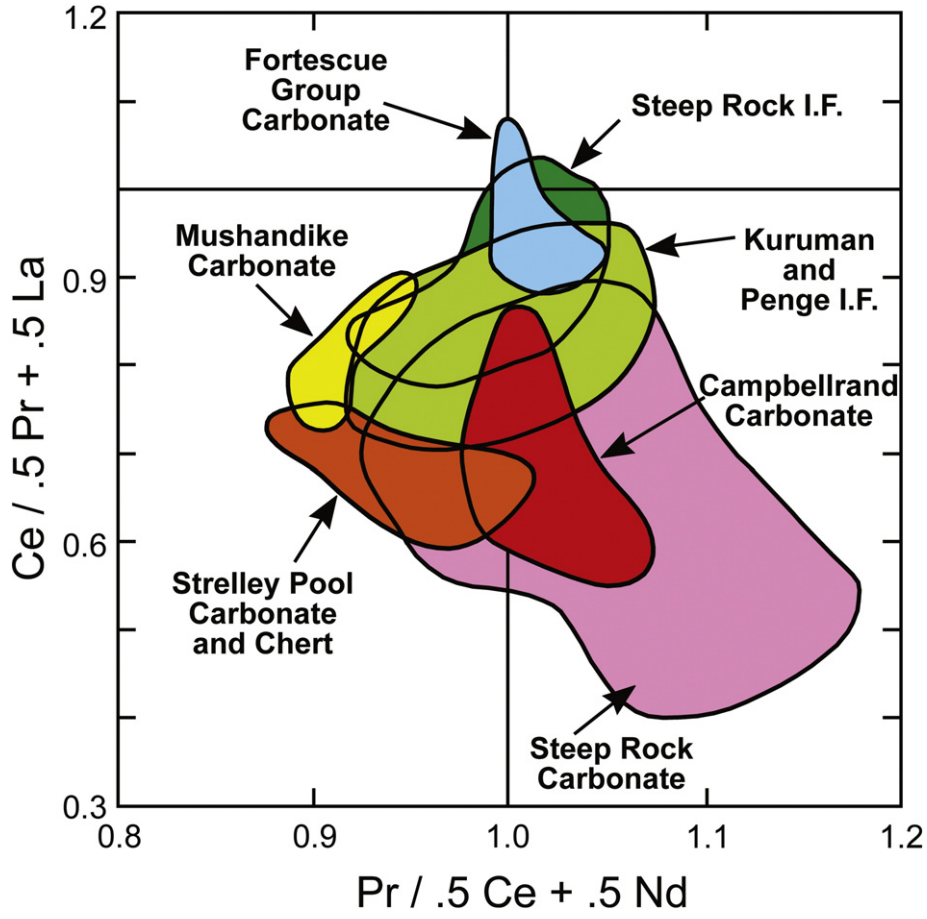

Fig. 30. Comparison of La (Y axis) and Ce (X axis) anomalies in Steep Rock carbonates and iron formation with those in other Meso- and Neoarchean carbonate deposits and associated iron formation. The Steep Rock iron formation samples show considerable overlap with Kuruman and Penge iron formation samples. Also, the plot for Steep Rock carbonates encloses the entire area of the plot for Campbellrand carbonates and extends further, as some Steep Rock crystal fan and cuspate fenestral fabric samples contain significant negative Ce anomalies. The larger plot area covered by the Steep Rock carbonates may reflect the larger sample size, or a larger original diversity in geochemistry. Two iron formation samples with slight positive Pr anomalies were not plotted, as this produces a spurious negative Ce anomaly.
Data for non-Steep Rock fields are from Bau and Dulski (1996), Kamber and Webb (2001), Bolhar et al. (2004), Kamber et al. (2004), and Bolhar and van Kranendonk (2007).

a change in the mineralogy of the precipitating carbonate phase rather than more restricted conditions. The high Sr contents of the crystal fan fabric in these domes are similar to the high Sr values found in Campbellrand crystal fans (Sumner and Grotzinger, 2000; Sumner, 2004) and supports interpretation that they were originally aragonite (Sumner and Grotzinger, 1996, 2004), although the possibility that Campbellrand examples were originally gypsum has also been advanced (Bertrand-Sarfati, 1976; Hardie, 2003, 2004; Gandin et al., 2005; Gandin and Wright, 2007). The crystal fan fabrics consistently contain larger amounts of strontium and barium and lesser amounts of manganese and iron than the layers of cuspate fenestral fabric they alternate with. This probably reflects original mineralogy; the aragonite lattice of the crystal fan fabrics would contain more Sr and Ba, but less Fe and Mn, than calcite if that mineral formed the cement in the cuspate fenestral fabric. Due to the inhibiting effect iron has on calcite precipitation (Herzog et al., 1989; Sumner and Grotzinger, 1996, 2004), the periodic incursion of iron-rich, off-shore waters could account for the alternation between these two minerals. This may have also resulted in the dissolution surfaces and iron-rich accumulations immediately below some crystal fan layers (Figs. 17C, 19A). However, the elevated $\delta^{13}C$ of the crystal fan fabrics suggests they were deposited during periods of maximum restriction, with draw-down of Ca^{+2} due to calcite precipitation leading to elevated Mg/Ca and aragonite precipitation. The negative Ce anomaly associated with the crystal fans reinforces this interpretation (Figs. 26, 28). The lack of negative Ce anomaly in the stromatolites of the Hogarth Member indicates that circulation was not restricted to the point of allowing significant oxygen build-up during their formation. However, negative Ce anomalies in most crystal fan and some cuspate fenestral fabric samples from Locality 6 indicate that heightened restricted circulation developed during deposition of the Elbow Point Member, leading to areas where significant free oxygen moved the redox boundary basinward. This agrees with the higher $\delta^{13}C$ values of the crystal fans (Fig. 22).

Whichever of the above scenarios is correct, the cause of the alternation of water masses with differing chemistries in the area precipitating crystal fan fabric domes is difficult even to speculate on without knowledge of the time-spans represented by individual layers. It is also possible that the differences in chemistry do not reflect original differences in water body chemistry but were caused by diagenesis. Nothdurft et al. (2004) found that well preserved Devonian microbial carbonate contained less Sr (100 to 200 ppm) than other carbonates in the unit they studied, and concluded that the delicate microbial carbonate lost the greatest proportion of its Sr to the escaping fluid (Kamber et al., 2004). This explanation is unlikely to be the cause of the differences here as Fe and Mn are enriched rather than depleted in the cuspate fenestral fabric of Steep Rock giant domes. However, geochemical differences between areas millimeters apart that are the result of diagenesis do exist in our samples. The three samples that were sub-sampled for clear, void-filling cement and organic carbon-rich areas show distinct geochemical differences between these two components, with the cements being systematically lower in Sr and Ba and higher in Mn. Kamber and Webb (2001) found that void-filling cements in Campbellrand carbonates had different geochemistry than the more organic-rich microbial carbonate, with more REEs, U, Pb, Cs and Rb in the latter. Thus, the difference between the crystal fan fabrics and cuspate fenestral layers may reflect that the fans precipitated directly from seawater, whereas the majority of carbonate in the cuspate fenestral fabric formed as cements from pore fluids during early diagenesis. At Steep Rock, as in most carbonates, precipitation occurred directly from the water mass (e.g., crystal fan fabrics), in the mat (carbonate in association with organic material), during shallow burial (early cements), and during deeper progressive diagenesis (later cements). The fluid at each of these stages will have different geochemical characteristics, which the precipitate may inherit. This is a subject requiring further investigation; possibly laser ablation technology, combined with an understanding of the sample's diagenetic history.

12.2. Carbonate sediments

12.2.1. Bedded limestone facies

Assuming that Locality 4 and the section north of it is downfaulted Elbow Point Member (and therefore not part of the Hogarth Member), we recognize three parts to the Hogarth Member: (i) In the lower part, exposed at Locality 1, bedded limestone with stromatolite horizons overlies the tonalite. The stromatolites include domes, pseudocolumns, and columns with irregular laminae and we interpret them as lithified microbial mats (see Section 12.2.4). This sequence also contains at least two atikokania crystal layers one meter apart in Unit 7 (Figs. 5, 7), and numerous horizons of Fe-carbonate (Fig. 29). These suggest that during this initial phase of shelf development the seawater precipitating calcite was prone to influence by more open marine, iron-rich water that promoted Fe-carbonate and aragonite precipitation. (ii) The middle part, exposed in the lower portion of Locality 5, is mainly banded limestone with large domes (Fig. 13A). Some of these fine-grained carbonates may represent water-column precipitates in a relatively protected inner platform environment. Consistent with this, scarcity of Fe-carbonates in this part of the sequence suggests little influence from more open marine water. (iii) The upper part, exposed in the upper section of Locality 5, is dominated by layered fenestral — probably stromatolitic — limestones, with Fe-carbonate horizons. These suggest influence of iron- and carbonate-rich seawater that promoted early seafloor lithification, due to increased proximity to the shelf margin. Thus, in contrast with the Elbow Point Member, and also with the basal part of the Mosher Carbonate, the mid-upper part of the Hogarth Member is relatively Fe-poor and lacking in precipitated crystal fans and crusts.

Recrystallization hindered positive identification of grainy fabrics in the Mosher Carbonate. We only unequivocally observed grains between stromatolite columns at Locality 1. Martin et al. (1980, Fig. 23) also reported detrital intercolumn fill in Cheshire stromatolites. Oolite is well-developed in the Tumbiana Formation, ~2720 Ma (Awramik and Buchheim, 2009) and also forms a minor component at Campbellrand, 2600–2520 Ma (Beukes, 1987, Table 1). Bed thickness and sharp contacts of the strata in the upper part of the section at Locality 1 and the basal part of Locality 2, including an erosive contact and trough cross-stratification, suggest the presence of at least some packstone/grainstone units in the upper Bedded Limestone at these locations. These may represent sand shoals, but the evidence is fragmentary.

12.2.2. Stromatolites

Giant domes (see below) are the most conspicuous stromatolite-like structures at Steep Rock, and create one of the best known features of the succession (Fig. 18A). They were not the first stromatolites recognized at Steep Rock, probably because they were mainly either below lake level or covered by overburden prior to mining operations, and due to their unusual hybrid composition of relatively thick alternations of cuspate fenestral fabric and crystal fan fabric. More typical stromatolites, and the ones that first attracted attention at Steep Rock, are much smaller and generally readily recognized by their domal or columnar forms and distinctive crinkly laminae. Examples were described by Rothpletz (1916), who named them *C. walcotti*, even though he regarded them as stromatoporoids. However, at least one of these specimens (Rothpletz, 1916, pl. 8 Fig. 1) resembles the columnar and pseudocolumnar stromatolites described by Hofmann (1971, pl. 22, fig. 2) and Wilks and Nisbet (1985, fig. 6) (Fig. 8C). So it seems that at least some of Rothpletz's (1916) specimens were the first stromatolites recorded from Steep Rock, and possibly the first Archean stromatolites to be described anywhere.

We recognize four main categories of stromatolites and domal structures at Steep rock: (i) Small (<1 m) domes, low cones, pseudocolumns, and columns, typically with irregular laminae and poor inheritance. We interpret these diverse morphotypes as lithified microbial mats. They mainly occur as thin beds in the lower part of the Hogarth Member at Locality 1. Some of the columns are very thin and elongate and show

alpha branching. (ii) Stratiform stromatolites probably are present in both the lower and upper parts of the Hogarth Member. In the upper part they are closely associated with fenestrae and sheet-cracks. They may not be essentially microbial, and their lack of vertical relief makes them less distinct in areas where structural deformation has blurred their original fabric. (iii) Giant domes: major rock-builders that dominate the Elbow Point Member. We regard them as a distinctive variant of hybrid stromatolite (see Riding, 2008). (iv) Meter-scale banded limestone domes in the upper part of the Hogarth Member are enigmatic; they are not laminated and are mainly composed by dark–light alternations of apparently relatively fine-grained sediment, but they are locally steep sided. We do not regard them as stromatolites, but their origins remain uncertain.

In addition to their distinct differences in appearance, the small crinkly laminated stromatolites and the giant domes occur at different stratigraphic levels. Stratiform, small domal and columnar forms mainly appear in the lower and upper parts of the Hogarth Member, whereas the metric-scale domes constitute the overlying Elbow Point Member.

12.2.3. Small stromatolites with crinkly lamination

These occur interbedded with other carbonates throughout the Hogarth Member. Walter (1983, p. 209) concluded that late Archean stromatolites, including those at Steep Rock, reflect a diverse marine benthic microbiota likely to include photoautotrophs. Schopf (2006, table 1, fig. 2) also emphasized the morphologic diversity of late Archean stromatolites, and noted that this first appears in the Insuzi Group (~2985 Ma) and then at Steep Rock, both of which are reported to contain stratiform, pseudocolumnar, domal, conical, columnar, and branching forms. He noted that this degree of diversity 'suggests that such forms are not a product of a single set of nonbiogenic accretionary processes'. The Insuzi stromatolites, well-preserved in partly silicified dolomite, occur on a tidal flat and in the adjacent channel. In addition to forms also present at Steep Rock, they include steep-sided cones and microstromatolites (Beukes and Lowe, 1989, Figs. 7, 8, 10). The oldest stromatolites known, in several horizons at Pilbara (~3.4 Ga), are reported to include stratiform, domal and conical morphotypes (Schopf, 2006, table 1), plus pseudocolumns and branched pseudocolumns (Hofmann et al., 1999, fig. 2c) also described as branched columnar (Van Kranendonk, 2011, fig. 9c, d). These general comparisons suggest that Steep Rock stromatolites are not more diverse than Insuzi, and scarcely more than Pilbara. On the other hand, the Giant Dome Lithofacies at Steep Rock does appear to mark a new development.

12.2.4. Biogenicity and processes

Stromatolites are commonly considered lithified microbial mats, formed by a variety of processes (Awramik and Margulis, 1974; Konhauser and Riding, 2012). Previous workers have drawn attention to the generally good preservation of Steep Rock stromatolites (Walter, 1983) and their morphologic diversity (Schopf et al., 2007). Two features supporting biogenicity in Steep Rock stromatolites are locally relatively well-preserved microfabrics argued to contain evidence of filaments and grain trapping (Walter, 1983, 1994), and the variety of morphotypes present which 'suggests that such forms are not a product of a single set of nonbiogenic accretionary processes' (Schopf, 2006, p. 875). Morphologic arguments for biogenicity rely primarily on irregular crinkly lamination with poor inheritance that suggest lithified microbial mats, and vertically extended columns that lack an obvious abiotic origin.

Martin et al. (1980, fig. 23) drew attention to detrital intercolumn fill in a Cheshire stromatolite. Walter (1983) described one Steep Rock columnar layered stromatolite (Walter, 1983, photo 8-12) as having trapped detrital particles up to 1 mm in size, and another (Walter, 1983, photo 8-13) with 'film microstructure suggestive of construction by finely filamentous organisms', and in combination he suggested these as 'the oldest known example of a stromatolite apparently formed via sediment trapping by filamentous organisms.' He concluded 'the abundant presence of detritus may be indirect evidence that the constructing organisms were phototactic' (Walter, 1983). These interpretations are difficult to evaluate. The preservation in our specimens and in those of Walter (1983) does not seem sufficient to remove the possibility that putative coarse grains and filaments (perpendicular dark streaks, Walter, 1983, photo 8-13b) could be recrystallization products.

Irrespective of whether grain trapping was important in Steep Rock stromatolites, early lithification is also essential for accretion (Logan, 1961; Ginsburg, 1991; Riding, 2000). In Phanerozoic stromatolites, bacterial sulfate reduction (BSR) and cyanobacterial photosynthesis are commonly invoked as mechanisms to promote stromatolite lithification (Visscher and Stolz, 2005; Dupraz et al., 2009; Konhauser and Riding, 2012). Neither of these can be excluded at Steep Rock, although calcified cyanobacterial filaments have not been reported. There is evidence for BSR at ~3.47 Ga (Shen et al., 2001). Archean seawater sulfate concentrations have been suggested to be too low to sustain significant levels of BSR (Habicht et al., 2002; Crowe et al., 2014), but if these reached ~80 μM 2.7 Ga ago, then BSR may not have been insignificant (Jamieson et al., 2013).

Bacterial iron reduction could also have contributed to stromatolite lithification at Steep Rock. There is geochemical evidence that bacterial iron reduction was operating on the deeper areas of the Hamersley Platform (Czaja et al., 2010). Microbial iron reduction can promote precipitation of calcium-rich siderite which could be a precursor to calcite and dolomite (Zeng and Tice, 2014), although siderite is considered by some to be a diagenetic mineral (Beukes and Gutzmer, 2008). This process may have operated beneath the surface of Steep Rock stromatolites where bacterial degradation of organic matter was taking place. In shallow benthic cyanobacterial mats the presence of cyanobacterial organic matter together with low levels of both Fe(II) and Fe(III) would permit iron oxidation-reduction favoring Ca-carbonate and, locally, siderite precipitation. This could occur in mats with diurnal cycles of oxygen-level, creating mats lithified mainly by calcite and partly by siderite.

We envisage that mid-Archean anoxic seawater would precipitate Fe-carbonates so long as iron levels were high, and that this could occur in the water column (see Rajan et al., 1996, Black Sea). This would not preclude either diagenetic siderite precipitation (as Beukes and Gutzmer, 2008, suggest) or anaerobic iron oxidation (as Konhauser et al., 2005, suggest) in banded iron formation. Cyanobacterial oxygen production would remove dissolved iron by promoting water column iron oxidation. This would promote Ca-carbonate precipitation in shallow areas with restricted interchange with the ocean.

12.2.5. Giant Domes

The Hogarth Member shows a transition to the Giant Domes lithofacies at Localities 2 and 3, and the ~70 m Elbow Point Member at Locality 6 appears to consist entirely of Giant Domes without intervening sediment. Giant domes are unusual in their combination of external form (smooth oriented inflated metric scale domes) and internal structure (alternating layers of crystal fan fabric and cuspate fenestral fabric). These distinctive limestone deposits appear almost unique to Steep Rock. 'Fenestrate microbialite' (Sumner, 2000) fabrics are well-known in the 2600–2520 Ma Campbellrand Subgroup where they alternate with laminated dolomite (Beukes, 1987, fig. 6a) and small laminated domes and contorted mat (Sumner and Grotzinger, 2004, figs. 9, 12). They are clearly very similar to cuspate fenestral fabric, but often thicker and more complex. They form extensive cm–dm beds (Sumner and Grotzinger, 2000), and cyclic beds capped by dark 'precipitated crust' (Sumner, 1997b, fig. 4c). They are also 'interbedded with giant, elongate stromatolite mounds' (Sumner, 2000), although their volumetric importance in these is not clear. Campbellrand fenestrate microbialite is generally regarded as a deep water and/or low energy deposit (Sumner and Grotzinger, 2000, 2004) due to its 'delicate nature' (Sumner, 2000).

Crystal fan fabric layers, described as crystal pseudomorphs, form layers up to 20 cm thick interbedded with stromatolite laminae (Martin et al., 1980; Abell et al., 1985a) and with grainstones (Sumner and Grotzinger, 2000), in the Cheshire Formation, ~2650 Ma. Some stromatolite domes are 40 cm across and form thick units (Martin et al., 1980, fig. 15; Abell et al., 1985a, fig. 7a). However, further to the north-west, in the ~2600 Ma Huntsman Limestone, crystal fan fabrics are cyclically interbedded with cuspate fenestral fabric (Sumner and Grotzinger, 2000) and crystal pseudomorphs locally penetrate the cuspate fenestral fabric which are associated with 'giant stromatolite mounds' (Sumner, 2000). Some upside down Huntsman cuspate fenestral fabric specimens were previously misinterpreted as columnar stromatolites (Schopf et al., 1971; Walter, 1983; see Sumner, 1997a). In Western Australia, inflated domes up to 10 m in height in the ~2630 Ma Carawine Dolomite (Simonson et al., 1993, figs. 8, 27; Murphy and Sumner, 2008, fig. 4a) locally contain decimetric layers of crystal pseudomorphs (Simonson et al., 1993, figs. 16, 19, table 2). However, the large domes contain a variety of diverse stromatolite morphotypes (Murphy and Sumner, 2008) that do not appear to be constructed either by crystal fan fabric or by cuspate fenestral fabric, and Carawine cuspate fenestral fabric occurs in deep-water environments (Murphy and Sumner, 2008). In the same general area, the ~2720 Ma Tumbiana Formation contains cuspate structures, described as 'coniformly laminated columns connected by regularly occurring inter-column laminae' (Flannery and Walter, 2012, fig. 3b) that resemble cuspate fenestral fabric, and the slightly older (~2740 Ma) Mopoke Member of the Kylena Formation has centimetric crystal crusts (Flannery et al., 2012, fig. 3g), but these do not appear to occur together or to participate in large dome formation. Fabric similar to cuspate fenestral fabric was described as the stromatolite *Thesaurus* in 2730–2720 Ma allochthonous limestone blocks at Joutel, Québec (Hofmann and Masson, 1994), but is not reported to be associated there with crystal fan fabric.

Thus, Archean domes are well known at Campbellrand (Truswell and Eriksson, 1973; Beukes, 1987), and in the Carawine Dolomite (Simonson et al., 1993) and Huntsman Limestone (Sumner and Grotzinger, 2000, fig. 9). Fenestral fabrics and crystal fan fabric form discrete hybrid interbeds at both Campbellrand (2600–2520 Ma) (Sumner, 1997b, fig. 4c) and in the ~2600 Ma Huntsman Limestone (Sumner and Grotzinger, 2000). However, apart from Steep Rock, crystal fan fabric and cuspate fenestral fabric-type deposits only appear to combine to form 'giant stromatolite mounds' in the Huntsman (Sumner, 2000; Sumner and Grotzinger, 2000). Murphy and Sumner (2008) state that there are no reports of fenestrate microbialite younger than Campbellrand. We conclude that cuspate fenestral/fenestrate microbialite fabric and its distinctive hybrid alternation with crystal fan fabric appears to be an essentially Neoarchean phenomenon. These distinctive deposits appear to have been initiated by changes in microbial growth and Ca-carbonate deposition associated with areally limited oxygenation near the Meso-Neoarchean transition.

12.3. Succession and platform geometry

12.3.1. Facies polarity

Contrasting interpretations of the development of the Steep Rock limestone succession have been suggested. Wilks (1986) considered that the Mosher carbonate represents a shallowing sequence. Wilks and Nisbet (1988) interpreted the Mosher Carbonate to reflect a diversity of shallow-water settings 'from sabkha to intertidal to subtidal'. They compared the stromatolite morphologies to Shark Bay and suggested they formed on a shelf margin or in a lagoonal environment. In contrast, Grotzinger (1989) argued that the Steep Rock succession was more likely to be deepening, because many Proterozoic shallowing stromatolitic successions show larger forms overlain by smaller ones. However, there are several examples of large Precambrian stromatolite mounds at shallow shelf margins that appear to have been produced by platform progradation (e.g., Ricketts, 1983; Beukes, 1987; Ross and Donaldson, 1989). Some of these mounds consist of numerous small stromatolites, but nonetheless retain overall metric dimensions and substantial synoptic relief, and also show orientation.

Many features of the Steep Rock carbonate succession are consistent with a shallow water succession on a marine platform where limestone deposition kept pace with relative sea-level rise. The Elbow Point Member can be interpreted as a platform margin reef complex and the Hogarth Member as a more platform interior facies (Riding et al., 2014). The Giant Dome Lithofacies is central to this interpretation, and to understanding the sequence as a whole. The absence of particulate sediment, together with well-defined orientation and smooth dome surfaces, suggest that the giant domes formed under current influence that promoted seafloor precipitation, molded the dome shapes, and removed any allochthonous sediment. However, wave activity at a shallow shelf margin should create clastic sediment by erosion of even rigid bodies, and the giant domes could be expected to show signs of erosion and the local accumulation of reef-derived fragments. This may occur but seems relatively rare (Fig. 20D). It is difficult to explain why this was not prevalent if the Giant Dome Lithofacies occupied a shallow shelf margin. On the other hand, if the Giant Domes lithofacies formed below wave-base on the outer platform slope or in an off-shore ramp setting, then it would be reasonable to expect fine-grained sediment to have accumulated on or around them, especially since this sediment appears to be a major component of the Hogarth Member. Thus, in either case, the paucity of allochthonous sediment associated with the giant domes is problematic. A factor that may be implicated is the effect of air density (Som et al., 2012) and seawater viscosity (Fralick and Carter, 2011) on Archean wave and current intensities, and therefore on sediment production and transportation; these remain to be further resolved. At present, the evidence appears to support Wilks (1986) view that, except for the lowermost strandline and shallow offshore deposits the Mosher Carbonate is a shallowing sequence. Rare desiccation cracks on Giant Dome surfaces (Fig. 20C) support a shallow water setting. The heavy-enriched $\delta^{13}C$, negative Ce anomalies and high Sr/Fe ratios of the crystal fan layers, as at Locality 6, suggest that the Giant Dome Lithofacies was wide enough for some areas to develop restricted circulation. If so, these areas must have been somewhat removed from the platform edge and it is possible that the Elbow Point Member at Locality 6 represents a more interior, back-reef, location within the Giant Dome reef facies.

The even and lateral persistence of the alternating layers of cuspate fenestral and crystal fan fabric in the giant domes suggest fluctuating episodes of microbial growth and abiotic precipitation, respectively. This could have been produced at a shelf margin adjacent to a redox chemocline between oxygenated shelf waters and suboxic, iron-rich offshore/basinal waters influenced by periodic upwelling. The periodicity of the giant dome alternations is difficult to assess. A range from seasonal to decadal seems possible. Present-day studies indicate that seasonal, intra-annual and inter-annual variability in temperature, wind, and currents can influence shallow-marine conditions (García-Reyes and Largier, 2010), and that regional climate forcing may be preserved in stromatolite layering (Petryshyn et al., 2012).

12.3.2. Platform geometry and seawater chemistry

Transgressive flooding created a stable platform environment (Wilks and Nisbet, 1985) in which shallow water carbonate sedimentation kept pace with relative sea-level rise. We infer that aggradation ultimately constructed a more or less flat topped carbonate platform with a rimmed margin. This is consistent with fine-grained (platform interior) sediments in the Hogarth Member overlain by the giant domes of the Elbow Point Member (shallow margin).

We infer that the Mosher Carbonate accumulated when localized cyanobacterial oxygenic photosynthesis in an 'oxygen oasis' removed sufficient ferrous iron to promote significant $CaCO_3$ precipitation (Riding et al., 2014) (see below). Seawater chemistry over the platform

probably varied with the extent of oxygen production, initial terrestrial run-off, and incursion of off-shore, sub- or anoxic water, rich not only in bicarbonate but also in dissolved iron, as well as with water depth and platform size. The thickness of the Steep Rock carbonate platform indicates it existed for an extended period of time. During that interval, water composition may have varied considerably in space and time. At the simplest, we envisage significant changes with distance from the open sea and degree of bathymetric restriction, depending on the stage of platform development. These include the early transgressive stage of Hogarth Member deposition, commensurate initially with open marine influence during that stage of platform development, and cyclically during the formation of the Elbow Point Member, which we interpret as a platform-margin deposit. The contrasting, laterally extensive, hybrid layers of the giant domes appear to reflect fluctuating conditions that alternately favored microbial growth and early lithification on the one hand, and precipitation of dense sparry crystal fans on the other. These changes are likely to include water chemistry influenced by periodic upwelling, major storm forcing, and/or overturn. A tendency for calcite to preferentially precipitate on the inner part of the Steep Rock platform, whereas aragonite, in places bounded by dissolution surfaces with Fe-carbonate present, formed on the outer platform, would be consistent with differences in the influence from more Fe-rich offshore waters.

Thus, based on conventional facies assumptions, it can be suggested that the Hogarth Member, characterized by banded limestones that appear fine-grained, not only formed the initial deposits of the carbonate platform but may have persisted and become more restricted platform interior facies as the overlying giant domes of the Elbow Point Member built a barrier to circulation on the platform margin (Riding et al., 2014) (Fig. 31). However, the steep dip of the outcrops that we examined makes it difficult to verify this interpretation. In addition, our REE values indicating oxygenation are limited to giant domes of the Elbow Point Member, and these deposits also have carbon isotope values consistent with elevated salinity.

These observations raise a number of questions and possibilities. Firstly, failure to detect a negative cerium anomaly in the Hogarth Member does not necessarily imply that these sediments lacked partial oxygenation if limestone precipitation at the margins of otherwise iron-rich seas is itself an indication of oxygenation (Riding et al., 2014). Nonetheless, it is possible that both oxygenation and salinity increased as the Steep Rock 'oxygen oasis' developed, and that weaker oxygenation limited negative cerium anomaly development in the Hogarth carbonates. Secondly, it remains possible that we have not seen (or sampled) platform interior carbonates that were coeval with the Elbow Point giant domes. This is because the outcrops we studied leave questions concerning the lateral relationships of the Hogarth and Elbow Point members. Thirdly, our conventional facies interpretation is based on the view that the Steep Rock carbonate platform, like much younger examples, accumulated sediments that were finer in the interior and more reefal near the margin (cf., Grotzinger, 1989). In this view, it seems unlikely that the Giant Dome Lithofacies expanded into the platform interior, because if that happened it should have been inter-bedded with the finer banded limestone of the Hogarth Member. However, these inferences are uncertain and we cannot exclude the possibility that Steep Rock carbonates, and the processes that formed them, may have been fundamentally different from those in younger platforms. Thus, if at least some parts of the Giant Dome Lithofacies developed in more platform interior conditions, this might account for both their more oxygenated REE values and elevated carbon isotope values. Nonetheless, we still find a more nuanced interpretation more plausible, i.e., that the giant dome samples preserving a negative Ce anomaly were located on the back-reef side of the Giant Dome reef margin, and that this location was both more oxygenated and more saline than the outer margin facing the anoxic basin (Fig. 31). All these considerations, and uncertainties, underscore the need for further studies, in particular more analyses, of the Steep Rock carbonates to elucidate facies distribution, oxygenation, and platform geometry.

12.4. Archean carbonate platforms

Compilation of published reports on Archean sedimentary Ca-carbonate deposits indicates eight that are older than Steep Rock

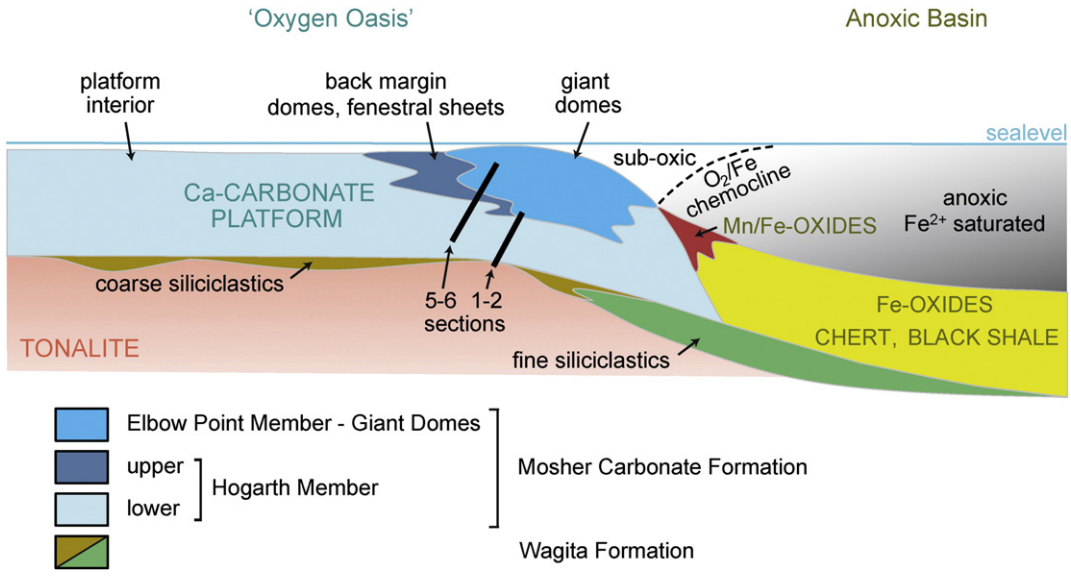

Fig. 31. Interpretive cross-section of Steep Rock platform-basin facies. The Hogarth Member at Localities 1 to 2 consists of banded limestone with thin Fe-carbonate layers and small stromatolite domes and columns, possibly becoming grainstone-dominated in its mostly hematized upper part. The upper Hogarth Member at Locality 5 consists mainly of banded limestone domes passing upwards into fenestral layers and small stromatolite domes. The Elbow Point Member at Locality 6 consists entirely of juxtaposed giant domes, each composed of thick alternations of cuspate fenestral and radial fan fabric. The balance between rate of oxygen production and rate of delivery of offshore Fe^{2+} saturated anoxic water to the shallow carbonate areas determined the position of the chemocline. Onshore water movement, possibly caused by storm surge, would result in the chemocline moving into the platform interior, with the formation of a thin Fe-carbonate layer in the platform assemblage and the offshore switching from iron hydroxide to chert and/or carbonaceous mud deposition. During periods of restricted circulation on the shallow platform the oxygen gradient represented by the chemocline would move offshore, possibly as a bottom proximal wedge, due to the existence of a salinity gradient. During these times crystal fans would precipitate on the giant domes and Mn oxides and Fe hydroxides would form offshore. Not to scale; platform sedimentary sequence thickness several 100 m, horizontal distance ~10–15 km.

(Riding et al., 2014, Fig. 1 and supplementary data), only two of which are more than 60 m thick: Red Lake and Mushandike. The 2940–2925 Ma ~300 m Ball assemblage at Red Lake, ~300 km NNW of Steep Rock, is mainly marble (Hofmann et al., 1985; Corfu and Wallace, 1986). The 2839 or 2817 Ma ~200 m Mushandike Formation, Zimbabwe, contains stromatolites that retain lamination (Orpen and Wilson, 1981), but the sequence is generally recrystallized (Abell et al., 1985b) and as a whole is 'too strongly deformed to reconstruct the broad depositional setting and palaeogeography from sedimentological evidence alone' (Kamber et al., 2004). Of the twelve Archean Ca-carbonate deposits younger than Steep Rock, only three exceed 80 m. These are the 225 m Carawine Dolomite (<2630 Ma) and 475 m Wittenoom Formation (2597–2504 Ma) in the Hamersley Group (Murphy and Sumner, 2008, fig. 2), and the 1900 m Campbellrand platform (2600–2520 Ma, Schröder et al., 2009, Fig. 2). Thus, at 2801–2780 Ma, Steep Rock is the oldest thick and relatively well-preserved limestone deposit, and similar (e.g., Wittenoom) or larger (e.g., Campbellrand) well-preserved examples are unknown until ~2600 Ma. Steep Rock therefore offers insights into the nature and formation of the first thick carbonate platforms, as well as into early Neoarchean conditions and life. Relatively abrupt appearance of thick limestones ~3 Ga could be a vagary of preservation (Nisbet et al., 2007) since limestones older than ~3 Ga are not only thin, but scarce. Nonetheless, well-preserved shallow water siliciclastic and cherty sediments do occur during the ~3.0–3.4 Ga interval when Ca-carbonates appear very scarce, e.g., in the 3.1–3.2 Ga Moodies Group (Heubeck and Lowe, 1994), which includes microbial mats (Heubeck, 2009), and in the 3.4 Ga Buck Reef Chert (Tice and Lowe, 2004), both in the Barberton Greenstone Belt. It is therefore possible that the appearance of thick carbonate platforms in the mid-Archean could reflect a significant environmental threshold.

12.5. Oxygen oases

The iron formations that are common in the Archean are thought to have been precipitated from seawater rich in dissolved iron (Fe^{+2} in the range 40–120 μmol l^{-1} (Canfield, 2005)), and consist of Fe-carbonate and other iron minerals (Bekker et al., 2014). Even if calcium were abundant, it is expected that Ca-Mg carbonate precipitation would be inhibited at these levels of dissolved iron (Herzog et al., 1989; Sumner and Grotzinger, 1996, 2004). In the younger (~2.55 Ga) Campbellrand platform, precipitation of shallow-water aragonite and calcite has been attributed to the presence of oxygen produced by cyanobacterial photosynthesis (Klein and Beukes, 1989). Nisbet et al. (2007) suggested that the increased productivity resulting from the evolution of oxygenic photosynthesis could have caused CO_2 drawdown sufficient to promote $CaCO_3$ precipitation. Iron-rich seawater, widely inferred for the Archean from widespread iron-formation deposition and the lack of evidence for any significant level of free oxygen (Canfield, 2005; Holland, 2006), is not expected to promote precipitation of Ca-carbonate. Instead Fe-carbonate precipitation would have been favored, and the critical effect of oxygenation would be to remove ferrous iron from seawater by precipitating it as ferric hydroxide (Riding et al., 2014). The evolution of oxygenic photosynthesis in cyanobacteria is likely to have created oxygenated areas of seawater depleted in iron (Hayes, 1983). We infer that this was necessary to permit Ca-carbonate precipitation. These environments would be most likely to develop in shallow-water areas that were supplied with nutrients for cyanobacterial growth and protected from open marine circulation that would immediately scavenge the oxygen (Hayes, 1983), and would therefore likely be near-shore shelf environments (Kasting, 1991, 1992; Pavlov and Kasting, 2002). This description fits the Steep Rock limestone: a shallow platform-sea accumulating Ca-carbonate sediments and with stromatolites. We therefore propose Steep Rock as an early example of a marine oxygen oasis in which removal of Fe^{2+} led to the inception of marine $CaCO_3$ precipitation (Fralick and Riding, 2012; Riding et al., 2014).

If Archean seas were iron-rich and anoxic, then all Archean marine limestones must reflect local oxygen production. In contrast, non-marine environments would not necessarily have been affected, and could have precipitated Ca-carbonates under anoxic conditions so long as they were also iron-free. This reading of the Archean limestone record suggests that inception of the development of thick carbonate platforms adjacent to anoxic iron-rich marine basins marks significant accumulation of free oxygen in oxygen oases and possibly the evolution of oxygenic photosynthesis itself. It also implies that limestones predating oxygenation must be non-marine. These inferences require further investigation. They suggest that stromatolites much older than Steep Rock may not be marine (cf., Schopf, 2006, table 3; Buick, 2008). On the other hand, evolution of oxygenic photosynthesis at ~3 Ga is suggested by a number of possible proxies for oxygenation (Buick, 2008), although these could also reflect changes in preservation. An additional consideration is whether early cyanobacterial lineages were restricted to freshwater ecosystems before occupying marine environments (Blank and Sánchez-Baracaldo, 2010). This would not alter our rationale concerning Ca-carbonate precipitation in iron-rich seas (see above). However, it does raise the possibility that oxygenation commenced earlier in non-marine habitats and that cyanobacteria could have been involved in non-marine stromatolite formation.

The long Archean record of stromatolites ranges from a variety of relatively small forms at Pilbara ~3.4 Ga ago (Allwood et al., 2006; van Kranendonk, 2006, 2011) to huge barrel-shaped mounds in the Campbellrand Subgroup, 2.5–2.6 Ga (Truswell and Eriksson, 1973; Beukes, 1987). Steep Rock is one of the earliest examples with a wide range of morphotypes, which includes stratiform, pseudocolumnar, domal, conical, columnar, and branched forms (Wilks and Nisbet, 1985; Schopf, 2006). Although at least sixteen stromatolite-bearing deposits have been recognized that are older than Steep Rock, it seems likely that Steep Rock contains the earliest known relatively diverse suite of stromatolite morphotypes (Schopf, 2006). Walter (1994) commented 'about 2.8–2.7 Ga ago, something happened to allow stromatolites to become both more abundant and much more diverse morphologically'.

Marine transgression, probably related to isostatic loading of the volcanic plateau (Fralick et al., 2008), created a shallow marine platform on tonalite whose weathering could initially supply nutrients. We infer that cyanobacterial productivity in this shallow-water environment with limited incursion of open marine seawater locally created an oxygenated water-mass ('oxygen oasis') depleted in dissolved iron due to oxidative precipitation of ferric hydroxide and thereby favoring Ca-carbonate precipitation. On the platform, short term periods of mixing, possibly driven by large storm events, could have caused thin iron carbonate horizons to develop and more substantial intervals could have led to the deposition of thicker, iron-rich carbonate units with columnar stromatolites that lack a negative Ce anomaly. This interpretation is supported by the presence of REE values indicating oxygenation. The Steep Rock carbonate platform was terminated by inundation by sub-oxic and anoxic seawater that covered it with manganese- and then iron-rich sediments (Riding et al., 2014, Fig. 6), and the effects of oxygenation are reflected in the initial manganese oxide-bearing 'Paint Rock' deposits of this transgression (Nisbet et al., 2007). Based on Phanerozoic rates of carbonate platform accumulation (Schlager, 2003), an assumption supported by rates of sedimentation calculated for the Campbellrand/Malmani carbonate platform (Altermann and Nelson, 1998), the Steep Rock 'oxygen oasis' could have persisted for at least 5 Ma (Riding et al., 2014).

In addition to the activity of cyanobacteria (Cloud, 1968, 1976) and availability of shallow protected shelf habitats (Hayes, 1983), oxygen oasis development would have been influenced by oceanic hydrothermal flux of Fe(II) related to mantle activity (Isley, 1995). Superplume events during the Archean and Paleoproterozoic can be linked to marine transgressions (Isley and Abbott, 1999), and Barley et al. (2005) suggested that plume activity in the late Archean (~2.72 to 2.65 Ga) and

near the Archean–Proterozoic transition (~2.51 to 2.45 Ga) may have been more important than biological controls on the rise of oxygen. Swanner et al. (2015) suggested that drowning of the Campbellrand/Malmani carbonate platform by iron formation might be directly related to plume-driven upwelling of Fe(II)-rich seawater. In this context it is necessary to distinguish between short-term ocean basin upwelling plumes (Beukes and Gutzmer, 2008) and mantle plume events with durations of tens of million years, far longer than single transgressive episodes. Nonetheless, it remains possible that termination of the Steep Rock Platform by iron- and manganese-rich waters (Riding et al., 2014) could reflect increased hydrothermal activity near the onset of the major mantle plume event, widely inferred to have commenced prior to 2.7 Ga (Barley et al., 1998, 2005; Bekker et al., 2010).

12.6. Oxygen, calcium and metabolic evolution

Concentrations of oxygen and calcium significantly affect cell chemistry; both can be highly toxic and require careful regulation (Shi et al., 2006; Verret et al., 2010). Cells of prokaryotes and eukaryotes maintain Ca^{2+} homeostasis, and numerous cellular processes are controlled by Ca^{2+} signaling (Berridge, 2007). Considering cellular ion carrier evolution in the context of early ocean composition, calcium may have been favored for its ability (based on size and coordination number) to interact with biological molecules (Carafoli, 1987, p. 397). In addition, homeostasis and signaling could be related, if homeostatic systems that protect against calcium ultimately led to the Ca^{2+} signaling system that provides cells with an extraordinarily 'versatile regulatory machinery' (Case et al., 2007, pp. 345–346; Petersen et al., 2005). Calcium concentrations may have been relatively high in Archean oceans (Grotzinger and Kasting, 1993). This is consistent with the view that hydrothermal vents and interactions between seawater and ocean crust supplied calcium to the ocean (Russell et al., 2010, 2014; Shibuya et al., 2010; Sleep et al., 2011), as they do today (Ludwig et al., 2006; Schrenk et al., 2013), and also consistent with maintenance of high saturation states for $CaCO_3$ minerals in Archean seawater due to the abundance of dissolved iron (Sumner, 1997b; Holland, 2006) and scarcity of sulfate (Habicht et al., 2002; Crowe et al., 2014). Similarly, cyanobacteria require Fe(II) (Saito et al., 2003) but can also be stressed by Fe(II) concentrations >10 μM (Shcolnick et al., 2009). Swanner et al. (2015) suggested that Fe(II)-rich water would have limited cyanobacterial productivity in the late Archean and that oxygenation depended on the timing of submarine volcanism and upwelling rates. Sustained removal of dissolved Fe(II) by oxidation in oxygen oases can be expected to have lowered the stress on cyanobacteria created by high levels of Fe(II).

In environments such as the Mosher Carbonate, factors that combined to promote oxygen oasis development could therefore have created positive feedbacks maintaining and expanding conditions favorable to oxygen production. We envisage that in these near-shore conditions cyanobacterial growth was promoted by nutrients from terrestrial run-off and that the oxygen released accumulated in shallow seawater partially isolated from anoxic iron-rich open-marine circulation. Under overall conditions where phosphorus may have been limited (Jones et al., 2015), increased recycling of phosphorus by oxygenation of seafloor organic matter (Van Cappellen and Ingall, 1996) could have significantly increased nutrient availability. Furthermore, oxygenation promoted Ca-carbonate precipitation by removing ferrous iron that otherwise would have promoted Fe-carbonate (e.g., siderite) precipitation (Klein and Beukes, 1989; Riding et al., 2014). This in turn alleviated both Fe(II) and Ca^{2+} stress on cells. Accumulation of carbonate sediment at rates exceeding relative sea-level rise further enhanced shallow-water conditions, increasing cyanobacterial growth and oxygenation. Thus, once initiated, carbonate platform oxygen oases tended to maintain long lasting, relatively O_2-rich and Fe(II)- and Ca^{2+}-poor conditions, under which cellular adaptations to these novel environments could progress.

Ultimately, oxygen stimulated the development of new cellular capabilities (da Silva and Williams, 1991; Saito et al., 2003) and diverse aerobic metabolisms (Baudouin-Cornu and Thomas, 2007; Raymond and Segrè, 2006), that included sterane biosynthesis (Waldbauer et al., 2011), the development of transmembrane proteins that facilitate cellular compartmentalization (Ren and Paulsen, 2005; Acquisti et al., 2007), and microbial pathways of Fe-oxidation, and nitrate and sulfate reduction (Nisbet and Sleep, 2001; Müller et al., 2012). In this view, Archean carbonate platforms could have provided stable relatively nutrient-rich environments for microbial communities to adapt to reactive oxygen species, oxidative stress, lower calcium, and organic carbon production. They may also have hosted some of the earliest eukaryotes (Knoll, 2014) that could sense, regulate and utilize light, oxygen and calcium, providing a cradle of shallow-marine evolution. Further research is needed to elucidate the effects of oxygenated carbonate platform inception, and its significance for biospheric evolution.

13. Conclusions

The Mosher Carbonate is ~2800 Ma old (Fralick et al., 2008), up to 500 m thick (Wilks and Nisbet, 1988), and can be traced laterally for at least 50 km. Apart from secondarily hematized areas it is essentially limestone, and accumulated following marine transgression of an eroded 3000 Ma tonalitic gneiss and basaltic land surface. Greenschist alteration hinders fine-fabric interpretation, but macrofabrics are generally well-preserved. We recognize a lower Hogarth Member, at least 120 m thick, and an upper Elbow Point Member, at least 70 m thick. The Hogarth Member typically consists of thin-layers of dark and light-colored limestone that locally contain numerous layers of Fe-carbonate. This banded lithotype shows some broad resemblances to fine-grained ribbon rock and locally forms large steep sided domes. At Locality 1, the Hogarth Member contains thin biostromes of small well-preserved domal and columnar stromatolites, very occasional thin horizons of atikokania crystal fans, and fenestral sheet-crack limestone that may be stratiform stromatolites. Well-preserved irregular laminae in some of the stromatolites resemble lithified microbial mats and biofilms, and might be cyanobacteria-dominated mats lithified by dissimilatory iron reduction (DIR). At Locality 5, the upper part of the Hogarth Member contains large banded limestone domes that pass upwards into fenestral layers with numerous small stromatolite domes, locally with radial crystal fans. The overlying Elbow Point Member at Localities 2, 3 and 6 consists entirely of juxtaposed elongate metric-scale domes, commonly 2–3 m across and up to 1 m thick, with smooth dimpled surfaces. Each dome consists of numerous centimetric alternations of precipitated crystal fan fabric, with strontium concentrations that suggest they were originally aragonite, and cuspate fenestral fabric that resembles microbial films and spar-filled vugs. The domes appear current-oriented and lack intervening sediment. Overall, we tentatively interpret the Mosher Carbonate as a shallow-water succession with interior platform banded limestone facies (e.g., lower Hogarth Member at Locality 1), back margin banded domes and fenestral facies (e.g., upper Hogarth Member at Locality 5), and Elbow Point platform margin facies of oriented giant domes (e.g., Locality 6).

Rare Earth Element (REE) values indicate that the seawater from which some Mosher carbonates precipitated was oxygenated. We infer that oxygenation promoted Ca-carbonate over Fe-carbonate precipitation and that Steep Rock represents a protected shallow marine platform environment in which, at times, oxygen removed sufficient dissolved iron to permit aragonite and calcite precipitation. The most likely source of the oxygen is oxygenic photosynthesis, and it is therefore likely that Steep Rock stromatolites harbored cyanobacteria. We identify the Steep Rock limestone as an early example of a marine oxygen oasis (Riding et al., 2014). This interpretation could be extended to other Archean limestones that were precipitated at the margins of otherwise iron-rich anoxic seas. Thin stratiform Fe-carbonate layers interbedded in the lower part of the Hogarth Member and in the giant

domes of the Elbow Point Member represent periods of mixing between more oxygenated iron-poor platform water and less oxygenated iron-rich offshore water. The 'hybrid' structure of the giant domes, with thickly interlayered crystal fan and cuspate fenestral fabric, may reflect fluctuating conditions near a redox chemocline. Limestone accumulation is estimated to have continued for 5 Ma or more. It was terminated by drowning beneath sub-oxic seawater that precipitated up to 400 m of first Mn-rich and then Mn-poor iron formation. The irregular upper contact of the limestone was probably produced during Phanerozoic alteration of this iron formation.

The geochemistry of the carbonate sediments is strongly correlated with their lithofacies. There are indications that their primary carbonate precipitates and secondary void filling cements have differing geochemistries. Systematic changes in carbonate geochemistry through the succession probably record interplay between more oxygenated waters on the shallow platform and oxygen-deficient offshore seawater. Future studies of Precambrian chemical sediments should maximize the information obtained by conducting not just geochemical analyses of their lithofacies, but also of the primary and secondary minerals these lithofacies contain.

Steep Rock could be Earth's oldest thick, well-preserved marine carbonate platform and it contains a variety of stromatolites, ranging from small domes and finger-like columns, to giant domes 5 m or more across. Numerous uncertainties remain to be elucidated. Notable challenges include discrimination and interpretation of the diverse lithofacies, together with their fabrics and geochemistry, as well their lateral variations. It is crucially important to establish the facies polarity of the succession, and also the roles of lateral fluctuations in geochemical gradients, driven by changes in the rate of oxygen production and physical processes, e.g., storms, in defining chemical and biological characteristics of the sediment. Calcium carbonate platform deposits have wide significance for understanding interactions between life and environments in the mid-Archean.

Acknowledgements

We are grateful to Raymond Bernatchez for introducing us to Steep Rock outcrops and providing sample 8-44, and to Linda Jahnke for loaning the sample in Fig. 17E. Maureen Wilks kindly advised us on localities. This work was supported by a NSERC Discovery grant and Lakehead University Research Chair to PF. Drafting was conducted by Sam Spivak with assistance from Fabio Tosti. RR thanks Maribel Benito, Ramón Mas and Pablo Suarez-Gonzalez for guidance in the Cameros Basin, Spain. We are very grateful to editor André Strasser and two anonymous reviewers for helpful comments and advice that improved the manuscript. Finally, we thank Tim Horscroft for inviting us to prepare this article.

Appendix A. Supplementary data

Supplementary data to this article can be found online at http://dx.doi.org/10.1016/j.earscirev.2015.10.006.

References

Abbott, G., 1914. Is "Atikokania lawsoni" a concretion? Nature 94, 477–478.
Abell, P.I., McClory, J., Martin, A., Nisbet, E.G., 1985a. Archaean stromatolites from the Ngesi Group, Belingwe greenstone belt, Zimbabwe; preservation and stable isotopes — preliminary results. Precambrian Res. 27, 357–383.
Abell, P.I., McClory, J., Martin, A., Nisbet, E.G., Kyser, T.K., 1985b. Petrography and stable isotope ratios from Archaean stromatolites, Mushandike Formation, Zimbabwe. Precambrian Res. 27, 385–398.
Acquisti, C., Kleffe, J., Collins, S., 2007. Oxygen content of transmembrane proteins over macroevolutionary time scales. Nature 445, 47–52.
Aitken, J.D., 1967. Classification and environmental significance of cryptalgal limestones and dolomites, with illustrations from the Cambrian and Ordovician of southwestern Alberta. J. Sediment. Petrol. 37, 1163–1178.
Alibert, C., McCulloch, M.T., 1993. Rare earth element and neodymium isotopic compositions of the banded iron-formations and associated shales from Hamersley, Western Australia. Geochim. Cosmochim. Acta 57, 187–204.
Allwood, A.C., Walter, M.R., Kamber, B.S., Marshal, C.P., Burch, I.W., 2006. Stromatolite reef from the Early Archaean era of Australia. Nature 441, 714–718.
Allwood, A.C., Walter, M.R., Burch, I.W., Kamber, B.S., 2007. 3.43 billion-year-old stromatolite reef from the Pilbara Craton of Western Australia: ecosystem-scale insights to early life on Earth. Precambrian Res. 158, 198–227.
Allwood, A.C., Kamber, B.S., Walter, M.R., Burch, I.W., Kanik, I., 2010. Trace elements record depositional history of an Early Archean stromatolitic carbonate platform. Chem. Geol. 270, 148–163.
Altermann, W., 2008. Accretion, trapping and binding of sediment in Archean stromatolites — morphological expression of the antiquity of life. Space Sci. Rev. 135, 55–79.
Altermann, W., Lenhardt, N., 2012. The volcano-sedimentary succession of the Archean Sodium Group, Ventersdorp Supergroup, South Africa: volcanology, sedimentology and geochemistry. Precambrian Res. 214–215, 60–81.
Altermann, W., Nelson, D.R., 1998. Sedimentation rates, basin analysis and regional correlations of three Neoarchaean and Palaeoproterozoic sub-basins of the Kaapvaal craton as inferred from precise U–Pb zircon ages from volcaniclastic sediments. Sediment. Geol. 120, 225–256.
Altermann, W., Siegfried, H.P., 1997. Sedimentology and facies development of an Archaean shelf: carbonate platform transition in the Kaapvaal Craton, as deduced from a deep borehole at Kathu, South Africa. J. Afr. Earth Sci. 24, 391–410.
Anbar, A.D., Duan, Y., Lyons, T.W., Arnold, G.L., Kendall, B., Creaser, R.A., Kaufman, A.J., Gordon, G.W., Scott, C., Garvin, J., Buick, R., 2007. A whiff of oxygen before the Great Oxidation Event? Science 317, 1903–1906.
Anbar, A.D., Kendall, B., Reinhard, C.T., Lyons, T.W., 2011. Whither the whiff? Goldschmidt Confer. Abs. Mineral. Mag. 75, 433.
Awramik, S.M., Buchheim, H.P., 2009. A giant, Late Archean lake system: the Meentheena Member (Tumbiana Formation; Fortescue Group), Western Australia. Precambrian Res. 174, 215–240.
Awramik, S.M., Margulis, L., 1974. Stromatolite Newsl. 2, 5.
Barley, M.E., Bekker, A., Krapez, B., 2005. Late Archean to Early Paleoproterozoic global tectonics, environmental change and the rise of atmospheric oxygen. Earth Planet. Sci. Lett. 238, 156–171.
Barley, M.E., Krapez, B., Groves, D.I., Kerrich, R., 1998. The Late Archaean bonanza: metallogenic and environmental consequences of the interaction between mantle plumes, lithospheric tectonics and global cyclicity. Precambrian Res. 91, 65–90.
Barrett, T.J., Fralick, P.W., 1989. Turbidites and iron formation, Beardmore–Geraldton, Ontario: application of a combined ramp/fan model to Archean clastic and chemical sedimentation. Sedimentology 36, 221–234.
Barrett, T.J., Fralick, P.W., Jarvis, I., 1988. Rare-earth-element geochemistry of some Archean iron formations north of Lake Superior, Ontario. Can. J. Earth Sci. 25, 570–580.
Bartley, J.K., Kah, L.C., Frank, T.D., Lyons, T.W., 2014. Deep-water microbialites of the Mesoproterozoic Dismal Lakes Group: microbial growth, lithification, and implications for coniform stromatolites. Geobiology http://dx.doi.org/10.1111/gbi.12114.
Bau, M., 1993. Effects of syn- and post-depositional processes on the rare-earth element distribution in Precambrian iron-formations. Eur. J. Mineral. 5, 257–267.
Bau, M., Dulski, P., 1996. Distribution of yttrium and rare-earth elements in the Penge and Kuruman iron-formations, Transvaal Supergroup, South Africa. Precambrian Res. 79, 37–55.
Bau, M., Moller, P., 1993. Rare earth element systematics of the chemically precipitated component in Early Precambrian iron formations and the evolution of the terrestrial atmosphere–hydrosphere–lithosphere system. Geochim. Cosmochim. Acta 57, 2239–2249.
Baud, A., Richoz, S., Pruss, S., 2007. The lower Triassic anachronistic carbonate facies in space and time. Glob. Planet. Chang. 55, 81–89.
Baudouin-Cornu, P., Thomas, D., 2007. Oxygen at life's boundaries. Nature 445, 35–36.
Beakhouse, G.P., Stott, G.M., Blackburn, C.E., Breaks, F.W., Ayer, J., Stone, D., Farrow, C., Corfu, F., 1996. Western superior province (field trips A5 and B6). Geol. Ass. of Canada/Mineral. Ass. of Canada, Ann. Meeting, Winnipeg, Manitoba, May 27–29 (107 pp.).
Becker, R.H., Clayton, R.N., 1972. Carbon isotopic evidence for the origin of a banded iron-formation in Western Australia. Geochim. Cosmochim. Acta 36, 577–595.
Bekker, A., Eriksson, K.A., 2003. A Paleoproterozoic drowned carbonate platform on the southeastern margin of the Wyoming Craton: a record of the Kenorland breakup. Precambrian Res. 120, 327–364.
Bekker, A., Karhu, J.A., Eriksson, K.A., Kaufman, A.J., 2003. Chemostratigraphy of Paleoproterozoic carbonate successions of the Wyoming Craton: tectonic forcing of biogeochemical change? Precambrian Res. 120, 279–325.
Bekker, A., Holland, H.D., Wang, P.L., Rumble, D., Stein, H.J., Hannah, J.L., Coetzee, L.L., Beukes, N.J., 2004. Dating the rise of atmospheric oxygen. Nature 427, 117–120.
Bekker, A., Slack, J.F., Planavsky, N., Krapez, B., Hofmann, A., Konhauser, K.O., Rouxel, O.J., 2010. Iron formation: the sedimentary product of a complex interplay among mantle, tectonic, oceanic and biospheric processes. Econ. Geol. 105, 467–508.
Bekker, A., Planavsky, N.J., Rasmussen, B., Krapez, B., Hoffman, A., Slack, J.F., Rouxel, O.J., Konhauser, K.O., 2014. Iron Formations: their origins and implications for seawater chemistry. In: Holland, H., Turekian, K. (Eds.), Treatise on Geochemistry, 2nd ed. Elsevier, pp. 561–628.
Berridge, M.J., 2007. Calcium signalling, a spatiotemporal phenomenon. New Compr. Biochem. 41, 485–502.
Bertrand-Sarfati, J., 1976. Pseudomorphoses de gypse en rosettes dans un calcaire cryptalgo-laminaire du Précambrien inférieur (Système du Transvaal, Afrique du Sud). Bull. Soc. Geol. Fr. 1976 (3), 99–102 (Suppl.).
Beukes, N.J., 1987. Facies relations, depositional environments and diagenesis in a major early Proterozoic stromatolitic carbonate platform to basinal sequence, Campbellrand Subgroup, Transvaal Supergroup, Southern Africa. Sediment. Geol. 54, 1–46.

Beukes, N.J., Gutzmer, J., 2008. Origin and paleoenvironmental significance of major iron formations at the Archean–Paleoproterozoic boundary. In: Hagemann, S., Rosiere, C., Gutzmer, J., Beukes, N.J. (Eds.), Banded Iron Formation-related High-grade Iron Ore. Rev. in Econ. Geol., Soc. of Econ. Geol., Denver 15, pp. 5–47.

Beukes, N.J., Lowe, D.R., 1989. Environmental control on diverse stromatolite morphologies in the 3000 Myr Pongola Supergroup, South Africa. Sedimentology 36, 383–397.

Beukes, N.J., Klein, C., Kaufman, A.J., Hayes, J.M., 1990. Carbonate petrology, kerogen distribution, and carbon and oxygen isotope variations in an early Proterozoic transition from limestone to iron-formation deposition, Transvaal Supergroup, South Africa. Econ. Geol. 85, 663–690.

Bickle, M.J., Martin, A., Nisbet, E.G., 1975. Basaltic and peridotitic komatiites and stromatolites above a basal unconformity in the Belingwe greenstone belt, Rhodesia. Earth Planet. Sci. Lett. 27, 155–162.

Bishop, J.W., Sumner, D.Y., 2006. Molar tooth structures of the Neoarchean Monteville Formation, Transvaal Supergroup, South Africa. I: constraints on microcrystalline $CaCO_3$ precipitation. Sedimentology 53, 1049–1068.

Blackwelder, E., 1926. Precambrian geology of the Medicine Bow Mountains. Geol. Soc. Am. Bull. 37, 615–658.

Blank, C.E., Sánchez-Baracaldo, P., 2010. Timing of morphological and ecological innovations in the cyanobacteria — a key to understanding the rise in atmospheric oxygen. Geobiology 8, 1–23.

Bolhar, R., Kamber, B.S., Moorbath, S., Fedo, C.M., Whitehouse, M.J., 2004. Characterisation of early Archaean chemical sediments by trace element signatures. Earth Planet. Sci. Lett. 222, 43–60.

Bolhar, R., van Kranendonk, M.J., 2007. A non-marine depositional setting for the northern Fortescue Group, Pilbara Craton, inferred from trace element geochemistry of stromatolitic carbonates. Precambrian Res. 155, 229–250.

Bourque, P.-A., Boulvain, F., 1993. Model for the origin and petrogenesis of the red stromatactis limestone of Paleozoic carbonate mud mounds. J. Sediment. Petrol. 63, 607–619.

Buick, R., 1992. The antiquity of oxygenic photosynthesis: evidence from stromatolites in sulphate-deficient Archaean lakes. Science 255, 74–77.

Buick, R., 2007. The earliest records of life. In: Sullivan, W.T., Baross, J.A. (Eds.), Planets and Life: The Emerging Science of Astrobiology. Cambridge Un. Press, Cambridge, UK, pp. 237–264.

Buick, R., 2008. When did oxygenic photosynthesis evolve? Philos. Trans. R. Soc. B 363, 2731–2743.

Buick, R., Dunlop, J.S.R., 1990. Evaporitic sediments of Early Archaean age from the Warrawoona Group, North Pole, Western Australia. Sedimentology 37, 241–277.

Burnham, O.M., Schweyer, J., 2004. Trace element analysis of geological samples by ICP–MS at the Geoscience Laboratories: revised capabilities due to improvements to instrumentation. Summary of Field Work and Other Activities 2004. Ont. Geol. Surv., Open File Rept. 6145 (54–1 to 54–20).

Button, A., 1973. The stratigraphic history of the Malmani Dolomite in the eastern and northeastern Transvaal. Geol. Soc. S. Afr. Trans. 76, 229–247.

Button, A., 1976. Iron-formation as an end member in carbonate sedimentary cycles in the Transvaal Supergroup, South Africa. Econ. Geol. 71, 193–201.

Byrne, R.H., Kim, K.H., 1990. Rare earth element scavenging in seawater. Geochim. Cosmochim. Acta 54, 2645–2656.

Canfield, D.E., 2005. The early history of atmospheric oxygen: homage to Robert M. Garrels. Annu. Rev. Earth Planet. Sci. 33, 1–36.

Carafoli, E., 1987. Intracellular calcium homeostasis. Annu. Rev. Biochem. 56, 395–433.

Casanova, J., Marcell, C.H., 1993. Carbon and oxygen isotopes in African lacustrine stromatolites: palaeohydrological interpretations. In: Swart, P.K., Lohmann, K.C., McKenzie, J., Savin, S. (Eds.), Climate Change in the Continental Isotopic Record. Am. Geophy. Union, Geophys. Monogr. 94, pp. 123–133.

Case, R.M., Eisner, D., Gurney, A., Jones, O., Muallem, S., Verkhratsky, A., 2007. Evolution of calcium homeostasis: from birth of the first cell to an omnipresent signalling system. Cell Calcium 42, 345–350.

Catling, D.C., Claire, M.W., 2005. How Earth's atmosphere evolved to an oxic state: a status report. Earth Planet. Sci. Lett. 237, 1–20.

Chafetz, H.S., Folk, R.L., 1984. Travertines: depositional morphology and the bacterially constructed constituents. J. Sediment. Petrol. 54, 289–316.

Chafetz, H.S., Guidry, S.A., 2003. Bacterial shrubs, crystal shrubs, and ray-crystal shrubs: bacterial vs. abiotic precipitation. Sediment. Geol. 126, 57–74.

Cloud Jr., P.E., 1960. Gas as a sedimentary and diagenetic agent. Am. J. Sci. 258A, 35–45.

Cloud Jr., P.E., 1968. Atmospheric and hydrospheric evolution on the primitive Earth: both secular accretion and biological and geochemical processes have affected Earth's volatile envelope. Science 160, 729–736.

Cloud Jr., P.E., 1972. A working model of the primitive Earth. Am. J. Sci. 272, 537–548.

Cloud Jr., P.E., 1976. Beginnings of biospheric evolution and their biogeochemical consequences. Paleobiology 2, 351–387.

Cloud Jr., P.E., Semikhatov, M.A., 1969. Proterozoic stromatolite zonation. Am. J. Sci. 267, 1017–1061.

Cloud Jr., P.E., Wright, L.A., Williams, E.G., Diehl, P., Walter, M.R., 1974. Giant stromatolites and associated vertical tubes from the Upper Proterozoic Noonday Dolomite, Death Valley Region, eastern California. Geol. Soc. Am. Bull. 85, 1861–1882.

Coleman, A.P., 1898. Clastic Huronian rocks of western Ontario. Geol. Soc. Am. Bull. 9, 223–238.

Corfu, F., Wallace, H., 1986. U–Pb zircon ages for magmatism in the Red Lake greenstone belt, northwestern Ontario. Can. J. Earth Sci. 23, 27–42.

Corkeron, M., 2007. 'Cap carbonates' and Neoproterozoic glacigenic successions from the Kimberley region, north-west Australia. Sedimentology 54, 871–903.

Cowan, C.A., James, N.P., 1993. Diastasis cracks: mechanically generated synaeresis-like cracks in Upper Cambrian shallow water oolite and ribbon carbonates. Sedimentology 39, 1101–1118.

Craig, H., 1954. Carbon 13 in plants and the relationships between carbon 13 and carbon 14 variations in nature. J. Geol. 62, 115–149.

Crowe, S.A., Døssing, L.N., Beukes, N.J., Bau, M., Kruger, S.J., Frei, R., Canfield, D.E., 2013. Atmospheric oxygenation three billion years ago. Nature 501, 535–539.

Crowe, S.A., Paris, G., Katsev, S., Jones, C.-A., Kim, S.-T., Zerkle, A.L., Nomosatryo, S., Fowle, D.A., Adkins, J.F., Sessions, A.L., Farquhar, J., Canfield, D.E., 2014. Sulfate was a trace constituent of Archean seawater. Science 346, 735–739.

Czaja, A.D., Johnson, C.M., Beard, B.L., Eigenbrode, J.L., Freeman, K.H., Yamaguchi, K.E., 2010. Iron and carbon isotope evidence for ecosystem and environmental diversity in the ~2.7 to 2.5 Ga Hamersley Province, Western Australia. Earth Planet. Sci. Lett. 292, 170–180.

Czaja, A.D., Johnson, C.M., Roden, E.E., Beard, B.L., Voegelin, A.R., Nägler, T.F., Beukes, N.J., Wille, M., 2012. Evidence for free oxygen in the Neoarchean ocean based on coupled iron–molybdenum isotope fractionation. Geochim. Cosmochim. Acta 86, 118–137.

da Silva, J.J.R.F., Williams, R.J.P., 1991. The Biological Chemistry of the Elements: The Inorganic Chemistry of Life. Oxford University Press, Oxford, p. 561.

Danielson, A., Moller, P., Dulski, P., 1992. The europium anomalies in banded iron formation and the thermal history of the oceanic-crust. Chem. Geol. 97, 89–100.

Davis, D.W., 1993. Report on U–Pb geochronology in the Atikokan area, Wabigoon Subprovince. Royal Ontario Museum Report, p. 9.

Davis, D.W., Jackson, M.C., 1988. Geochronology of the Lumby Lake greenstone belt: a 3 Ga complex within the Wabigoon subprovince, northwest Ontario. Geol. Soc. Am. Bull. 100, 818–824.

De Baar, H.J.W., Brewer, P.G., Bacon, M.P., 1985. Anomalies in rare earth distributions in seawater: Gd and Tb. Geochim. Cosmochim. Acta 49, 1961–1969.

De Baar, H.J.W., Schijf, J., Byrne, R.H., 1991. Solution chemistry of the rare earth elements in seawater. Eur. J. Solid State Inorg. Chem. 28, 357–373.

DeCarlo, E.H., Wen, X.Y., Irving, M., 1998. The influence of redox reactions on the uptake of dissolved Ce by suspended Fe and Mn oxide particle. Aquat. Geochem. 3, 357–392.

Demicco, R.V., 1983. Wavy and lenticular-bedded carbonate ribbon rocks of the Upper Cambrian Conococheague Limestone, central Appalachians. J. Sediment. Petrol. 53, 1121–1132.

Derry, L.A., Jacobsen, S.B., 1990. The chemical evolution of Precambrian seawater — evidence from REEs in banded iron formations. Geochim. Cosmochim. Acta 54, 2965–2977.

Donaldson, J.A., 1976. Palaeoecology of *Conophyton* and associated stromatolites in the Precambrian Dismal Lakes and Rae groups, Canada. In: Walter, M.R. (Ed.), Stromatolites. Elsevier, Amsterdam, The Netherlands, pp. 523–534.

Dupraz, C., Reid, P., Braissant, O., Decho, A.W., Norman, R.S., Visscher, P.T., 2009. Processes of carbonate precipitation in modern microbial mats. Earth Sci. Rev. 96, 141–162.

Eigenbrode, J.L., Freeman, K.H., 2006. Late Archean rise of aerobic microbial ecosystems. PNAS 103, 15759–15764.

Eigenbrode, J.L., Freeman, K.H., Summons, R.E., 2008. Methylhopane biomarker hydrocarbons in Hamersley Province sediments provide evidence for Neoarchean aerobiosis. Earth Planet. Sci. Lett. 273, 323–331.

Elderfield, H., Upstillgoddard, R., Sholkovitz, E.R., 1990. The rare earth elements in rivers, estuaries and costal seas and their significance to the composition of ocean waters. Geochim. Cosmochim. Acta 54, 971–991.

Eriksson, K.A., Krapez, B., Fralick, P.W., 1994. Sedimentology of greenstone belts: signatures of tectonic evolution. Earth Sci. Rev. 37, 1–88.

Farquhar, J., Wing, B.A., 2003. Multiple sulfur isotopes and the evolution of the atmosphere. Earth Planet. Sci. Lett. 213, 1–13.

Farquhar, J., Bao, H., Thiemens, M., 2000. Atmospheric influence of Earth's earliest sulfur cycle. Science 289, 756–758.

Farquhar, J., Zerkle, A.L., Bekker, A., 2011. Geological constraints on the origin of oxygenic photosynthesis. Photosynth. Res. 107, 11–36.

Fenton, C.L., Fenton, M.A., 1933. Algal reefs or bioherms in the Belt Series of Montana. Geol. Soc. Am. Bull. 44, 1135–1142.

Fenwick, K.G., 1976. Geology of the Finlayson Lake area, district of Rainy River. Ont. Div. of Mines, GeoSci. Rept No. 145, p. 86.

Fischer, A.G., 1964. The Lofer cyclothems of the Alpine Triassic. In: Merriam, D.F. (Ed.), Symposium on Cyclic Sedimentation. Kansas Geol. Surv. Bull. 169, pp. 107–149.

Fischer, A.G., 1965. Fossils, early life, and atmospheric history. Proc. Natl. Acad. Sci. U. S. A. 53, 1205–1215.

Fischer, W.W., Schroeder, S., Lacassie, J.P., Beukes, N.J., Goldberg, T., Strauss, H., Horstmann, U.E., Schrag, D.P., Knoll, A.H., 2009. Isotopic constraints on the Late Archean carbon cycle from the Transvaal Supergroup along the western margin of the Kaapvaal Craton, South Africa. Precambrian Res. 169, 15–27.

Flannery, D.T., Walter, M.R., 2012. Archean tufted microbial mats and the Great Oxidation Event: new insights into an ancient problem. Aust. J. Earth Sci. 59, 1–11.

Flannery, D.T., Hoshino, Y., George, S.C., Walter, M.R., 2012. Field observations relating to the c. 2740 Ma Mopoke Member, Kylena Formation, Fortescue Group, Pilbara region, Western Australia. Geol. Sur. of W. Austral. Rec. 2012/8, p. 12.

Fralick, P., 1989. Microbial bioherms, Lower Proterozoic Gunflint Formation, Thunder Bay, Ontario. In: Geldsetzer, H.H.J., James, N.P., Tebbutt, G.E. (Eds.), Reefs Canada and Adjacent Areas. Can. Soc. of Petrol. Geol. Mem. 13, pp. 24–29.

Fralick, P., Carter, J.E., 2011. Neoarchean deep marine paleotemperature: evidence from turbidite successions. Precambrian Res. 191, 78–84.

Fralick, P.W., King, D., 1996. Mesoarchean evolution of western Superior Province: evidence from metasedimentary sequences near Atikokan. In: Harrap, R.M., Helmstaedt, H. (Eds.), Western Superior Transect Third Annual Workshop, University of British Columbia, LITHOPROBE Secretariat. LITHOPROBE Rept 53, pp. 29–35.

Fralick, P.W., Pufahl, P.K., 2006. Iron formation in Neoarchean deltaic successions and the microbially mediated deposition of transgressive systems tracts. J. Sediment. Res. 76, 1057–1066.

Fralick, P.W., Riding, R., 2012. Steep Rock carbonate platform: an early marine oxygen oasis. Goldschmidt Conference, Montreal, Abst.

Fralick, P.W., Hollings, P., King, D., 2008. Stratigraphy, geochemistry and depositional environments of Mesoarchean sedimentary units in Western Superior Province: implications for generation of early crust. In: Condie, K.C., Pease, V. (Eds.), When did Plate Tectonics Begin on Planet Earth? Geol. Soc. of Am. Spec. Paper 440, pp. 77–96.
Fralick, P.W., Wu, J., Williams, H.R., 1992. Trench and slope basin deposits in an Archean metasedimentary belt, Superior Province, Canadian Shield. Can. J. Earth Sci. 29, 2551–2557.
Frei, R., Gaucher, C., Poulton, S.W., Canfield, D.E., 2009. Fluctuations in Precambrian atmospheric oxygenation recorded by chromium isotopes. Nature 461, 250–253.
Furniss, G., Rittel, J.F., Winston, D., 1998. Gas bubble and expansion crack origin of "molar-tooth" calcite structures in the Middle Proterozoic Belt Supergroup, western Montana. J. Sediment. Res. 68, 104–114.
Gandin, A., Wright, D.T., 2007. Evidence of vanished evaporates in Neoarchean carbonates of South Africa. In: Schreiber, B.C., Lugli, S., Babel, M. (Eds.), Evaporites Through Space and Time. Geol. Soc. Spec. Pub 285, pp. 285–308.
Gandin, A., Wright, D.T., Melezhik, V., 2005. Vanished evaporates and carbonate formation in the Neoarchaean Kogelbeen and Gamohaan formations of the Campbellrand Subgroup, South Africa. J. Afr. Earth Sci. 41, 1–23.
García-Reyes, M., Largier, J., 2010. Observations of increased wind-driven coastal upwelling off central California. J. Geophys. Res. 115, C04011. http://dx.doi.org/10.1029/2009JC005576.
German, C.R., Hergt, J., Palmer, M.R., Edmond, J.M., 1999. Geochemistry of a hydrothermal sediment core from the OBS vent-field, 21 degrees N East Pacific Rise. Chem. Geol. 155, 65–75.
Ginsburg, R.N., 1991. Controversies about stromatolites: vices and virtues. In: Muller, D.W., McKenzie, J.A., Weissert, H. (Eds.), Controversies in Modern Geology; Evolution of Geological Theories in Sedimentology, Earth History and Tectonics. Academic Press, London, pp. 25–36.
Glaessner, M.F., 1962. Pre-cambrian fossils. Biol. Rev. 37, 467–493.
Godfrey, L.V., Chan, L.-H., Alonso, R.N., Lowenstein, T.K., McDonough, W.F., Houston, J., Li, J., Bobst, A., Jordan, T.E., 2013. The role of climate in the accumulation of lithium-rich brine in the central Andes. Appl. Geochem. 38 (920102).
Grassineau, N.V., Nisbet, E.G., Fowler, C.M.R., Bickle, M.J., Lowry, D., Chapman, H.J., Mattey, D.P., Abell, P., Yong, J., Martin, A., 2002. Stable isotopes in the Archaean Belingwe belt, Zimbabwe: evidence for a diverse prokaryotic mat ecology. In: Fowler, C.W.R., Ebinger, C.J., Hawkesworth, C.J. (Eds.), The Early Earth: Physical, Chemical and Biological Development. Geol. Soc. Spec. Pub., Geol. Soc. of London Spec. Pub. 199, pp. 309–328.
Grassineau, N.V., Appel, P.W.U., Fowler, C.M.R., Nisbet, E.G., 2005. Distinguishing biological from hydrothermal signature via sulphur and carbon isotopes in Archean mineralizations at 3.8 and 2.7 Ga. In: McDonald, I. (Ed.), Mineral Deposits and Earth Evolution. Geol. Soc. of London, Spec. Pub. 248, pp. 195–212.
Grassineau, N., Abell, P., Appel, P.W.U., Lowry, D., Nisbet, E., 2006. Early life signatures in sulfur and carbon isotopes from Isua, Barberton, Wabigoon (Steep Rock), and Belingwe Greenstone Belts (3.8 to 2.7 Ga). In: Kesler, S.E., Ohmoto, H. (Eds.), Evolution of Early Earth's Atmosphere, Hydrosphere, and Biosphere — Constraints from Ore Deposits. Geol. Soc. of Am. 198, pp. 33–52.
Grassineau, N.V., Nisbet, E.G., 2008. Early evolution of photosynthetic processes before the Great Oxidation: a C and S isotopes perspective. Goldschmidt Conference Abst. 72, p. A324.
Grey, K., 1981. Small conical stromatolites from the Archaean near Kanowna, Western Australia. W. Austral. Geol. Surv. Ann. Rept. for 1980, pp. 90–94.
Grotzinger, J.P., 1986. Cyclicity and paleoenvironmental dynamics, Rocknest platform, northwest Canada. Geol. Soc. Am. Bull. 97, 1208–1231.
Grotzinger, J.P., 1989. Facies and evolution of Precambrian carbonate depositional systems: emergence of the modern platform archetype. In: Crevello, P.D., Wilson, J.L., Sarg, J.F., Read, J.F. (Eds.), Controls on Carbonate Platform and Basin Development. SEPM Spec. Pub 44, pp. 79–106.
Grotzinger, J.P., Kasting, J.F., 1993. New constraints on Precambrian ocean composition. J. Geol. 101, 235–243.
Grotzinger, J.P., Knoll, A.H., 1999. Stromatolites in Precambrian carbonates: evolutionary mileposts or environmental dipsticks? Annu. Rev. Earth Planet. Sci. 27, 313–358.
Grotzinger, J.P., Read, J.F., 1983. Evidence for primary aragonite precipitation, lower Proterozoic (1.9-Ga) Rocknest Dolomite, Wopmay orogen, northwest Canada. Geology 11, 710–713.
Grover, G., Read, J.F., 1978. Fenestral and associated vadose diagenetic fabrics of tidal flat carbonates, Middle Ordovician, New Market Limestone, southwestern Virginia. J. Sediment. Petrol. 48, 453–473.
Habicht, K.S., Gade, M., Thamdrup, B., Berg, P., Canfield, D.E., 2002. Calibration of sulfate levels in the Archean ocean. Science 298, 2372–2374.
Hall, J., 1883. *Cryptozoön*, n.g.; *Cryptozoön proliferum*, n.sp. New York State Museum of Nat. Hist. 36th Ann. Rept. of the Trustees, Plate 6.
Ham, W.E., 1952. Algal origin of the "birdseye" limestone in the McLish Formation. Oklahoma Acad. Sci. Proc. 33, 200–203.
Hannigan, R.E., Sholkovitz, E.R., 2001. The development of middle rare earth element enrichments in freshwaters: weathering of phosphate minerals. Chem. Geol. 175, 495–508.
Hardie, L.A., 2003. Secular variations in Precambrian seawater chemistry and the timing of Precambrian aragonite seas and calcite seas. Geology 31, 785–788.
Hardie, L.A., 2004. Secular variations in Precambrian seawater chemistry and the timing of Precambrian aragonite seas and calcite seas: reply. Geol. e1–e2.
Hayes, J.M., 1983. Geochemical evidence bearing on the origin of aerobiosis, a speculative hypothesis. In: Schopf, J.W. (Ed.), Earth's Earliest Biosphere, Its Origin and Evolution. Princeton University Press, pp. 291–301.
Hayes, J.M., 1994. Global methanotrophy at the Archean–Proterozoic transition. In: Bengtson, S. (Ed.), Early Life on Earth. Nobel Symp. No. 84. Columbia Univ. Press, New York, pp. 220–236.
Heimann, A., Johnson, C.M., Beard, B.L., Valley, J.W., Roden, E.E., Spicuzza, M.J., Beukes, N.J., 2010. Fe, C, and O isotope compositions of banded iron formation carbonates demonstrate a major role for dissimilatory iron reduction in ~2.5 Ga marine environments. Earth Planet. Sci. Lett. 294, 8–18.
Herzog, R.E., Shi, Q., Patil, J.N., Katz, J.L., 1989. Magnetic water treatment: the effect of iron on calcium carbonate nucleation and growth. Langmuir 5, 861–867.
Heubeck, C., 2009. An early ecosystem of Archean tidal microbial mats (Moodies Group, South Africa, ca. 3.2 Ga). Geology 37, 931–934.
Heubeck, C., Lowe, D.R., 1994. Depositional and tectonic setting of the Archean Moodies Group, Barberton Greenstone Belt, South Africa. Precambrian Res. 68, 257–290.
Hladil, J., 2005. The formation of stromatactis-type fenestral structures during the sedimentation of experimental slurries — a possible clue to a 120-year-old puzzle about stromatactis. Bull. Geosci. 80, 193–211 (Czech Geological Survey, ISSN 1214–1119).
Hoffman, P., 1967. Algal stromatolites: use in stratigraphic correlation and paleocurrent determination. Science 157, 1043–1045.
Hoffman, P., 1973. Evolution of an early Proterozoic continental margin: the Coronation geosyncline and associated aulacogens, northwestern Canadian Shield. In: Sutton, J., Windley, B.F. (Eds.), Evolution of the Precambrian Crust. Royal Soc. London Phil. Trans. Series A 273, pp. 547–581.
Hoffman, P., 1974. Shallow and deepwater stromatolites in Lower Proterozoic platform-to-basin facies change, Great Slave Lake, canada. Am. Assoc. Pet. Geol. Bull. 58, 856–867.
Hoffman, P., 1976a. Stromatolite morphogenesis in Shark Bay, Western Australia. In: Walter, M.R. (Ed.), Stromatolites, Developments in Sedimentology 20. Elsevier, Amsterdam, pp. 261–271.
Hoffman, P., 1976b. Environmental diversity of Middle Precambrian stromatolites. In: Walter, M.R. (Ed.)Stromatolites, Developments in Sedimentology 20. Elsevier, Amsterdam, pp. 599–611.
Hoffman, P.F., 1980. Wopmay Orogen: a Wilson Cycle of early Proterozoic age in the northwest of the Canadian Shield. In: Strangway, D.W. (Ed.), The Continental Crust and Its Mineral Resources. Geol. Ass. of Can. Spec. Paper 20, pp. 523–549.
Hoffman, P.F., 1989. Pethei reef complex (1.9 Ga), Great Slave Lake, N.W.T. In: Geldsetzer, H.H.J., James, N.P., Tebbutt, G.E. (Eds.), Reefs Canada and Adjacent Areas. Can. Soc. of Petrol. Geol. Mem 13, pp. 38–48.
Hoffman, P.F., Macdonald, F.A., 2010. Sheet-crack cements and early regression in Marinoan (635 Ma) cap dolostones: regional benchmarks of vanishing ice-sheets? Earth Planet. Sci. Lett. 300, 374–384.
Hofmann, H.J., 1971. Precambrian fossils, pseudofossils, and problematica in Canada. Geol. Surv. Can. Bull. 189, 146.
Hofmann, H.J., 1973. Stromatolites: characteristics and utility. Earth-Sci. Rev. 9, 339–373.
Hofmann, H.J., Masson, M., 1994. Archean stromatolites from Abitibi greenstone belt, Quebec, Canada. Geol. Soc. Am. Bull. 106, 424–429.
Hofmann, H.J., Snyder, G.L., 1985. Archean stromatolites from the Hartville Uplift, eastern Wyoming. Geol. Soc. Am. Bull. 96, 842–849.
Hofmann, H.J., Thurston, P.C., Wallace, H., 1985. Archean stromatolites from Uchi greenstone belt, northwestern Ontario. In: Ayres, L.D., Thurston, P.C., Card, K.D., Weber, W. (Eds.), Evolution of Archean Supracrustal Sequences. Geol. Ass. of Can. Spec. Paper 28, pp. 125–132.
Hofmann, H.J., Sage, R.P., Berdusco, E.N., 1991. Archean stromatolites in Michipicoten Group siderite ore at Wawa, Ontario. Econ. Geol. 86, 1023–1030.
Hofmann, H.J., Grey, K., Hickman, A.H., Thorpe, R.I., 1999. Origin of 3.45 Ga coniform stromatolites in Warrawoona Group, Western Australia. Geol. Soc. Am. Bull. 111, 1256–1262.
Holland, H.D., 1973. The oceans: a possible source of iron in iron-formations. Econ. Geol. 68, 1169–1172.
Holland, H.D., 1978. The Chemistry of the Atmosphere and Oceans. Wiley, New York, p. 351.
Holland, H.D., 2006. The oxygenation of the atmosphere and oceans. Philos. Trans. R. Soc. B 361, 903–915.
Hollings, P., Wyman, D., 1999. Trace element and Sm–Nd systematics of volcanic and intrusive rocks from the 3 Ga Lumby Lake Greenstone belt, Superior Province: evidence for Archean plume–arc interaction. Lithos 46, 189–213.
Hollings, P., Wyman, D., Kerrich, R., 1999. Komatiite–basalt–rhyolite volcanic associations in Northern Superior Province greenstone belts: significance of plume–arc interaction in the generation of the proto continental Superior Province. Lithos 46, 137–161.
Huston, W.J., 1956. The Steeprock Manganiferous Footwall Paint M.Sc. thesis Queen's University, Kingston, Ontario, p. 76.
Isley, A.E., 1995. Hydrothermal plumes and the delivery of iron to banded iron formation. J. Geol. 103, 169–185.
Isley, A.E., Abbott, D.H., 1999. Plume-related mafic volcanism and the deposition of banded iron formation. J. Geophys. Res. 104 (B7), 15461–15477.
James, N.P., Narbonne, G.M., Kyser, T.K., 2001. Late Neoproterozoic cap carbonates: Mackenzie Mountains, northwestern Canada: precipitation and global glacial meltdown. Can. J. Earth Sci. 38, 1229–1262.
Jamieson, J.W., Wing, B.A., Farquhar, J., Hannington, M.D., 2013. Neoarchaean seawater sulphate concentrations from sulphur isotopes in massive sulphide ore. Nat. Geosci. 6, 61–64.
Jolliffe, A.W., 1955. Geology and iron ores of Steep Rock Lake. Econ. Geol. 50, 373–398.
Jolliffe, A.W., 1966. Stratigraphy of the Steeprock Group, Steep Rock Lake, Ontario. In: Goodwin, A.M. (Ed.), Precambrian Symposium on the Relationship of Mineralization to Precambrian Stratigraphy in Certain Mining Areas of Ontario and Quebec. Geol. Ass. of Can. Spec. Paper 3, pp. 75–98.
Jones, C., Nomosatryo, S., Crowe, S.A., Bjerrum, C.J., Canfield, D.E., 2015. Iron oxides, divalent cations, silica, and the early earth phosphorus crisis. Geology 43, 135–138.
Kakegawa, T., Haikawa, M., 2007. Aerobic and anaerobic ecosystem recorded in the Steep Rock Group, Ontario, Canada. Goldschmidt Conf., Cologne, Abst. Geochim. Cosmochim. Acta 71 (15), A458 (supplement).

Kamber, B.S., Bolhar, R., Webb, G.E., 2004. Geochemistry of late Archaean stromatolites from Zimbabwe: evidence for microbial life in restricted epicontinental seas. Precambrian Res. 132, 379–399.
Kamber, B.S., Webb, G.E., 2001. The geochemistry of late Archaean microbial carbonate: implications for ocean chemistry and continental erosion history. Geochim. Cosmochim. Acta 65, 2509–2525.
Kasting, J.F., 1991. Box models for the evolution of atmospheric oxygen, an update. Palaeogeogr. Palaeoclimatol. Palaeoecol. 97, 125–131 (Global and Planetary Change Section).
Kasting, J.F., 1992. Models relating to Proterozoic atmospheric and oceanic chemistry. In: Schopf, J.W., Klein, C. (Eds.), The Proterozoic Biosphere, a Multidisciplinary StudyCambridge University Press. Cambridge, UK, pp. 1185–1187.
Kato, Y., Nakamura, K., 2003. Origin and global tectonic significance of Early Archean cherts from the Marble Bar greenstone belt, Pilbara Craton, Western Australia. Precambrian Res. 125, 191–243.
Kaufman, A.J., Hayes, J.M., Klein, C., 1990. Primary and diagenetic controls of isotopic compositions of iron-formation carbonates. Geochim. Cosmochim. Acta 54, 3461–3473.
Kaufman, A.J., Johnston, D.T., Farquhar, J., Masterson, A.L., Lyons, T.W., Bates, S., Anbar, A.D., Arnold, G.L., Garvin, J., Buick, R., 2007. Late Archean biospheric oxygenation and atmospheric evolution. Science 317, 1900–1906.
Kazmierczak, J., Altermann, W., Kremer, B., Kempe, S., Eriksson, P., 2009. Mass occurrence of benthic coccoid cyanobacteria and their role in the production of Neoarchean carbonates of South Africa. Precambrian Res. 173, 79–92.
Kendall, B., Reinhard, C.T., Lyons, T.W., Kaufman, A.J., Poulton, S.W., Anbar, A.D., 2010. Pervasive oxygenation along late Archaean ocean margins. Nat. Geosci. 3, 647–652.
Kendall, B., Gordon, G.W., Poulton, S.W., Anbar, A.D., 2011. Molybdenum isotope constraints on the extent of late Paleoproterozoic ocean euxinia. Earth Planet. Sci. Lett. 307, 450–460.
Kerrich, R., Said, N., 2011. Extreme positive Ce-anomalies in a 3.0 Ga submarine volcanic sequence, Murchison Province: oxygenated marine bottom waters. Chem. Geol. 280, 232–241.
Kershaw, S., et al., 2011. Earliest Triassic microbialites in Çürük Dag, southern Turkey: composition, sequences and controls on formation. Sedimentology 58, 739–755.
Kim, K.H., Byrne, R.H., Lee, J.H., 1991. Gadolinium behaviour in seawater: a molecular basis for gadolinium anomalies. Mar. Chem. 36, 107–120.
Kimberley, M.M., Sorbara, J.P., 1976. Post-Archean weathering of Steep Rock Group iron formation. Proceedings of the 1976 Geotraverse Workshop. University of Toronto Press, Toronto, Canada (32–1 to 32–17).
Klein, C., 2005. Some Precambrian banded iron-formations (BIFs) from around the world: their age, geologic setting, mineralogy, metamorphism, geochemistry, and origins. Am. Mineral. 90, 1473–1499.
Klein, C., Beukes, N.J., 1989. Geochemistry and sedimentology of a facies transition from limestone to iron-formation deposition in the Early Proterozoic Transvaal Supergroup, South Africa. Econ. Geol. 84, 1733–1774.
Klinkhammer, G., Elderfield, H., Hudson, A., 1983. Rare earth elements in seawater near hydrothermal vents. Nature 305, 185–188.
Klinkhammer, G.P., Elderfield, H., Edmond, J.M., Mitra, A., 1994. Geochemical implications of rare earth element patterns in hydrothermal fluids from mid-ocean ridges. Geochim. Cosmochim. Acta 58, 5105–5113.
Knight, S.H., Keefer, D.K., 1966. Preliminary report on the Precambrian stromatolites in the Nash Formation, Medicine Bow Mountains, Wyoming. Contributions to Geol. 5. University of Wyoming, pp. 1–11
Knoll, A.H., 2014. Paleobiological perspectives on early eukaryotic evolution. Cold Spring Harbor Perspec. in Biol. 6, no. 1.
Knoll, A.H., Beukes, N.J., 2009. Introduction: initial investigations of a Neoarchean shelf margin-basin transition (Transvaal Supergroup, South Africa). Precambrian Res. 169, 1–14.
Konhauser, K.O., Riding, R., 2012. Bacterial biomineralization. In: Knoll, A.H., Canfield, D.E., Konhauser, K.O. (Eds.), Fundamentals of Geobiology. John Wiley and Sons, Chichester, UK, pp. 105–130.
Konhauser, K.O., Newman, D.K., Kappler, A., 2005. The potential significance of microbial Fe(III) reduction during deposition of Precambrian banded iron formations. Geobiology 3, 167–177.
Kopp, R.E., Kirschvink, J.L., Hilburn, I.A., Nash, C.Z., 2005. Natl. Acad. Sci. 102, 11131–11136.
Korolyuk, I.K., 1959. Undulatory-bedded stromatolites (*Stratifera*) in the Cambrian rocks of southeastern Siberia. Byull. Mosk. Obshch. Ispyt. Prir. Otd. Geol. 34 (3), 76–95 (in Russian).
Korolyuk, I.K., 1960. Stromatolites of the Lower Cambrian and Proterozoic of the Irkutsk Amphitheatre. Trudy Inst. Geol. Razrab. Goryuchikhina Iskop., Akad. Nauk. SSSR 1, 112–161 (in Russian).
Krylov, I.N., 1976. Approaches to the classification of stromatolites. In: Walter, M.R. (Ed.), StromatolitesDevelopments in Sedimentology 20. Elsevier, Amsterdam, pp. 31–43.
Kusky, T.M., Hudleston, P.J., 1999. Growth and demise of an Archean carbonate platform, Steep Rock Lake, Ontario, canada. Can. J. Earth Sci. 36, 565–584.
Lawson, A.C., 1912. The geology of Steeprock Lake Ontario. Can. Dept. Mines, Geol. Sur. Branch, Mem. 28, 7–15.
Lazar, B., Erez, J., 1990. Extreme ^{13}C depletion in seawater-derived brines and their implications for the past geochemical carbon cycle. Geology 18, 1191–1194.
Lees, A., 1964. The structure and origin of the Waulsortian (Lower Carboniferous) 'reefs' of west-central Eire. Philos. Trans. R. Soc. Lond. Ser. B Biol. Sci. 247, 483–531.
Lehrmann, D.J., Wan, Y., Wei, J., Yu, Y.-Y., Xiao, J., 2001. Lower Triassic peritidal cyclic limestone: an example of anachronistic carbonate facies from the Great Bank of Guizhou, Nanpanjiang Basin, Guizhou province, South China. Palaeogeogr. Palaeoclimatol. Palaeoecol. 173, 103–123.
Logan, B.W., 1961. *Cryptozoon* and associated stromatolites from the Recent, Shark Bay, Western Australia. J. Geol. 69, 517–533.
Logan, B.W., Rezak, R., Ginsburg, R.N., 1964. Classification and environmental significance of algal stromatolites. J. Geol. 72, 68–83.
Lowe, D.R., Byerly, G.R., 2007. An overview of the geology of the Barberton greenstone belt and vicinity: implications for early crustal development. Dev. Precambian. Geol. 15, 481–526.
Ludwig, K.A., Kelley, D.S., Butterfield, D.A., Nelson, B.K., Früh-Green, G., 2006. Formation and evolution of carbonate chimneys at the Lost City Hydrothermal Field. Geochim. Cosmochim. Acta 70, 3625–3645.
Lyons, T.W., Gill, B.C., 2010. Ancient sulfur cycling and oxygenation of the early biosphere. Elements 6, 93–99.
MacGregor, A.R., 1927. The problem of the Precambrian atmosphere. S. Afr. J. Sci. 24, 155–172.
MacGregor, I.M., 1941. A Precambrian algal limestone in southern Rhodesia. Geol. Soc. S. Afr. Trans. 43, 9–15.
Machado, A.B., 1987. On the origin and age of the Steep Rock buckshot, Ontario, Canada. Chem. Geol. 60, 337–349.
Martin, A., Nisbet, E.G., Bickle, M.J., 1980. Archaean stromatolites of the Belingwe Greenstone Belt, Zimbabwe (Rhodesia). Precambrian Res. 13, 337–362.
McInnes, W., 1899. Report on the geology of the area covered by the Seine River and Lake Shebandowan map-sheets, comprising portions of Rainy River and Thunder Bay districts, Ontario. Ann. Rept. Geol. Sur. Can. 10, 5–65 (part H).
McLennan, S.M., 1994. Rare earth element geochemistry and the "tetrad" effect. Geochim. Cosmochim. Acta 58, 2025–2033.
Mel'nik, Y.P., 1982. Precambrian banded iron formations. Developments in Precam. Geol. 5. Elsevier, Amsterdam, p. 310
Misra, Y., Kumar, S., 2005. Coniform stromatolites and the Vindhyan Supergroup, central India: implication for basinal correlation and age. J. Palaeontol. Soc. India 50, 153–167.
Moffett, J.W., 1990. Microbially mediated cerium oxidation in sea water. Nature 345, 421–423.
Moore, E.S., 1938. The steep rock series. Trans. of the Royal Soc. of Can. Section 4, 3rd Series. 32, pp. 11–23.
Moore, E.S., 1939. Geology and ore deposits of the Atikokan area. Ont. Dept. of Mines 48th Ann. Rept. 48, pp. 1–34
Müller, M., Mentel, M., van Hellemond, J.J., Henze, K., Woehle, C., Gould, S.B., Yu, R.-Y., van der Giezen, M., Tielens, A.G.M., Martin, W.F., 2012. Biochemistry and evolution of anaerobic energy metabolism in eukaryotes. Microbiol. Mol. Biol. Rev. 76, 444–495.
Murphy, M.A., Sumner, D.Y., 2008. Variations in Neoarchean microbialite morphologies: clues to controls on microbialite morphologies through time. Sedimentology 55, 1189–1202.
Murray, R.W., Tenbrink, M.R.B., Gerlach, D.C., Russ, G.P., Jones, D.L., 1992. Interoceanic variation in the rare-earth, major, and trace-element depositional chemistry of chert — perspectives gained from the DSDP and ODP record. Geochim. Cosmochim. Acta 56, 1897–1913.
Nisbet, E.G., Grassineau, N.V., Howe, C.J., Abell, P.I., Regelous, M., Nisbet, R.E.R., 2007. The age of Rubisco: the evolution of oxygenic photosynthesis. Geology 5, 311–335.
Nisbet, E.G., Sleep, N.H., 2001. The habitat and nature of early life. Nature 409, 1083–1091.
Nisbet, E.G., Wilks, M.E., 1989. Archaean stromatolite reef at Steep Rock Lake, Atikokan, Northwestern Ontario. In: Geldsetzer, H.H.J., James, N.P., Tebbutt, J.E. (Eds.), Reefs Canada and Adjacent Areas. Can. Soc. of Petrol. Geol. Mem. 13, pp. 89–92.
Nothdurft, L.D., Webb, G.E., Kamber, B.S., 2004. Rare earth element geochemistry of Late Devonian reefal carbonates, Canning Basin, Western Australia: confirmation of a seawater REE proxy in ancient limestones. Geochim. Cosmochim. Acta 68, 263–283.
Ono, S., Kaufman, A.J., Farquhar, J., Sumner, D.Y., Beukes, N., 2009. Lithofacies control on multiple-sulfur isotope records and Neoarchean sulfur cycles. Precambrian Res. 169, 58–67.
Orpen, J.L., Wilson, J.F., 1981. Stromatolites at ≈3500 Myr and a greenstone–granite unconformity in the Zimbabwean Archaean. Nature 291, 218–220.
Pavlov, A.E., Kasting, J.F., 2002. Mass-independent fractionation of sulfur isotopes in Archean sediments: strong evidence for an anoxic Archean atmosphere. Astrobiology 2, 27–41.
Peckmann, J., Goedart, J.L., Thiel, V., Michaelis, W., Reitner, J., 2002. A comprehensive approach to the study of methane-seep deposits from the Lincoln Creek Formation, western Washington State, USA. Sedimentology 49, 855–873.
Pentecost, A., 2005. Travertine. Springer, Berlin Heidelberg, p. 445.
Percival, J.A., Sanborn-Barrie, M., Skulski, T., Stott, G.M., Helmstaedt, H., White, D.J., 2006. Tectonic evolution of the western Superior Province from NATMAP and Lithoprobe studies. Can. J. Earth Sci. 43, 1085–1117.
Petersen, O.H., Michalak, M., Verkhratsky, A., 2005. Calcium signalling: past, present and future. Cell Calcium 38, 161–169.
Petrov, P.Y., Semikhatov, M.A., 2001. Sequence organization and growth patterns of late Mesoproterozoic stromatolite reefs: an example from the Burovaya Formation, Turukhansk Uplift, Siberia. Precambrian Res. 111, 257–281.
Petryshyn, V.A., Corsetti, F.A., Berelson, W.M., Beaumont, W., Lund, S.P., 2012. Stromatolite lamination frequency, Walker Lake, Nevada: implications for stromatolites as biosignatures. Geology 40, 499–502.
Pfeil, R.W., Read, J.F., 1980. Cambrian carbonate platform margin facies, Shady Dolomite, southwestern Virginia, U.S.A. J. Sediment. Petrol. 50, 91–116.
Planavsky, N., Grey, K., 2008. Stromatolite branching in the Neoproterozoic of the Centralian Superbasin, Australian: an investigation into sedimentary and microbial control of stromatolite morphology. Geobiology 6, 33–45.
Planavsky, N.J., Asael, D., Hofmann, A., Reinhard, C.T., Lalonde, S.V., Knudsen, A., Wang, X., Ossa, F., Pecoits, E., Smith, A.J.B., Beukes, N.J., Bekker, A., Johnson, T.M., Konhauser, K.O., Lyons, T.W., Rouxel, O.J., 2014. Evidence for oxygenic photosynthesis half a billion years before the Great Oxidation Event. Nat. Geosci. 7, 283–286.
Planavsky, N., Bekker, A., Rouxel, O.J., Kamber, B., Hofmann, A., Knudsen, A., Lyons, T.W., 2010. Rare Earth Element and yttrium compositions of Archean and Paleoproterozoic

Fe formations revisited: new perspectives on the significance and mechanisms of deposition. Geochim. Cosmochim. Acta 74, 6387–6405.
Playford, P.E., Cockbain, A.E., 1976. Modern algal stromatolites in Hamelin Pool, a hypersaline barred basin in Shark Bay, Western Australia. In: Walter, M.R. (Ed.), 'Stromatolites' Chapter 8.2, Developments in Sedimentology 20. Amsterdam, Elsevier, pp. 389–411.
Poulton, S.W., Fralick, P.W., Canfield, D.E., 2010. Spatial variability in oceanic redox structure 1.8 billion years ago. Nat. Geosci. 3, 486–490.
Pratt, B.R., 1995. The origin, biota and evolution of deep-water mud-mounds. In: Monty, C.L.V., Bosence, D.W.J., Bridges, P.H., Pratt, B.R. (Eds.), Carbonate Mud-mounds, Their Origin and Evolution. International Association of Sedimentologists. Spec. Pub. 23, pp. 49–123.
Pruss, S.B., Corsetti, F.A., Fischer, W.W., 2008. Seafloor-precipitated carbonate fans in the Neoproterozoic Rainstorm Member, Johnnie Formation, Death Valley region, USA. Sediment. Geol. 207, 34–40.
Pufahl, P.K., Hiatt, E.E., 2012. Oxygenation of the Earth's atmosphere–ocean system: a review of physical and chemical sedimentologic responses. Mar. Pet. Geol. 1–20.
Rajan, S., Mackenzie, F.T., Glenn, C.R., 1996. A thermodynamic model for water column precipitation of siderite in the Plio-Pleistocene Black Sea. Am. J. Sci. 296, 506–548.
Ray, J.S., Veizer, J., Davis, W.J., 2003. C, O, Sr and Pb isotope systematics of carbonate sequences of the Vindhyan Supergroup, India: age, diagenesis, correlations and implications for global events. Precambrian Res. 121, 103–140.
Raymond, P.E., 1935. Pre-Cambrian life. Geol. Soc. Am. Bull. 46, 375–392.
Raymond, J., Segrè, D., 2006. The effect of oxygen on biochemical networks and the evolution of complex life. Science 311, 1764–1767.
Read, J.F., 1985. Carbonate platform facies models. Am. Assoc. Pet. Geol. Bull. 69, 1–21.
Ren, Q., Paulsen, I.T., 2005. Comparative analyses of fundamental differences in membrane transport capabilities in prokaryotes and eukaryotes. PLoS Comput. Biol. 1 (3), e27.
Rezak, R., 1957. Stromatolites of the belt series in Glacier National Park and vicinity. MontanaU. S. Geol. Surv. Prof. Paper 294-D, pp. 127–154.
Ricketts, B.D., 1983. The evolution of a middle Precambrian dolostone sequence — a spectrum of dolomitization regimes. J. Sediment. Petrol. 53, 565–586.
Ricketts, B.D., Donaldson, J.A., 1989. Stromatolite reef development on a mud-dominated platform in the middle Precambrian Belcher Group of Hudson Bay. In: Geldsetzer, H.H.J., James, N.P., Tebbutt, G.E. (Eds.), Reefs Canada and Adjacent Areas. Can. Soc. of Petrol. Geol. Mem 13, pp. 113–119.
Riding, R., 2000. Microbial carbonates: the geological record of calcified bacterial–algal mats and biofilms. Sedimentology 47 (Suppl. 1), 179–214.
Riding, R., 2008. Abiogenic, microbial and hybrid authigenic carbonate crusts: components of Precambrian stromatolites. Geol. Croat. 61, 73–103.
Riding, R., Fralick, P., Liang, L., 2014. Identification of an Archean marine oxygen oasis. Precambrian Res. 251, 232–237.
Rivera, M.J., Sumner, D.Y., 2014. Unraveling the three-dimensional morphology of Archean microbialites. J. Paleontol. 88, 719–726.
Rosing, M.T., Frei, R., 2004. U-rich Archaean sea-floor sediments from Greenland — indications of >3700 Ma oxygenic photosynthesis. Earth Planet. Sci. Lett. 217, 237–244.
Ross, G.M., Donaldson, J.A., 1989. Reef development and facies geometry on a high-energy early Proterozoic carbonate shelf (Hornby Bay Group, Northwest Territories, Canada). In: Geldsetzer, H.H.J., James, N.P., Tebbutt, G.E. (Eds.), Reefs Canada and Adjacent Areas. Can. Soc. of Petrol. Geol. Mem 13, pp. 120–128.
Rothpletz, A., 1916. Über die systematische Deutung und die stratigraphische Stellung der ältesten Versteinerungen Europas und Nordamerikas mit besonderer Berücksichtigung der Cryptozoen und Oolithe; Teil 2: Über Cryptozoon, Eozoon und Atikokania. Abhandlungen der Königlich Bayerischen Akademie der Wissenschaften. Mathematisch-physikalische Klasse, München, p. 92.
Rouxel, O.J., Bekker, A., Edwards, K.J., 2005. Iron isotope constraints on the Archean and Paleoproterozoic ocean redox state. Science 307, 1088–1091.
Russell, M.J., Barge, L.M., Bhartia, R., Bocanegra, D., Bracher, P.J., Branscomb, E., Kidd, R., McGlynn, S., Meier, D.H., Nitschke, W., Shibuya, T., Vance, S., White, L., Kanik, I., 2014. The drive to life on wet and icy worlds. Astrobiology 14, 308–343.
Russell, M.J., Hall, A.J., Martin, W., 2010. Serpentinization as a source of energy at the origin of life. Geobiology 8, 355–371.
Saito, M.A., Sigman, D.M., Morel, F.M.M., 2003. The bioinorganic chemistry of the ancient ocean: the co-evolution of cyanobacterial metal requirements and biogeochemical cycles at the Archean–Proterozoic boundary? Inorg. Chim. Acta 356, 308–318.
Schäfer, W., 1954. Dehnungsrisse unter Wasser im meerischen Sediment. Senckenb. Lethaea 35, 87–99.
Schau, M., Henderson, J.B., 1983. Archean chemical weathering at three localities on the Canadian Shield. Precambrian Res. 20, 189–224.
Schidlowski, M., 1988. A 3,800-million-year isotopic record of life from carbon in sedimentary rocks. Nature 333, 313–318.
Schidlowski, M., Matzigkeit, U., Mook, W.G., Krumbein, W.E., 1985. Carbon isotope geochemistry and ^{14}C ages of microbial mats from the Gavish Sabkha and the Solar Lake. In: Friedman, G.M., Krumbein, W.E. (Eds.), Hypersaline EcosystemsEcological Studies 5. Berlin, Springer-Verlag, pp. 381–401.
Schlager, W., 2003. Benthic carbonate factories of the Phanerozoic. Int. J. Earth Sci. 92, 445–464.
Schneiderhan, E.A., Gutzmer, J., Strauss, H., Mezger, K., Beukes, N.J., 2006. The chemostratigraphy of a Paleoproterozoic MnF–BIF succession — the Voelwater Subgroup of the Transvaal Supergroup in Griqualand West, South Africa. S. Afr. J. Geol. 109, 63–80.
Schofield, R.K., Keen, B.A., 1929. Rigidity in weak clay suspensions. Nature 123, 492–493.
Schopf, J.W., 2006. Fossil evidence of Archaean life. Philos. Trans. R. Soc. B 361, 869–885.
Schopf, J.W., Oehler, D.Z., Horodyski, R.J., Kvenvolden, K.A., 1971. Biogenicity and significance of the oldest known stromatolites. J. Paleontol. 45, 477–485.
Schopf, J.W., Kudryavtsev, A.B., Czaja, A.D., Tripathi, A.B., 2007. Evidence of Archean life: stromatolites and microfossils. Precambrian Res. 158, 141–155.
Schrenk, M.O., Brazelton, W.J., Lang, S.Q., 2013. Serpentinization, carbon, and deep life. Rev. Mineral. Geochem. 75, 575–606.
Schröder, S., Beukes, N.J., Sumner, D.Y., 2009. Microbialite-sediment interactions on the slope of the Campbellrand carbonate platform (Neoarchean, South Africa). Precambrian Res. 169, 68–79.
Scott, C.T., Lyons, T.W., Bekker, A., et al., 2008. Tracing the stepwise oxygenation of the Proterozoic biosphere. Nature 452, 456–459.
Scott, C.T., Bekker, A., Reinhard, C.T., Schnetger, B., Krapež, B., Rumble, D., Lyons, T.W., 2011. Late Archean euxinic conditions before the rise of atmospheric oxygen. Geology 39, 119–122.
Semikhatov, M.A., Raaben, M.E., 2000. Proterozoic stromatolite taxonomy and biostratigraphy. In: Riding, R., Awramik, S.M. (Eds.), Microbial Sediments. Springer-Verlag, Heidelberg, pp. 295–306.
Serebryakov, S.N., 1976. Distribution of stromatolites in Riphean deposits of the Uchur-Maya region of Siberia. In: Walter, M.R. (Ed.), StromatolitesDevelopments in Sedimentology 20. Elsevier, Amsterdam, pp. 613–633.
Shcolnick, S., Summerfield, T.C., Reytman, L., Sherman, L.A., Keren, N., 2009. The mechanism of iron homeostasis in the unicellular cyanobacterium *Synechocystis* sp. PCC 6803 and its relationship to oxidative stress. Plant Physiol. 150, 2045–2056.
Shen, Y., Buick, R., 2004. The antiquity of microbial sulfate reduction. Earth Sci. Rev. 64, 243–272.
Shen, Y., Buick, R., Canfield, D.E., 2001. Isotopic evidence for microbial sulphate reduction in the early Archaean era. Nature 410, 77–81.
Shepard, R.N., Sumner, D.Y., 2010. Undirected motility of filamentous cyanobacteria produces reticulate mats. Geobiology 8, 179–190.
Sheppard, S.M.F., Schwarcz, H.P., 1970. Fractionation of carbon and oxygen isotopes and magnesium between coexisting metamorphic calcite and dolomite. Contrib. Mineral. Petrol. 26, 161–198.
Shi, Y., Zhao, W., Zhang, W., Ye, Z., Zhao, J., 2006. Regulation of intracellular free calcium concentration during heterocyst differentiation by HetR and NtcA in *Anabaena* sp. PCC 7120. Proc. Natl. Acad. Sci. U. S. A. 103, 11334–11339.
Shibuya, T., Komiya, T., Nakamura, K., Takai, K., Maruyama, S., 2010. Highly alkaline, high-temperature hydrothermal fluids in the early Archean ocean. Precambrian Res. 182, 230–238.
Shinn, E.A., 1968. Practical significance of birdseye structures in carbonate rocks. J. Sediment. Petrol. 38, 215–223.
Shklanka, R., 1972. Geology of the Steep Rock Lake area. In: Geology of the Steep Rock Lake area, District of Rainy River. Geol. Rept. 93 Part 1 and map 2217, 1:12,000. Ont. Dept. of Mines and Northern Affairs, Toronto, Ont., pp. 78.
Sholkovitz, E.R., Schneider, D.L., 1991. Cerium redox cycles and rare earth elements in the Sargasso Sea. Geochim. Cosmochim. Acta 55, 2737–2743.
Simonson, B.M., Schubel, K.A., Hassler, S.W., 1993. Carbonate sedimentology of the early Precambrian Hamersley Group of Western Australia. Precambrian Res. 60, 287–335.
Sleep, N.H., Bird, D.K., Pope, E.C., 2011. Serpentinite and the dawn of life. Philos. Trans. R. Soc. B 366, 2857–2869.
Smith, W.H.C., 1893. The Archean rocks west of Lake Superior. Geol. Soc. Am. Bull. 4, 333–348.
Smith, F.G., 1942. Notes on the iron ores of Steeprock Lake, Ontario. University of Toronto Studies, Geological Series. 47, pp. 71–75.
Smyth, H.L., 1891. Structural geology of Steep Rock Lake, Ontario. Am. J. Sci. 42, 317–331.
Som, S.M., Catling, D.C., Harnmeijer, J.P., Polivka, P.M., Buick, R., 2012. Air density 2.7 billion years ago limited to less than twice modern levels by fossil raindrop imprints. Nature 484, 359–362.
Stiller, M., Rounick, J.S., Shasha, S., 1985. Extreme carbon-isotope enrichments in evaporating brines. Nature 316, 434–435.
Stone, D., 2008. Precambrian geology, Steep Rock Lake area (east). Ont. Geol. Surv. Preliminary Map P.3586, scale 1:10 000.
Stone, D., 2010. Precambrian geology of the central Wabigoon Subprovince area, Northwestern Ontario. Ont. Geol. Surv. Open File Rept. 5422, p. 129.
Stone, D., Pufahl, P., 1995. Project Unit 95-14. Geology of the Atikokan–Sapawe area: regional controls on gold mineralization in the Marmion batholith. Summary of Field Work and other Activities 1995. Ont. Geol. Surv. Misc. Pap. 164, pp. 45–47.
Stone, D., Kamineni, D.C., Jackson, M.C., 1992. Precambrian geology of the Atikokan area, northwestern Ontario. Geol. Surv. Can. Bull. 405, 106 Ottawa.
Stone, D., Tomlinson, K.Y., Davis, D.W., Fralick, P., Percival, J.A., Hallé, J., Pufahl, P., 2002. Geology and tectonostratigraphic assemblages, south-central Wabigoon Subprovince, Ontario. Western Superior NATMAP compilation series. Ont. Geol. Surv. Preliminary Map P3448, scale 1:250,000, Geol. Surv. of Can. Open File 4284.
Stüeken, E.E., Catling, D.C., Buick, R., 2012. Contributions to late Archaean sulphur cycling by life on land. Nat. Geosci. 5, 722–725.
Stumm, W., Morgan, J.J., 1996. Aquatic Chemistry: Chemical Equilibria and Rates in Natural Waters. Wiley-Interscience, New York, N.Y., p. 1022.
Sumner, D.Y., 1996. Evidence for low late Archean atmospheric oxygen from oceanic depth gradients in iron concentration. Geol. Soc. Am. Bull. 28, 218.
Sumner, D.Y., 1997a. Late Archean calcite-microbe interactions: two morphologically distinct microbial communities that affected calcite nucleation differently. PALAIOS 12, 302–318.
Sumner, D.Y., 1997b. Carbonate precipitation and oxygen stratification in late Archean seawater as deduced from facies and stratigraphy of the Gamohaan and Frisco formations, Transvaal Supergroup, South Africa. Am. J. Sci. 297, 455–487.
Sumner, D.Y., 2000. Microbial versus environmental influences on the morphology of Late Archean fenestrate microbialites. In: Riding, R., Awramik, S. (Eds.), Microbial Sediments, pp. 307–314.
Sumner, D.Y., 2002. Neoarchean carbonates — clues to early life and early ocean chemistry. International Ass. of Sedimentologists, 16th International Sedimentological Congress, Johannesburg, South Africa, Excursion A6, Field Guide, 1–6 July 2002, p. 24.

Sumner, D.Y., 2004. Secular variations in Precambrian seawater chemistry and the timing of Precambrian aragonite seas and calcite seas (Comment, Geology, Online Forum, p. e1).
Sumner, D.Y., Beukes, N.J., 2006. Sequence stratigraphic development of the Neoarchean Transvaal carbonate platform, Kaapvaal Craton, South Africa. S. Afr. J. Geol. 109, 11–22.
Sumner, D.Y., Grotzinger, J.P., 1996. Were the kinetics of calcium carbonate precipitation related to oxygen concentration? Geology 24, 119–122.
Sumner, D.Y., Grotzinger, J.P., 2000. Late Archean aragonite precipitation: petrography, facies associations, and environmental significance. In: Grotzinger, J.P., James, N.P. (Eds.), Carbonate Sedimentation and Diagenesis in the Evolving Precambrian World. SEPM Spec. Pub. Number 67, pp. 123–144.
Sumner, D.Y., Grotzinger, J.P., 2004. Implications for Neoarchaean ocean chemistry from primary carbonate mineralogy of the Campbellrand–Malmani platform, South Africa. Sedimentology 51, 1–27.
Swain, F.M., 2002. The Pseudofossil Atikokania in the Early Precambrian of Minnesota. Unpublished manuscript, Department of Geology and Geophysics, University of Minnesota, Minneapolis, USA, pp. 12.
Swanner, E.D., Mloszewska, A.M., Cirpka, O.A., Schoenberg, R., Konhauser, O., Kappler, A., 2015. Modulation of oxygen production in Archaean oceans by episodes of Fe(II) toxicity. Nat. Geosci. 8, 126–130.
Tamulonis, C., Kaandorp, J., 2014. A model of filamentous bacteria leading to reticulate pattern formation. Life 4, 433–456.
Taylor, M.E., Cook, H.E., 1976. Continental shelf and slope facies in the Upper Cambrian and lowest Ordovician of Nevada. Brigham Young Univ. Geol. Stud. 23 (2), 181–214.
Taylor, S.R., McLennan, S.M., 1985. The Continental Crust: Its Composition and Evolution. Blackwell, Oxford, p. 312.
Tice, M.M., Lowe, D.R., 2004. Photosynthetic microbial mats in the 3,416-Myr-old ocean. Nature 431, 549–552.
Tice, M.M., Thornton, D.C.O., Pope, M.C., Olszewski, T.D., Gong, J., 2011. Archean microbial mat communities. Annu. Rev. Earth Planet. Sci. 39, 297–319.
Tomlinson, K.Y., Hughes, D.J., Thurston, P.C., Hall, R.P., 1999. Plume magmatism and crustal growth at 2.9 to 3.0 Ga in the Steep Rock and Lumby Lake area, Western Superior Province. Lithos 46, 103–136.
Tomlinson, K.Y., Davis, D.W., Stone, D., Hart, T.R., 2003. U–Pb age and Nd isotopic evidence for Archean terrane development and crustal recycling in the south-central Wabigoon subprovince, Canada. Contrib. Mineral. Petrol. 144, 684–702.
Truswell, J.F., Eriksson, K.A., 1973. Stromatolitic associations and their palaeoenvironmental significance: a re-appraisal of a Lower Proterozoic locality from the Northern Cape Province, South Africa. Sediment. Geol. 10, 1–23.
Twenhofel, W.H., 1919. Pre-Cambrian and Carboniferous algal deposits. Am. J. Sci. 48, 339–352.
Valero-Garcés, B.L., Delgado-Huertas, A., Ratto, N., Navas, A., 1999. Large ^{13}C enrichment in primary carbonates from Andean Altiplano lakes, northwest Argentina. Earth Planet. Sci. Lett. 171, 253–266.
Van Cappellen, P., Ingall, E.D., 1996. Redox stabilization of the atmosphere and oceans by phosphorus-limited marine productivity. Science 271, 493–496.
Van Kranendonk, M.J., 2006. Volcanic degassing, hydrothermal circulation and the flourishing of early life on Earth: a review of the evidence from c. 3490–3240 Ma rocks of the Pilbara Supergroup, Pilbara Craton, Western Australia. Earth Sci. Rev. 74, 197–240.
Van Kranendonk, M.J., 2011. Morphology as an indicator of biogenicity for 3.5–3.2 Ga fossil stromatolites from the Pilbara Craton, Western Australia. In: Reitner, J., et al. (Eds.), Advances in Stromatolite GeobiologyLecture Notes in Earth Sciences 131. Springer-Verlag, Berlin Heidelberg, pp. 537–554. http://dx.doi.org/10.1007/978-3-642-10415-2_32.
Van Kranendonk, M.J., Webb, G.E., Kamber, B.S., 2003. New geological and trace element evidence from 3.45 Ga stromatolitic carbonates in the Pilbara Craton: support of a marine, biogenic origin and for a reducing Archean ocean. Geobiology 1, 91–108.
Veizer, J., Compston, W., Hoefs, J., Nielson, H., 1982. Mantle buffering of the early oceans. Naturwissenschaften 69, 173–180.
Veizer, J., Clayton, R.N., Hinton, R.W., von Brunn, V., Mason, T.R., Buck, S.G., Hoefs, J., 1990. Geochemistry of Precambrian carbonates: 3-shelf seas and non-marine environments of the Archean. Geochim. Cosmochim. Acta 54, 2717–2729.
Verret, F., Wheeler, G., Taylor, A.R., Farnham, G., Brownlee, C., 2010. Calcium channels in photosynthetic eukaryotes: implications for evolution of calcium-based signalling. New Phytol. 187, 23–43.
Visscher, P.T., Stolz, J.F., 2005. Microbial mats as bioreactors: populations, processes, and products. Palaeogeogr. Palaeoclimatol. Palaeoecol. 219, 87–100.
Vlasov, F.Y., 1977. Precambrian stromatolites from the Satkin Suite of the Southern Urals. In: Raaben, M.E. (Ed.), Materialy po Paleontologii Srednego Paleozoya Urala i Sibiri (Akad. Nauk SSSR, Uralskii Nauchnyi Tsentr), pp. 101–124 (in Russian).
Voegelin, A.R., Nägler, T.F., Beukes, N.J., Lacassie, J.P., 2010. Molybdenum isotopes in late Archean carbonate rocks: implications for early Earth oxygenation. Precambrian Res. 182, 70–82.
Walcott, C.D., 1912. Notes on fossils from limestone of Steeprock series, Ontario. Can. Dept. Mines, Geol. Surv. Branch Mem. 28, pp. 16–23
Walcott, C.D., 1914. Cambrian geology and paleontology III: Precambrian Algonkian algal flora. Smithsonian Miscellaneous Collection 64, pp. 77–156.
Waldbauer, J.R., Sherman, L.S., Sumner, D.Y., Summons, R.E., 2009. Late Archean molecular fossils from the Transvaal Supergroup record the antiquity of microbial diversity and aerobiosis. Precambrian Res. 169, 28–47.
Waldbauer, J.R., Newman, D.K., Summons, R.E., 2011. Microaerobic steroid biosynthesis and the molecular fossil record of Archean life. Proc. Natl. Acad. Sci. U. S. A. 108, 13409–13414.
Walker, J.C.G., Hays, P.B., Kasting, J.F., 1981. A negative feedback mechanism for the long-term stabilization of Earth's surface temperature. J. Geophys. Res. 86 (C10), 9776–9782.
Walter, M.R., 1972. Stromatolites and the biostratigraphy of the Australian Precambrian and Cambrian. Spec. Pap. Palaeontol. 11 (268 pp.).
Walter, M.R., 1983. Archean stromatolites: evidence of Earth's earliest benthos. In: Schopf, J.W. (Ed.), Earth's Earliest Biosphere. Princeton University Press, Princeton, NJ, pp. 187–213.
Walter, M.R., 1994. Stromatolites: the main geological source of information on the evolution of the early benthos. In: Bengtson, S. (Ed.), Early Life on EarthNobel Symposium 84. Columbia University Press, New York, pp. 270–286.
Walter, M.R., Bauld, J., Brock, T.D., 1976. Microbiology and morphogenesis of columnar stromatolites (*Conophyton*, *Vacerrilla*) from hot springs in Yellowstone National Park. In: Walter, M.R. (Ed.), StromatolitesDevelopments in Sedimentology 20. Elsevier, Amsterdam, pp. 273–310.
Webb, G.E., Nothdurft, L.D., Kamber, B.S., Kloprogge, J.T., Zhao, J., 2009. Rare earth element geochemistry of scleractinian coral skeleton during meteoric diagenesis: a sequence through neomorphism of aragonite to calcite. Sedimentology 56, 1433–1463.
Wegenast, W.G., 1954. The footwall rocks of the Steeprock orezone. Unpublished M.Sc. Thesis, Queen's University, Kingston, Ontario.
Wilks, M.E., 1986. The geology of the Steep Rock Group, N.W. Ontario: a major Archaean unconformity and Archaean stromatolites. Unpublished MS thesis, University of Saskatchewan, pp. 206.
Wilks, M.E., Nisbet, E.G., 1985. Archaean stromatolites from the Steep Rock Group, northwestern Ontario, canada. Can. J. Earth Sci. 22, 792–799.
Wilks, M.E., Nisbet, E.G., 1988. Stratigraphy of the Steep Rock Group, northwest Ontario: a major Archaean unconformity and Archaean stromatolites. Can. J. Earth Sci. 25, 370–391.
Williams, H.R., 1990. Subprovince accretion tectonics in the south-central Superior Province. Can. J. Earth Sci. 27, 570–581.
Wilson, J.L., 1975. Carbonate Facies in Geologic History. Springer, Berlin, p. 471.
Winefield, P.R., 2000. Development of late Paleoproterozoic aragonitic sea floor cements in the McArthur Group, Northern Australia. In: Grotzinger, J.P., James, N.P. (Eds.), Carbonate Sedimentation and Diagenesis in the Evolving Precambrian World. SEPM, Spec. Pub. 67, pp. 145–159.
Wright, D.T., Altermann, W., 2000. Microfacies development in Late Archaean stromatolites and oolites of the Ghaap Group of South Africa. Geol. Soc. Lond. Spec. Publ. 178, 51–70.
Wyman, D., Hollings, P., 1998. Long-lived mantle-plume influence on an Archean protocontinent: geochemical evidence from the 3 Ga Lumby Lake greenstone belt, Ontario. Can. Geogr. 26, 719–722.
Zeng, Z., Tice, M.M., 2014. Promotion and nucleation of carbonate precipitation during microbial iron reduction. Geobiology 12, 362–371.
Zhang, J., Nozaki, Y., 1996. Rare earth elements and yttrium in seawater: ICP-MS determinations in the East Caroline, Coral Sea, and South Fiji basins of the western South Pacific Ocean. Geochim. Cosmochim. Acta 60, 4631–4644.